Flow in air conditioned rooms

Model experiments and numerical solution of the flow equations.

Nielsen, Peter V.

Publication date:
1974

Document Version
Tidlig version også kaldet pre-print

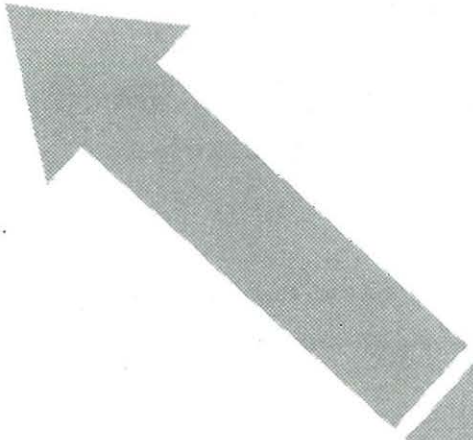

FLOW IN AIR CONDITIONED ROOMS

Model experiments and numerical solution of the flow equations.

Peter V. Nielsen

Abstract Flow in air conditioned rooms is examined by means of model experiments. The different geometries giving unsteady, steady three-dimensional and steady two-dimensional flow are determined. Velocity profiles and temperature profiles are measured in some of the geometries.

A numerical solution of the flow equations is demonstrated and the flow in air conditioned rooms in case of steady two-dimensional flow is predicted. Comparison with measured results is shown in the case of small Archimedes numbers, and predictions are shown at high Archimedes numbers.

A numerical prediction of flow and heat transfer in cavities is also shown.

Preface to the Danish edition.

The present thesis describes my work in the years 1970-1973. It is a part of the requirements for fulfilment of the degree of Lic.Techn. (Ph.D.) from the Technical University of Denmark under the supervision of Professor V. Korsgaard, Thermal Insulation Laboratory, and Professor Frank A. Engelund, Institute of Hydrodynamics and Hydraulic Engineering. The work was carried out at Danfoss A/S, Nordborg, Denmark, with occasional visits to my supervisors at the Technical University of Denmark. I should like to take this opportunity to thank my supervisors for helping me to establish and carry through this untraditional form of study.

The study was sponsored by the Danish Government Fund for Scientific and Industrial Research and by Danfoss A/S. I am deeply grateful for their support. My special thanks to M. Dyre, Head of Research at Danfoss A/S, for his kind assistance in arranging Danfoss sponsorship.

From the outset, it has been my intention in this study to use a numerical method for solving the flow equations. This brought me at an early stage into contact with the Department of Mechanical Engineering at the Imperial College of Science and Technology in London. I am grateful to the members of this department for their help, and, in particular I wish to thank Dr. B.E. Launder and Dr. A.D. Gosman for their support.

To the many persons at Danfoss A/S and the Technical University of Denmark who have assisted me in many ways I extend my grateful thanks. Especially I want to thank Mr. C. Schwarzbach, M.Sc., for carefully checking the manuscript and Mrs. K. Petersen for painstakingly typing the final copy.

Nordborg, february 1974

Peter V. Nielsen

Preface to the revised English edition.

Two years have passed since the publication of the Danish version of my thesis. I have therefore taken the opportunity to revise it, and added some results based on my work during the past years. Figures 2.4.2-1 and 2.4.5-3 have been changed and figures 2.4.5-4 and 3.4.1-6 have been added. In addition, several references have been added, throwing light on the penetration depth in rooms of small width, the influence of the side walls and the velocity decay in wall jets.

I should like to express my grateful thanks to M. Terp Paulsen, Ph.D., for his helpful comments in connection with the English manuscript. My sincere thanks also to R. St.John-Foster for his help with the English translation and Mrs. K. Petersen for her painstaking efforts in typing the final manuscript.

Danfoss A/S has readily placed its facilities at my disposal during these two years and also helped in many ways in the preparation of this English edition. I want at last to extend my grateful thanks for this assistance.

Nordborg, august 1976

Peter V. Nielsen

Index.

List of symbols.

a	Control surface at supply opening
Ar	Archimedes number
b	Control surface at supply opening
c_1	Constant in turbulence model
c_2	Constant in turbulence model
c_p	Specific heat
c_μ	Constant in turbulence model
C_E, C_N, C_S, C_W	Coefficients in difference equation
dA	Surface element
D	Source term in difference equation
D_T	Constant in equation for wall jet
D_V	Constant in equation for wall jet
e	Constant in equation for wall jet
E	Mean signal from anemometer
E'	Fluctuating part of signal from anemometer
g_i	Gravitational acceleration
Gr	Grashof number
Gr_w	Grashof number in case of convective heat transfer in a cavity
h	Height of supply opening
H	Height of room, model or cavity
k	Turbulent kinetic energy
K	Constant in equation for anemometer signal
K_1	Constant in equation for effective cooling velocity
K_2	Constant in equation for effective cooling velocity

K_T	Constant in equation for wall jet
K_V	Constant in equation for wall jet
l	Turbulent length scale
l_{re}	Penetration depth
L	Length of room or model
l/M	Scale
n	Outward normal to surface
n_p	Distance from a surface
p	Pressure
Pr	Prandtl number
q	Heat flux
r	Coefficient in equation for wall jet
Ra_w	Rayleigh number
Re	Reynolds number
R_t	Turbulent Reynolds number
R_φ	Residual
t	Time
T	Temperature
T_o	Supply temperature
T_{dA}	Temperature of surface element dA
T_m	Max. or min. temperature of wall jet
T_{ms}	Mean radient temperature
T_s	Surface temperature
T_u	Mean temperature along surface b
u	Height of return opening
v_i	Velocity vector
v_{eff}	Effective cooling velocity
v_{tot}	Total velocity
V_o	Supply velocity
V_m	Maximum velocity in wall jet

w	Width of supply opening
W	Width of room, model or cavity
x_o	Distance from supply opening to virtual origin of jet
x_a	Distance from surface 'a' to supply opening
x_d	Distance from wall to supply opening
x_s	Distance from ceiling to supply opening
x_i	Coordinate
z	Coefficient in equation for wall jet
α	Absorptivity
α_φ	Relaxation parameter
β	Volume expansion coefficient
δ_T	Thickness of thermal boundary layer in wall jet
δ_v	Thickness of boundary layer in wall jet
ΔT_o	Positive temperature difference between supply and return, or between hot and cold surface in a cavity
ε	Emissivity
ϵ	Dissipation
η	Coordinate in wall jet
$\varkappa$	Heat transfer coefficient
λ	Thermal conductivity
μ, μ_o	Molecular viscosity
μ_t	Turbulent viscosity
ρ, ρ_o	Density
σ	Stefan-Boltzmann constant
σ_h	Turbulent Prandtl number
σ_k	Constant in turbulence model
σ_ϵ	Constant in turbulence model
φ	Variable in the difference equation representing ω, ψ, T, k or ϵ respectively

φ_{sl}	Slip value for k, T, v_1 or v_2
ψ	Stream function
ψ_m	Maximum value of stream function
ω	Vorticity

The following indices are used for turbulent variables:

$\hat{}$	Instantaneous value
$'$	Instantaneous deviation from mean value

Variables without one of these indices are mean values, for example

$$\hat{v}_i = v_i + v_i'$$

The symbol 'bar' designates mean value in connection with correlations, for example

$$\overline{v_1' v_2'}$$

Dimensionless variables are denoted by $*$, for example

$$x_i^* = \frac{x_i}{h}$$

$f( )$ is a symbol for a function.

$$\hat{T} = f(x_j, t)$$

means for example that the instantaneous temperature is a function of the coordinates x_j and the time t.

1. Introduction.

One of the aims of an air conditioning system is to produce optimal conditions for the occupants of a room. This cannot be achieved simply by supplying a given amount of fresh air and by adding or removing heat to maintain a comfortable temperature level. It is also necessary to generate homogeneons thermal conditions everywhere in the occupied zone.

Thermal conditions, that is to say distribution of velocities and temperatures, are governed by many parameters, some of which are the distribution of heat sources, the dimensions of the room, air change, and the location and dimensions of the diffuser. It is the purpose of the present investigation to predict the combined influence of these parameters.

This investigation is made by means of a small-scale modelling technique and by numerical solution of the flow equations. The small-scale modelling technique is dealt with in part 2 and the numerical prediction of the flow in part 3. The two parts may be read independently, and it should be noted that the results in part 2 are general while those in part 3 apply in cases where the flow in the main part of the room is two-dimensional.

Part 4 gives a short description of the numerical prediction of convective heat transfer in cavities.

2. Model experiments.

Small-scale modelling techniques are used for many types of flow investigations. A variety of reasons can be named for making tests with models instead of making them in full-scale, but in heating and ventilation research their appeal lies first and foremost in the advantages of working with smaller dimensions and smaller systems. In the following, for example, experiments are made with flow in a model which simulates room lengths of 1o-2o m - an experiment which can be difficult to make in full-scale rooms owing to the space required. Small size models can also be made with a very flexible geometry, as is the case here, where experiments are made with about 25 different geometrical variations of the model. It is a primary purpose of these model experiments to obtain qualitative knowledge of the air distribution which takes place in rooms of different dimensions, i.e. whether the flow is steady or unsteady, two-dimensional or three-dimensional. The diffusers and room dimensions which give steady two-dimensional flow in the main body of the room are of special interest because we shall later demonstrate a calculation procedure capable of predicting the flow in these situations.

The model experiments must also yield quantitative data such as velocity profiles and temperature profiles. These data and results from other references will be used to check the solution procedure.

The following paragraphs on model experiments begin with the development of the governing laws, i.e. the theory of similarity. Particular attention should be given to the paragraph which demonstrates the influence of thermal radiation in model experiments, paragraph 2.2.2. This is followed by the paragraphs dealing with the actual model experiments, of which paragraph 2.3 is the first. If the reader is acquainted with the complex of problems surrounding the theory of similarity or does not wish to study the subject he would do well to begin reading at paragraph 2.3.

2.1. The basic equations

A set of basic equations is of interest for many reasons. With such a set of equations it is possible to describe the laws governing model experiments, and such systems also form the basis of the numerical method for prediction of flow distribution in a room, which is described later.

In the following we shall consider the flow in a cartesian coordinate system with the coordinates x_1, x_2, x_3. The basic equations describing the flow are the equation of continuity, the equations of motion and the equation of energy. The equations are given in detail in, for example, the reference [1].

If we assume that the flow is incompressible the equation of continuity will be

$$\frac{\partial \hat{v}_i}{\partial x_i} = 0 \qquad (2.1\text{-}1)$$

where $\hat{v}_i$ is the instantaneous velocity in direction x_i. All equations are written in abbreviated form according to the summation convention, where the subscript i takes the values 1, 2 and 3. In a case like this where the same subscript is repeated a summation over i is implied.

The equations of motion - also called the Navier Stokes equations - describe the balance of the forces in the three coordinate directions. If we assume that the flow is incompressible, the three equations of motion will be

$$\rho \left(\frac{\partial \hat{v}_i}{\partial t} + \hat{v}_j \frac{\partial \hat{v}_i}{\partial x_j} \right) = \rho g_i - \frac{\partial \hat{p}}{\partial x_i} + \mu \frac{\partial^2 \hat{v}_i}{\partial x_j \partial x_j} \qquad (2.1\text{-}2)$$

ρ is the density and μ the molecular viscosity. The instantaneous pressure is $\hat{p}$ and the gravitational acceleration is g_i.

The subscript i takes the values 1, 2, and 3 and describes three equations in three directions, and the subscript j is summed up in the single equations. The density ρ and viscosity μ are, in principle, functions of the instantaneous temperature $\hat{T}$. With the temperature differences that occur in practice this effect can be ignored except for the gravitational term ρg_i, see for example Rubel and Landis [30]. This assumption is called the Boussinesq approximation.

The dependence of density on temperature is expressed by an equation of state.

$$\rho = \rho_o - \rho_o \beta (\hat{T} - T_o) \qquad (2.1\text{-}3)$$

where ρ_o and T_o are reference values and β is the coefficient of thermal expansion.

If we apply the Boussinesq approximation and equation (2.1-3) to the equations (2.1-2) we get

$$\rho_o \left(\frac{\partial \hat{v}_i}{\partial t} + \hat{v}_j \frac{\partial \hat{v}_i}{\partial x_j} \right) = -\rho_o \beta g_i (\hat{T} - T_o) - \frac{\partial \hat{p}}{\partial x_i}$$

$$+ \mu_o \frac{\partial^2 \hat{v}_i}{\partial x_j \partial x_j} \qquad (2.1\text{-}4)$$

assuming that the hydrostatic term $\rho_o g_i$ is ignored. $\rho_o \beta g_i (\hat{T} - T_o)$ is the variation in the gravity as a function of the temperature, that is to say buoyancy.

The last equation in the set of basic equations is the energy equation, which expresses the energy conservation at a point. Energy is, in principle, the sum of internal energy, kinetic energy and potential energy. However, the last two can be ignored in our application. In a later chapter we will use an equation for that part of the kinetic energy which is connected with the turbulent eddies; not because they contain significant amounts of energy but because the transport of turbulent kinetic energy is important in connection with the description of turbulence.

The velocities are so low that we may consider the flow incompressible and ignore the energy produced by friction, viscous dissipation, and thus the energy equation remains

$$\rho_o c_p \left(\frac{\partial \hat{T}}{\partial t} + \hat{v}_j \frac{\partial \hat{T}}{\partial x_j} \right) = \lambda \frac{\partial^2 \hat{T}}{\partial x_j \partial x_j} \qquad (2.1\text{-}5)$$

Specific heat c_p and thermal conductivity λ are assumed to be uniform according to the Boussinesq approximation.

We have now set up a system of equations which gives a complete description of the flow in an area. It consists of the equation of continuity (2.1-1), three equations of motion (2.1-4) and the energy equation (2.1-5), and contains the five unknowns $\hat{v}_1$, $\hat{v}_2$, $\hat{v}_3$, $\hat{p}$ and $\hat{T}$.

It must be emphasized that the variables referred to are instantaneous velocity, pressure and temperature, and that in derivation of the equations nothing has been said about the type of flow. The set of equations describes every situation, regardless of whether it is steady, unsteady, turbulent or laminar.

A system consisting of differential equations is fully described when the boundary conditions, i.e. the values along the boundary of the area of integration, are known. The boundary conditions for the velocity are, in a diffuser, a velocity profile of the type

$$\hat{v}_i = f(x_j, t) \qquad (2.1\text{-}6)$$

The boundary conditions for the velocity on a surface are

$$\hat{v}_i = 0 \qquad (2.1\text{-}7)$$

The boundary conditions for the temperature are, in a diffuser and along surfaces, of the type

$$\hat{T} = f(x_j, t) \qquad (2.1\text{-}8)$$

The differential equations may have gradients as boundary conditions at some parts of the boundary. For example, a return opening may be described as follows

$$\frac{\partial v_1}{\partial x_1} = 0 \qquad (2.1\text{-}9)$$

$$\frac{\partial T}{\partial x_1} = 0 \qquad (2.1\text{-}10)$$

where v_1 and T are mean values, assuming flow parallel to the walls in the return opening.

The temperature at a surface may have a boundary condition of the type

$$\left(\frac{\partial \hat{t}}{\partial n}\right)_{n=0} = \text{const.} \qquad (2.1\text{-}11)$$

where n is normal for the surface ,and the heat flow to or from the surface is constant. The description of boundary conditions will be more complicated when thermal radiation is involved. This question will be dealt with in paragraph 2.2.2.

2.2. Principle of similarity.

2.2.1. Dimensionless equations

We shall demonstrate how it is possible, by means of dimensionless equations to evaluate rules which have to be observed when making a model experiment.

The following parameters are selected in order to characterize the situation in an air conditioned room: Diffuser velocity V_o, height of diffuser h, supply temperature T_o, and the positive temperature difference between supply and return ΔT_o.

It should be noticed that the height of the room H or its hydraulic diameter may be used as a reference length in other papers on the subject.

The set of basic equations is made dimensionless by introducing the dimensionless variables

$$x_i^* = \frac{x_i}{h} \qquad (2.2.1\text{-}1)$$

$$\hat{v}_i^* = \frac{\hat{v}_i}{V_o} \qquad (2.2.1\text{-}2)$$

$$\hat{p}^* = \frac{\hat{p}}{V_o^2 \rho_o} \qquad (2.2.1\text{-}3)$$

$$t^* = \frac{t V_o}{h} \qquad (2.2.1\text{-}4)$$

$$\hat{T}^* = \frac{\hat{T} - T_o}{\Delta T_o} \qquad (2.2.1\text{-}5)$$

These variables are introduced in the equations (2.1-1), (2.1-4) and (2.1-5), and we will thus get the following equations.

$$\frac{\partial \hat{v}_i^*}{\partial x_i^*} = 0 \qquad (2.2.1\text{-}6)$$

$$\frac{\partial \hat{v}_i^*}{\partial t^*} + \hat{v}_j^* \frac{\partial \hat{v}_i^*}{\partial x_j^*} = - \frac{\beta g_i h \Delta T_o}{V_o^2} \hat{T}^*$$

$$- \frac{\partial \hat{p}^*}{\partial x_i^*} + \frac{\mu_o}{\rho_o V_o h} \frac{\partial^2 \hat{v}_i^*}{\partial x_j^* \partial x_j^*} \qquad (2.2.1\text{-}7)$$

$$\frac{\partial \hat{T}^*}{\partial t^*} + \hat{v}_j^* \frac{\partial \hat{T}^*}{\partial x_j^*} =$$

$$\frac{\lambda}{c_p \rho_o V_o h} \frac{\partial^2 \hat{T}^*}{\partial x_j^* \partial x_j^*} \qquad (2.2.1\text{-}8)$$

It will be seen that the solution of the set of equations is dependent on some dimensionless numbers comprising physical constants of the fluid, and reference values of the problem.

$$Ar = \frac{\beta g_2 h \Delta T_o}{V_o^2} \qquad (2.2.1\text{-}9)$$

$$\frac{1}{Re} = \frac{\mu_o}{\rho_o V_o h} \qquad (2.2.1\text{-}10)$$

$$\frac{1}{Pr\ Re} = \frac{\lambda}{c_p \rho_o V_o h} \qquad (2.2.1\text{-}11)$$

where Ar is the Archimedes number, Re is the Reynolds number, and Pr is the Prandtl number. It is assumed that the gravity acts in the positive direction of the x_2-axis.

The use of the Archimedes number is common in air conditioning references, while in fluid dynamics it is often written as.

$$Ar = \frac{Gr}{Re^2} \qquad (2.2.1\text{-}12)$$

where Gr is the Grashof number.

By means of fig. 2.2.1-1 we can now specify the conditions to be fulfilled when a model experiment is to be made. The figure shows a section of a room and a section of a geometrically similar model.

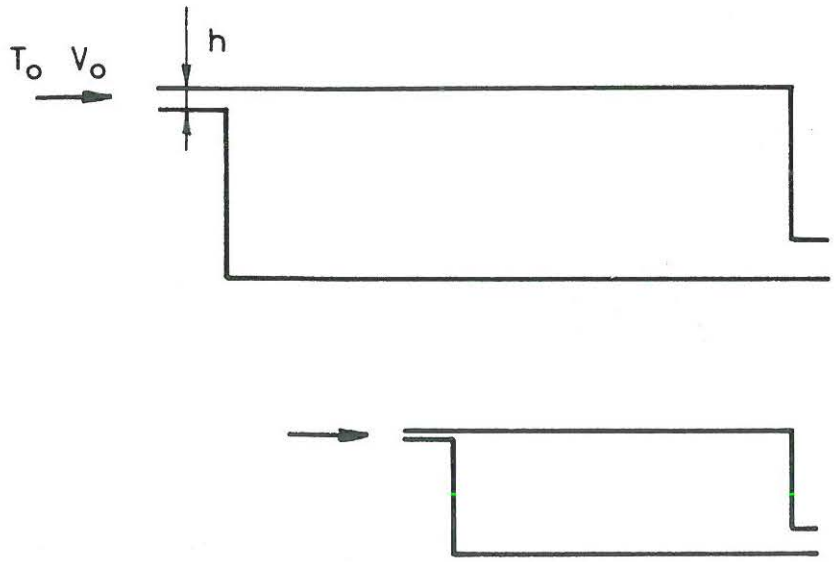

Fig. 2.2.1-1. Section of a room and section of a geometrically similar model. The reference variables are shown on the figure.

The basic flow equations of the form (2.1-1), (2.1-4), and (2.1-5) as well as the boundary conditions (2.1-6) to (2.1-1o) are set up for room and model respectively. After this, we make the two sets of equations and the boundary conditions dimensionless by introducing the variables (2.2.1-1) to (2.2.1-5) into the equations. These variables contain reference values from the full size room and from the model respectively. For example, the velocity in a room is described dimensionless by dividing with the diffuser velocity in the room, and the velocity in the model is described dimensionless by dividing with the supply velocity in the model.

The two sets of equations will now have the form (2.2.1-6), (2.2.1-7) and (2.2.1-8), and it will be seen that they are identical and thus describe the same solution, provided that:

1. the dimensionless boundary conditions, including geometry, are identical

2. the dimensionless numbers in the equations (2.2.1-9), (2.2.1-1o) and (2.2.1-11) are identical, i.e. the Archimedes number, the Reynolds number and the Prandtl number are the same for room and model.

2.2.2. Heat flow at surfaces.

Item 1 of the principle of similarity requires that boundary conditions for the temperature must be indentical in room and model. How, then is it possible to establish the correct boundary conditions in a model ?

The influence of a surface can in certain situations be described thus: The surface has a given temperature or temperature distribution, as is the case, for example, with heat loss through a window if the outdoor temperature is low. The boundary condition is of the type (2.1-8), and it is easy to establish. If the dimensionless surface temperature in a room is known according to equation (2.2.1-5), the surface

temperature in the model is determined so that it gives the same dimensionless temperature. Thermal radiation between surfaces will not affect the model test, if all surfaces are kept at given temperatures, i.e. boundary conditions of the type (2.1-8).

However, the boundary conditions for the temperature are generally more complicated. Distribution of the surface temperature is dependent on radiation between the different surfaces, and it is dependent on the local heat flow to or from the surface and also on the local coefficient of heat transfer. This we will examine by setting up an equation for the heat balance for a surface element dA. This equation is rendered dimensionless in the same way as previous equations, and the dimensionless numbers thus obtained, are evaluated.

When forming the heat balance equation it is reasonable to ignore the heat capacity owing to the large time constant of the surface material in relation to the turbulent eddies. Situations where the time dependent changes of temperature are so great that the time constant of the building structures is significant - for example daily variation of sun gain and outdoor temperature - are not included in this analysis because in practice model experiments are only made for steady conditions.

Fig. 2.2.2-1 shows the surface element dA with the normal n. The surface element is exposed to radiation from the surrounding body with the instantaneous mean radiant temperature $\hat{T}_{ms}$, and the heat flow to the surface element is qdA.

The heat balance per unit area of the surface element is

$$\alpha \sigma \hat{T}_{ms}^4 + q = -\lambda \left(\frac{\partial \hat{T}}{\partial n}\right)_{n=0} + \varepsilon \sigma \hat{T}_{dA}^4 \qquad (2.2.2\text{-}1)$$

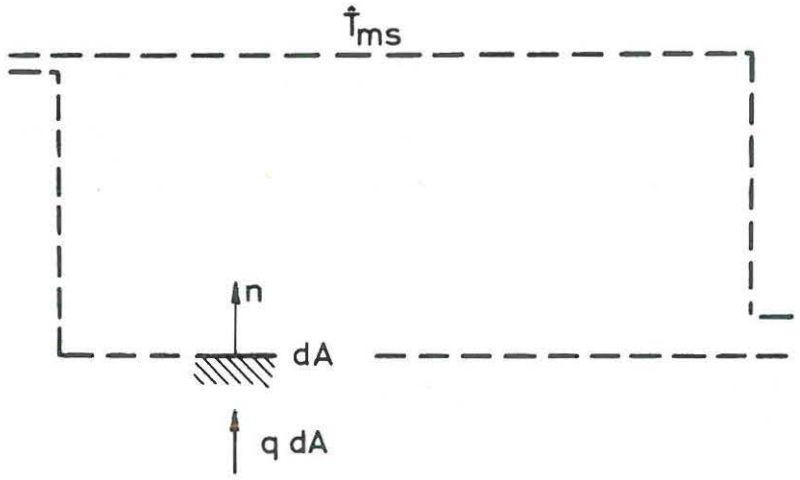

Fig. 2.2.2-1. Surface element and surroundings.

The first term in the equation is the thermal radiation received from the surroundings, while the second term is the heat flow to the surface. The first term on the right hand side is the conductive heat flow and the second term is the thermal radiation emitted from the surface. The thermal radiation is written as a product of the absorptivity α or the emissivity ε multiplied by the Stefan-Boltzmann's constant σ and by the mean radiant temperature $\hat{T}_{ms}$ to the fourth power or the instantaneous temperature T_{dA} of the surface element to the fourth power respectively.

The absorptivity α and the emissivity ε are in practice identical, because the received and emitted radiation is of the same wavelength distribution, 3.5 - 4o μm. Short wave sun radiation is ignored. Equation (2.2.2-1) can thus be written

$$q = -\lambda \left(\frac{\partial \hat{T}}{\partial n}\right)_{n=0} + \varepsilon \sigma (\hat{T}_{dA}^4 - \hat{T}_{ms}^4) \qquad (2.2.2\text{-}2)$$

When temperature differences are moderate we can linearize the term $(\hat{T}_{dA}^4 - \hat{T}_{ms}^4)$ and make the equation dimensionless by means of formulas (2.2.1-1) and (2.2.1-5).

$$\frac{q\,h}{\Delta T_o \lambda} = -\left(\frac{\partial \hat{T}^*}{\partial n^*}\right)_{n^*=0} + \frac{4\,\varepsilon\,\sigma\,T_o^3\,h}{\lambda}\,(\hat{T}_{dA}^* - \hat{T}_{ms}^*) \qquad (2.2.2\text{-}3)$$

Equation (2.2.2-3) contains two dimensionless numbers which must be identical for a surface element in a room and for a surface element placed in a similar position in a model.

We will first discuss the situation where radiation to and from the surface is negligible. This is the case when the air passing the surface has a high velocity or when the emissivity of the surface is small. Equation (2.2.2-3) now expresses that the dimensionless temperature gradient at the surface is equal to

$$-\frac{q\,h}{\Delta T_o\,\lambda} \qquad (2.2.2\text{-}4)$$

The condition that the same dimensionless temperature gradient should be present in room and model is now fulfilled by distributing the heat flux q in the model according to (2.2.2-4) in such a way that this number is identical in room and model at the same locations.

Let us now discuss the case where radiation is significant. The number

$$\frac{4\,\varepsilon\,\sigma\,T_o^3\,h}{\lambda} \qquad (2.2.2\text{-}5)$$

must be identical in room and model. The emissivity is 0.9 for common surfaces in a room by longwave thermal radiation. It is therefore not possible to raise this coefficient considerably in the model. T_o measured in Kelvin, is of the same magnitude in room and model.

We now see that it is not possible to make the dimensionless number (2.2.2-5) identical in room and model if we are working with air in the model.

The number will, in the model, be smaller according to the geometrical relation between model and room. This means that it is not possible when making model experiments with air to reproduce the influence of radiation in a room.

If the model experiment is made with water the influence of radiation has to be ignored, because water is opaque to long-wave thermal radiation.

When a model experiment is to be made in a situation where radiation is significant the only possibility in practice is to give the model a dimensionless temperature distribution which accords with the distribution which can be foreseen in a room under the combined influence of radiation, convection and conduction to and from the surfaces.

2.2.3. Practical use of the similarity principle.

In this paragraph we shall examine some examples of the use of the similarity principle and show how we can, in certain situations, reduce the requirements.

First let us consider the situation where the velocities in a room are high and the temperature differences are small. The forced convection is dominant compared with the free convection. This corresponds to the situation that the buoyancy terms in the equations (2.1-4) are becomming small compared to the other terms. We can in this situation ignore the buoyancy and the Archimedes number will not appear in the dimensionless equations. It is not important to the model experiment.

In the following example we assume that the Archimedes number is of a size such that the buoyancy shall be taken into consideration. We also assume that full consideration is given to the similarity principle, i.e. the following three dimensionless numbers must be identical in the room and in the model

$$Pr = \frac{\mu_o c_p}{\lambda} \qquad (2.2.3\text{-}1)$$

$$Re = \frac{V_o h \rho_o}{\mu_o} \qquad (2.2.3\text{-}2)$$

$$Ar = \frac{\beta g_2 h \Delta T_o}{V_o^2} \qquad (2.2.3\text{-}3)$$

The model experiment is made in air, so in this way the same Prandtl number is secured in room and model.

The factor by which the room is bigger than the model is called M, which means that the model is manufactured in the scale 1/M. The requirement that the same Reynolds number shall apply in room and model means that the velocity in the model increases with the factor M, because the height of the supply opening h is M times as small. The supply opening in the model is M times as small and the square of the supply velocity is M^2 times as big as in the room. Therefore the Archimedes number requires that ΔT_o in the model shall be M^3 times as big as in the room. We see that the temperatures in the model will reach very high values if the scale 1/M is to be reduced significantly.

If the model experiment is only to predict the general stream line pattern, which is mainly governed by free turbulence, it is possible to ignore the Reynolds number and the Prandtl number.

This simplification is possible because the structure of the turbulence at a sufficiently high level of velocity will be similar at different supply velocities and therefore independent of the Reynolds number. Likewise the transport of thermal energy by turbulent eddies will dominate the molecular diffusion and will therefore be independent of the Prandtl number.

Turbulent free jets and wall jets are examples of flows which can be similar at different Reynolds numbers and Prandtl numbers, see Schwarz and Cosart [32] and Schmidt [31]. Müllejans [25] has also shown how the general stream line pattern in a series of model tests was similar at different Reynolds numbers and only dependent on buoyancy and, with it, the Archimedes number.

There is a big advantage to be gained in ignoring the Reynolds number. In the example it was shown that the temperature difference in the model was M^3 times greater than in the room. If we ignore the Reynolds number it is possible to lower the velocity in the model to a value at which the flow is still suitably turbulent. The lower velocity will give a smaller denominator in the Archimedes number (2.2.3-3) and therefore also a lower temperature difference ΔT_o in the model. However, it is not possible to ignore the Reynolds number or Prandtl number if it is the heat transfer from the surface which is to be studied in the model experiment. The viscosity and molecular diffusion will always be important close to a surface

When a model experiment is made with water as fluid it is necessary to ignore the Prandtl number, because water at normal temperature and pressure has a Prandtl number which is 10 times greater than the Prandtl number for air.

2.3. Test set up.

This paragraph deals with the construction of a model and the necessary measuring equipment. The model works with air as experimental fluid and it has given the results discussed in paragraphs 2.4. and 2.5.

Fig. 2.3-1 shows a sketch of model and measuring equipment. The model (1) comprises a box with a length of 1.8o m, a width of o,6o m and a height of o.6o m. It is made of wooden frames, of which the bottom and both ends are coated with hard masonite and insulated with polystyrole. The side walls are double glazed, and the top of the model is of plexiglass with loose insulation in sections. By means of a light box (2) a beam of light can be applied at different places in the model and the stream line pattern in the model can be observed.

Air is sucked in through the box (3) and the nozzle (4). The nozzle ends in a supply opening (5), which is aligned with the top of the model and has a height of 7.2 mm. The inlet opening follows the whole width of the model and is divided up into 5 sections. They can be closed independently if it is wished to examine the flow in situations where the inlet opening only covers part of the width of the model.

The air leaves the model via a return opening (6) and is led to the blowers (7). By placing the blowers after the model, the risk of upsetting the measurements in the model by heat emitted from the blowers is avoided.

Inside the model is fitted an extra floor section (9) and an end wall (1o). We can thus examine various geometrical situations by varying the length and the heigth of this sub-model, and the width can be varied by placing a couple of plexiglass walls parallel with the side walls.

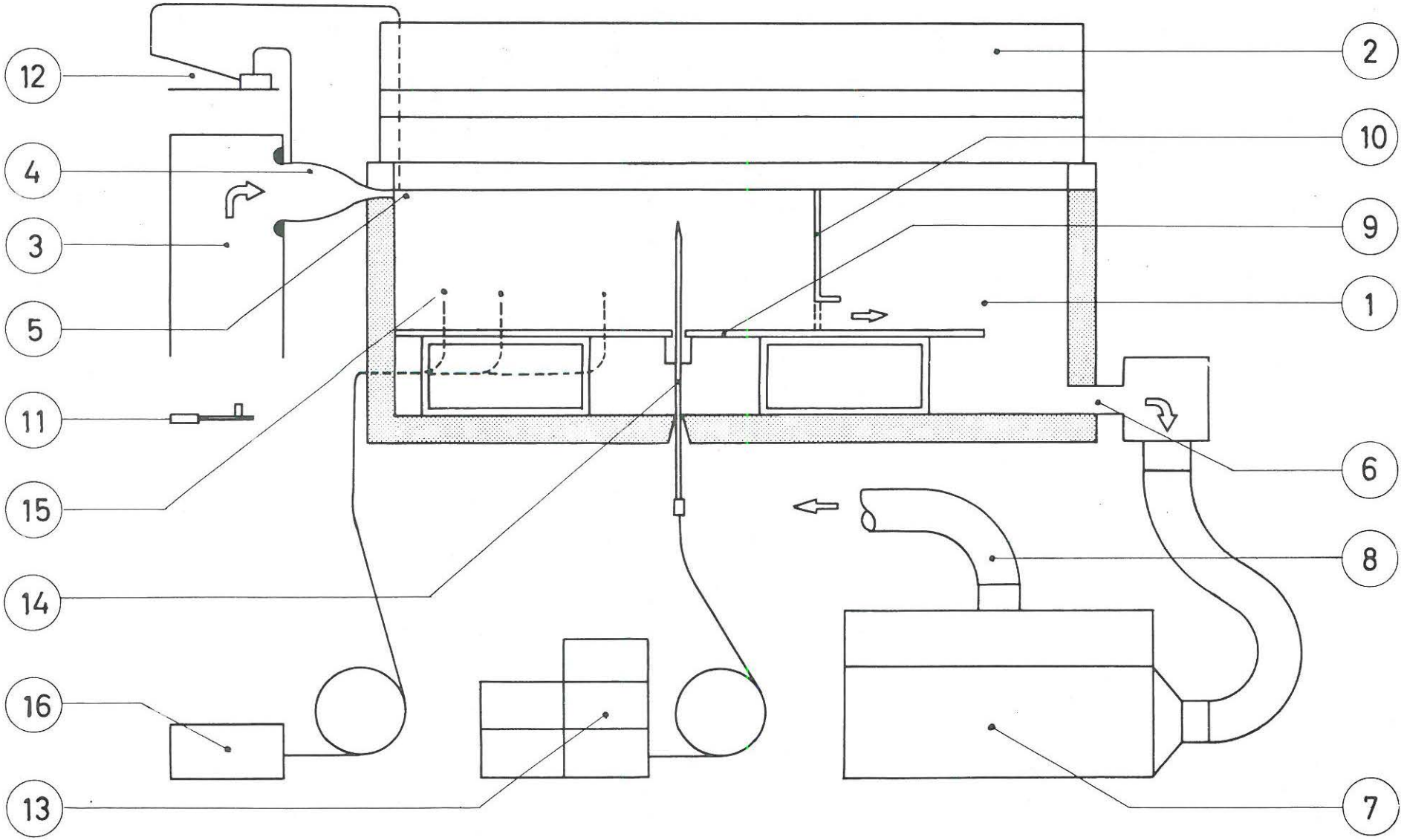

Fig. 2.3-1. Test set up with model and measuring equipment.

The model is designed for three types of experiments:

1. Measurement of stream line pattern
2. Measurement of a vertical velocity and turbulence profile
3. Measurement of temperature distribution.

The stream line pattern is measured by introducing light weight particles to the air, which are illuminated and photographed or filmed. The particles used are metaldehyde particles. These particles have a very big and crystal-like structure, which gives them high drag in proportion to their weight. The settling speed of the particles is so low that it is negligible even in experiments at very low velocities such as full scale experiments with free convection, see Daws et al.[6] .

The particles are formed by heating metaldehyde*) on a hot surface, in this case a soldering iron (11). When metaldehyde is heated a poisonous gas is produced and therefore the model is equipped with a box (3) so that all gas is led through the model and out into the free air (8).

The particles are illuminated in a section by means of a looo W halogen lamp (2) and are photographed or filmed through the side wall. By taking pictures with different exposure times it is possible to determine the stream line pattern and also make a qualitative evaluation of the mean velocity and turbulence.

The supply velocity is determined by measuring the pressure drop across the nozzle (4) by means of a micromanometer (12). The nozzle (4) has a contraction of 2o:1 and its shape is determined according to a method described by Libby and Reiss [18] .

---

*) META, Lonza A.G., Basel

Test measurements show that in practice the nozzle gives a friction free flow and it therefore creates an almost rectangular velocity profile in the supply opening. This velocity profile is a welldefined boundary condition for a model experiment and it is easy to repeat in other tests.

The vertical velocity profile in the model is measured with a DISA CTA-anemometer type 55D01 (13) and (14). The signal is linearized with a DISA linearizer type 55D10 and the mean value as well as the root-mean-square value is measured.

The anemometer is calibrated before and after a set of measurements in a known, uniform velocity core from a free jet. This free jet has the same temperature as the air in the model.

A DISA CTA-anemometer type 55K01 is used in some new measurements made in 1976.

For temperature experiments heat is supplied along the bottom of the model. The heat is generated by an ESWA electric heating film which is mounted on the surface (9) and is supplied via a variable transformer. Surface temperatures and the temperatures in the flow are measured by o.2 mm copper-constantan thermocouples (15), and the temperatures are recorded on a pen recorder (16).

2.4. Isothermal model experiments.

2.4.1. Parameters of the model experiments.

A model experiment in air with isothermal flow is fully characterized by the Reynolds number and by the geometry of the model, see paragraph 2.2.3. The geometry for all the experiments made, can be expressed by the dimensions given on fig. 2.4.1-1. H is the height of the model, L is its length or depth, and W is its width. h is the height of the supply opening and w is the width. u is the height of the return opening.

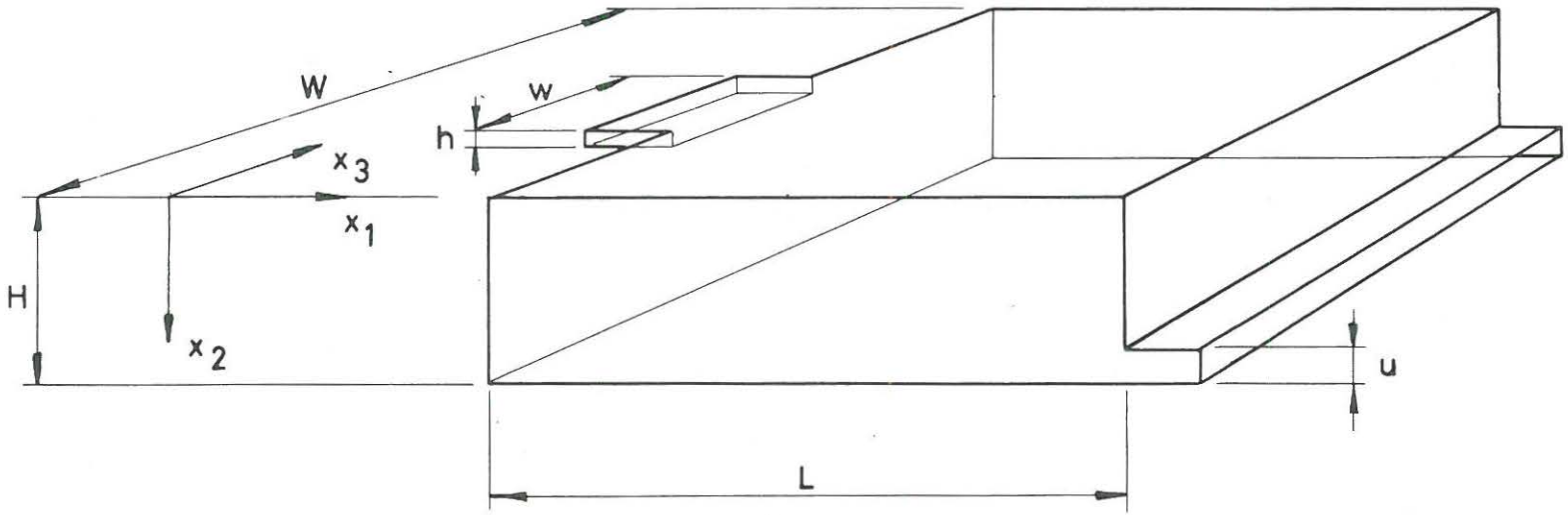

Fig. 2.4.1-1. Definition of geometry and coordinates in the model.

All the geometrical parameters are expressed in the following dimensionless ratios

h/H, L/H, W/H, u/H and w/W

Fig. 2.4.1-1 also shows the location of the coordinate axis. The coordinate system is placed with its centre in the upper left corner of the model, and all distances in the model are expressed in the dimensionless coordinates

x_1/H, x_2/H and x_3/W.

2.4.2. Flow in models with big depths.

This paragraph examines the results of a series of tests in which the depth L/H of the model is so great that the flow is not influenced by the end wall.

The results simulate a deep room and, of course, also rooms where the "effective" value of L/H is high. This may be the case in, for example, a storage room filled with goods and consequently having a small "effective" height H.

A jet will have a limited penetration into the model. Entrainment in the jet means that air must be led back along the bottom of the model and at a given distance this air will disperse or deflect the jet.

We define the penetration l_{re} as the distance from the wall with the supply opening to the point in the bottom of the model where the stream lines diverge :- reattachment point, see fig. 2.4.2-1 at the top. The penetration l_{re} must not be confused with the throw. The throw is, in the case of isothermal flow, a variable describing the velocities in a room, and it is defined as the length from the diffuser to a point with a given velocity (e.g. 25 cm/s) in a wall jet or free jet.

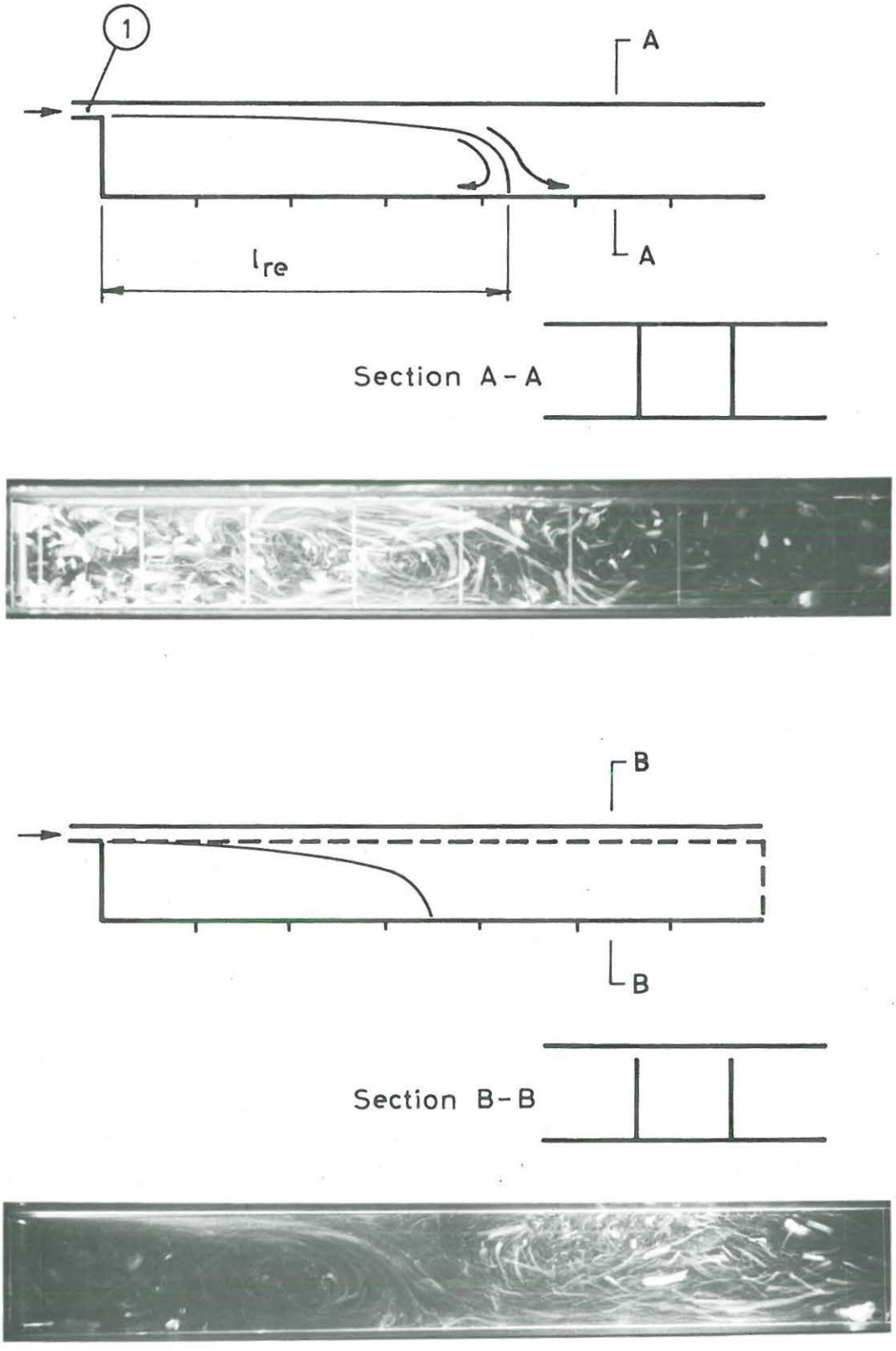

Fig. 2.4.2-1. Flow in model with big depth.
The upper picture shows the result for the pressure tight setup and the lower picture shows the result for the setup where the side walls are as high as the lower edge of the nozzle. h/H = 0.056, w/W = 1.0, W/H = 1.0 and Re = 4700.

At distances from the supply opening which are greater than the penetration the velocity is very low, since the injected air is distributed over the whole area, while at distances which are less than the penetration the velocities are very high, because big volumes of air are set in motion by the injected jet. The penetration is therefore an important parameter in the discussion of room air distribution.

Fig. 2.4.2-1 shows the two different setups resulting in two different penetration depths. They both have the following dimensions

$$h/H = 0.056$$
$$w/W = 1.0$$
$$W/H = 1.0$$

In the upper setup the side walls are made in such a way that they form a pressure-tight seal against the floor and ceiling. The side walls are also extended into the nozzle itself by means of two spacers, see point (1) on the figure.

The experiments show a penetration depth of $l_{re}/H \sim 4.3$, independent of the Reynolds number from Re = 4700 to Re = 9400.

In the lower setup on fig. 2.4.2-1 the side walls are as high as the lower edge of the nozzle. In this instance the experiments show that the penetration depth will be $l_{re}/H \sim 3.4$ at Reynolds numbers from 2900 to 9300. It will thus be seen that the penetration depth is greatly dependent on minor details in the construction of the model, and the latter result cannot be regarded as characteristic of a closed room.

Urbach [34] has with the aid of smoke visualization found a penetration at about 3.0 for values of h/H between 0.1 and 0.02 and Reynolds numbers between 3500 and 12000. The width of the model was W/H = 1.0.

Katz [14] has measured the penetration depth in models built up in an open water channel. He has found the penetration depth l_{re}/H between 3 and 4.5. His experiments show that the penetration depth is to some extent dependent on the location of the end wall. He explains this as a tendency of the water to form circular movements between the end wall and the point of reattachment so that this distance becomes a multiple of H. The models used for the experiments had a small width W/H.

It will be seen that there is some difference between the penetration depth in the various experiments referred to. This is probably due to the influence of the supply opening itself and the contraction formed before this opening.

A completely new situation arises when we extend the width W/H of the model. On fig. 2.4.2-2 the geometry is specified as follows

$$h/H = 0.056$$
$$w/W = 1.0$$
$$W/H = 4.7$$

The two pictures on the figure show two instantaneous situations of the flow which occur. From the top picture we see that the illuminated part of the jet penetrates deep into the model. The jet entrains air from part of the jet outside the illuminated area, i.e. there occurs a instantaneous flow in the x_3 direction. A moment later it is the jet under the light opening which deflects in the direction of the x_3 axis, entrained by the jet beside it, as is evident from the bottom picture. Unsteady flow conditions are in evidence throughout the examined velocity ranges from Reynolds number 2000 to 10000.

The tests were repeated with a supply opening having an h/H dimension of 0.025. This did not bring about any change in the flow, which remained unsteady throughout the examined velocity ranges.

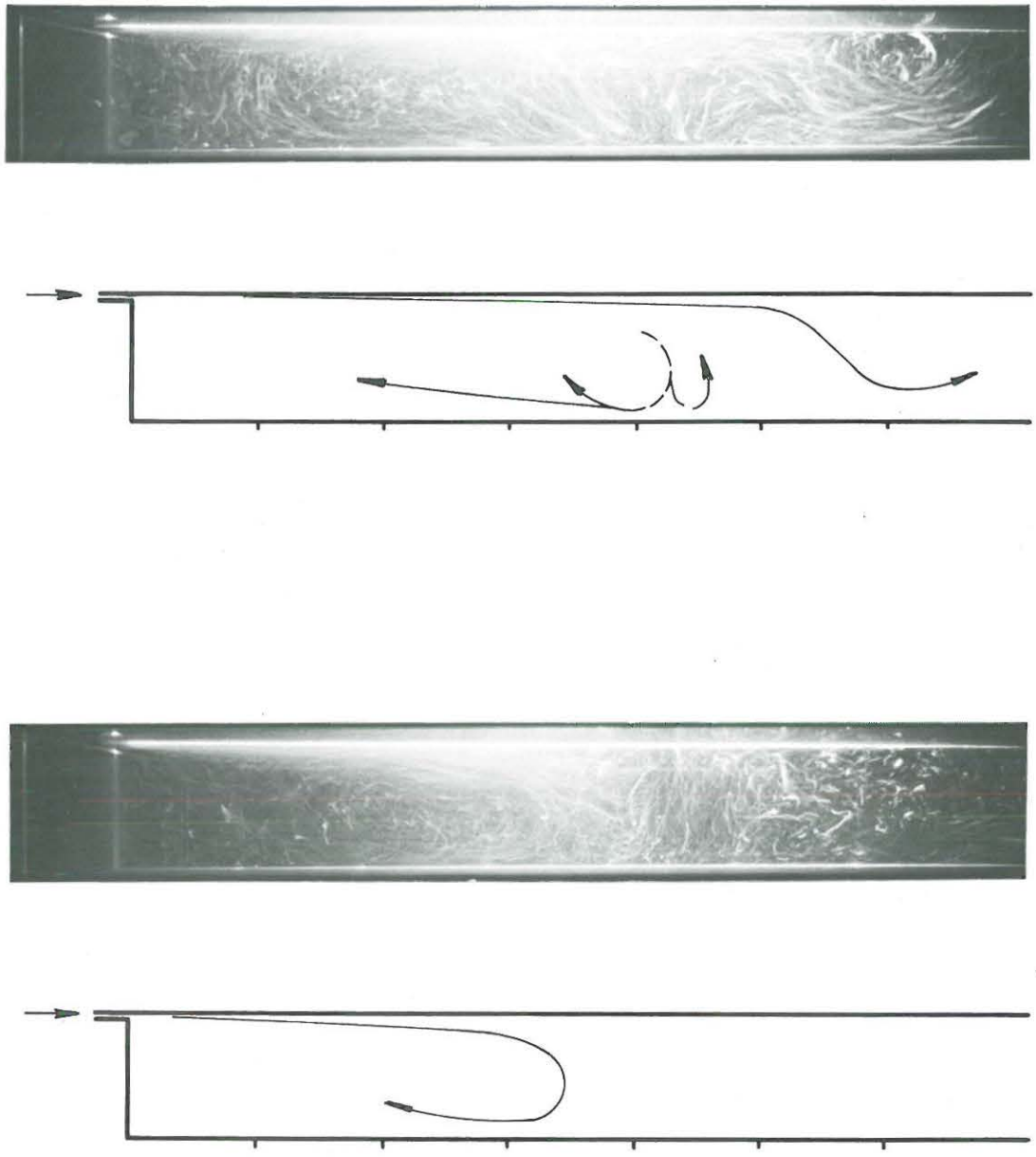

Fig. 2.4.2-2. Unsteady flow in a model of great depth. h/H = o.o56, w/W = 1.o, W/H = 4.7 and Re = 98oo.

The big width of the model makes unsteady flow possible and must therefore be considered an important parameter. No systematic determination of the influence of the width has been carried out, though it has been observed that with a width of W/H = 3 the flow is still unsteady.

The different forms of flow occuring in fig. 2.4.2-1 and in fig. 2.4.2-2 as the result of varying widths show that care must be displayed when making model tests or full scale tests which only represent a part of the room. As we have seen, it cannot be concluded that two-dimensional boundary conditions give two-dimensional flow. Later we shall see that boundary conditions that are symmetrical to a plane do not necessarily give a symmetrical flow.

Förthmann [9] has measured the velocity profiles in a deep model having the dimensions h/H = o.17 and W/H = 3.6. He has apparently not observed any unsteady flow. He has calculated the stream line distribution on the basis of the measured velocity profiles and finds a penetration depth l_{re}/H of 5.3.

In the next series of tests the width W/H is still 4.7 but an attempt has been made to damp the unsteady flow by means of longitudinal fins placed in the main flow direction having the height H/2. At the top of fig. 2.4.2-3 can be seen a sectional view in the direction of the x_3 axis showing the location of the fins. The flow will be partly two-dimensional because the injected jet is not disturbed by the side walls and because transverse unsteady flow is prevented by the fins.

Fig. 2.4.2-3 shows the stream line pattern at three different Reynolds numbers. An examination of photos shows that the average penetration l_{re}/H is 4.o to 4.5 for h/H = o.o56 and that the flow oscillates somewhat in the area of the reattachment point. The penetration is independent of Reynolds numbers in the range examined from 24oo to 93oo.

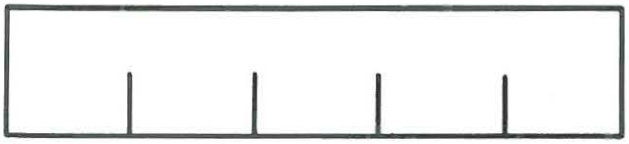

Re = 2300

Re = 4600

Re = 6300

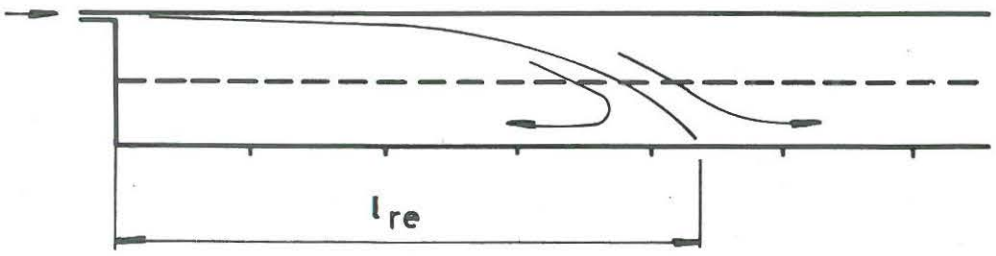

Fig. 2.4.2-3. Flow in model with great depth and longitudinal fins. h/H = 0.056, w/W = 1.0 and W/H = 4.7.

The last series of tests with a deep model concerns cases where the width of the supply opening is only part of the width of the model. The geometry is specified by the following dimensions

$$h/H = 0.025$$
$$w/W = 0.2$$
$$W/H = 4.7$$

At the top of fig. 2.4.2-4 will be seen a drawing of the flow which now occurs. The drawing shows the model from above. The injected air will after some distance stick to one side of the model owing to the Coanda-effect. With this deflection of the jet the vertical velocity gradient in the first part of the jet will be deflected onto a horizontal plane deeper in the model. This effect has two consequences of practical importance to room air distribution: Firstly, the primary jet will reach the bottom and therefore give rise to a rather high velocity in the area corresponding to the occupation zone. Secondly, the air which is entrained with the injected jet will return on the opposite side of the model, thus creating a quite rapid rotating movement below the supply opening. This flow is represented by the dotted line on fig. 2.4.2-4, and it runs in what corresponds to the occupied zone in a room.

At the start of a test the injected jet may tend to stick to either side, but once the flow is established it is completely steady and similar at the different Reynolds numbers throughout the examined velocity range from Re = 2000 to Re = 4800.

The two photos on fig. 2.4.2-4 show the stream line picture at two different Reynolds numbers. The horizontal rotating motion below the supply opening is clearly marked by particles of metaldehyde accumulated in this area.

The example demonstrates that boundary conditions which are plane symmetrically do not always result in a symmetrical flow.

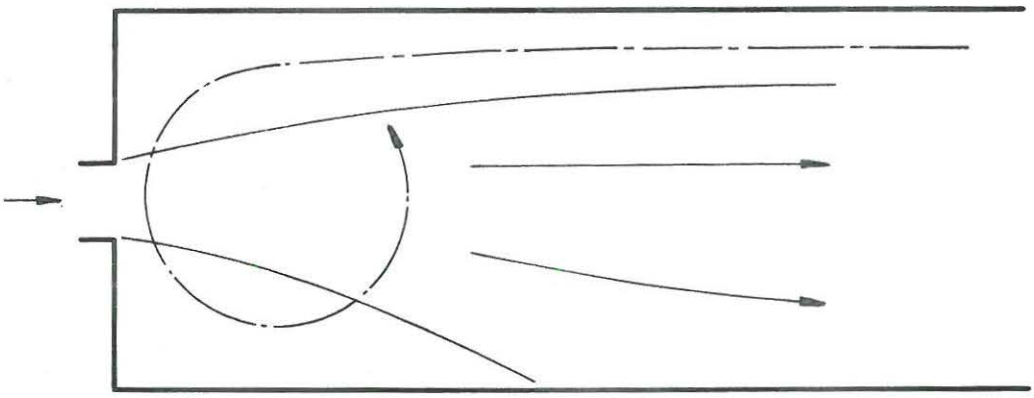

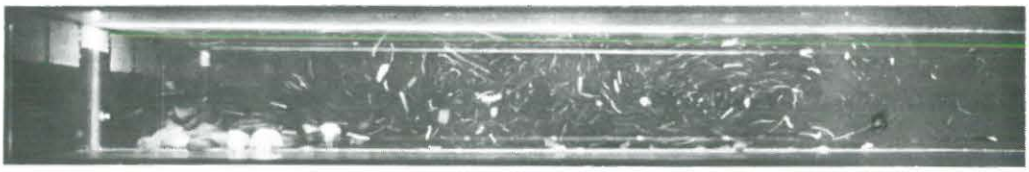

Re = 3200

Re = 4400

Fig. 2.4.2-4. Flow in model with big depth and small width of supply opening. h/H = o.o25, w/W = o.2 and W/H = 4.7.

2.4.3. Flow in models with width W/H = 4.7 and different depths.

In this paragraph we shall examine a series of tests in which the depth has influence on the flow. The object is to limit those dimensions of the model which, qualitatively, give two-dimensional flow. All of the tests are based on the geometry shown on fig. 2.4.2-2, except that an end wall has been introduced. The geometry is specified by the following parameters

$$h/H = 0.056$$
$$w/W = 1.0$$
$$W/H = 4.7$$

and by the location of the end wall L/H which lies between 6.0 and 2.0. The height of the return opening u/H is 0.16.

Fig. 2.4.3-1 and fig. 2.4.3-2 show that the original unsteady flow in wide deep rooms is still present with lengths of respectively L/H = 6.0 and L/H = 5.0.

On fig. 2.4.3-3 we see three typical photos of the flow for L/H = 4.0. There still occurs a weak oscillation of the stream line pattern on the right side of the model, but in practice, however, we may consider the flow as steady in the main part of the model. Visual observation of the flow shows that it is two-dimensional in this area. The penetration l_{re}/H ranges from 3.7 to 3.8.

Fig. 2.4.3-4 shows a single photo of the stream line pattern for L/H = 3.0. The flow is steady and two-dimensional both in the area of high velocity on the lower right side of the model and in the area of very low velocity on the lower left side of the model.

For L/H = 2.0 the flow is still two-dimensional throughout, see fig. 2.4.3-5.

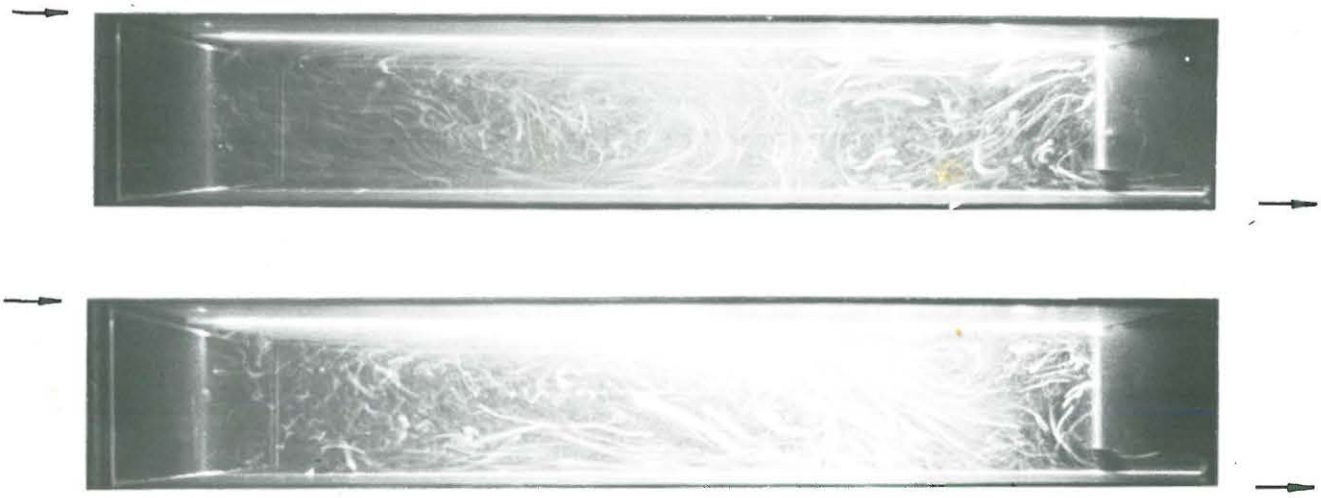

Fig. 2.4.3-1. Unsteady flow in model with length L/H = 6.o and big width. h/H = o.o56, w/W = 1.o, W/H = 4.7, u/H = o.16 and Re = 7ooo.

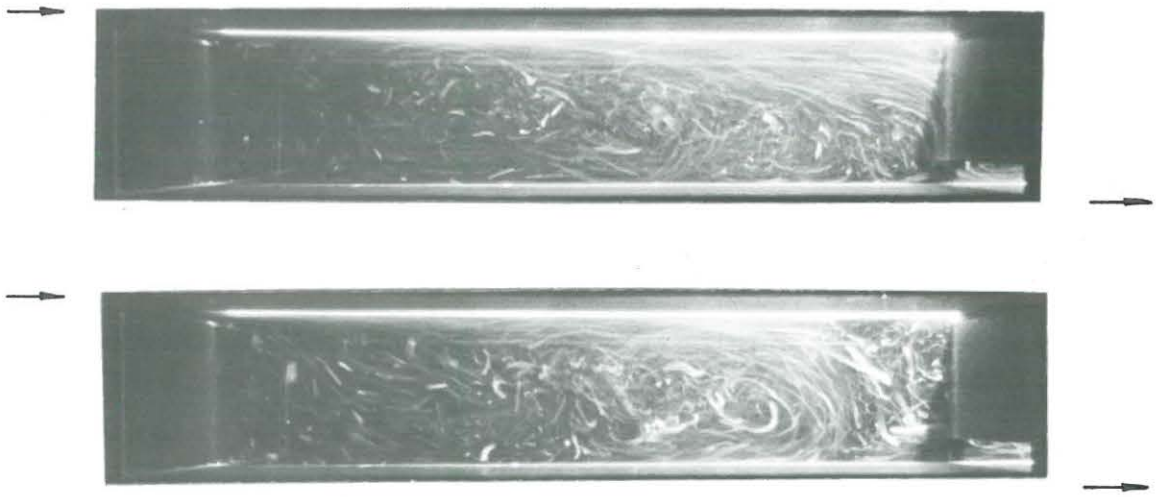

Fig. 2.4.3-2. Unsteady flow in model with length L/H = 5.o and big width. h/H = o.o56, w/W = 1.o, W/H = 4.7, u/H = o.16 and Re = 7ooo.

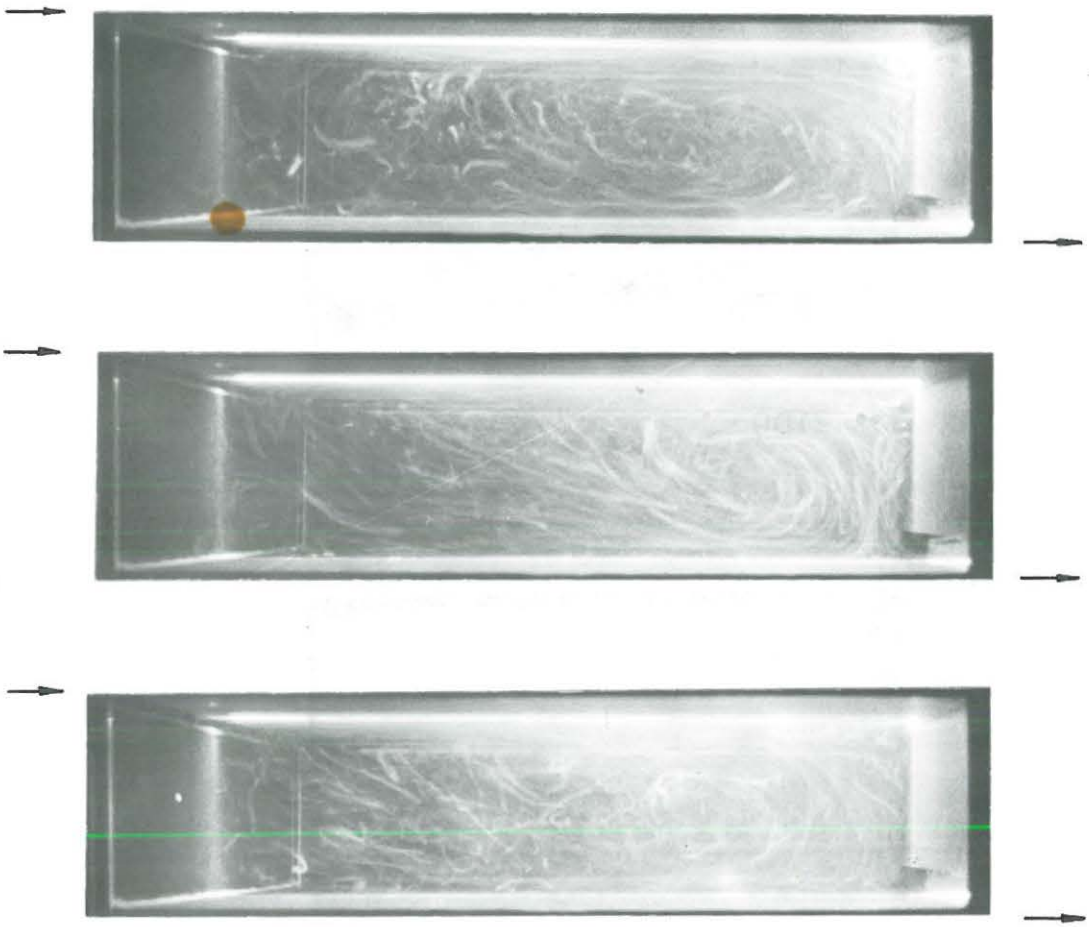

Fig. 2.4.3-3. Flow in model with length L/H = 4.o and big width. h/H = o.o56, w/W = 1.o, W/H = 4.7, u/H = o.16 and Re = 66oo.

Fig. 2.4.3-4. Flow in model with length L/H = 3.o and big width. h/H = o.o56, w/W = 1.o, W/H = 4.7 u/H = o.16 and Re = 7ooo.

Re = 2100

Re = 4500

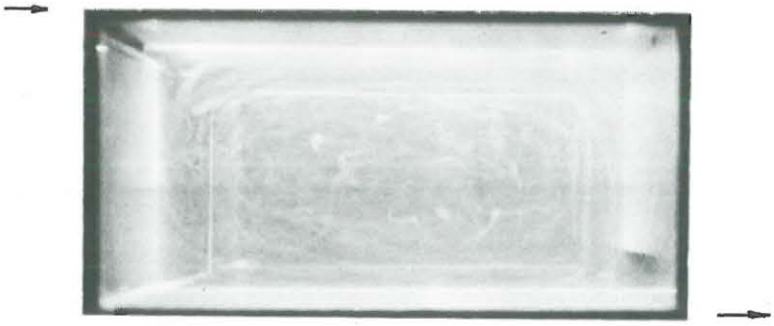

Re = 7000

Fig. 2.4.3-5. Flow in model with length L/H = 2.0 and big width. h/H = 0.056, w/W = 1.0, W/H = 4.7 and u/H = 0.16.

In the experiments discussed in this section, the supply opening has had a width equal to the width of the model, i.e. w/W is 1.o. In practice, the supply openings will often comprise a line of diffusers distributed across the width of the room. If these diffusers are placed at short distances from each other, the jets will, at a certain depth of the room, form a single, two-dimensional, wall jet. This means that the results also apply in this instance, provided that the line of single diffusers is replaced by one equivalent diffuser with w/W = 1.o, see section 3.3.1.

To exemplify what happens when there is a great distance between the diffusers, we shall examine a situation where there is only a single supply opening of the size w/W = o.2 and h/H = o.o25. The length of the model is 3.o and the width is 4.7. The height of the return opening u/H is o.16.

Fig. 2.4.3-6 shows a drawing of the flow conditions in the model as seen from above. The jet below the top of the model is a two-dimensional wall jet. When the jet reaches the end wall it is dispersed over an angle of 18o^{o} and acquires a character similar to that of a radial wall jet, where the decrease in velocity along the jet will be far greater than in the two-dimensional wall jet. The upper part of the radial jet from the end wall reaches the side walls and runs back and down these sides. This is indicated by a solid line on fig. 2.4.3-6. The bottom and middle parts of the radial jet from the end wall run down the wall where they are dispersed over the floor as illustrated by the dotted lines on the drawing. Part of this jet reaches the side walls and runs up these, meeting the downward jet in the area near the end wall. Together, the two jets run into the centre of the model. In the two corners below the diffuser a rotational upward motion occurs, the effect of which may be seen from the picture of the stream lines on fig. 2.4.3-6.

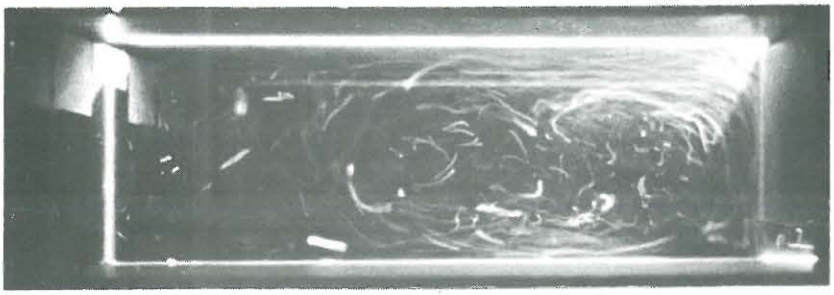

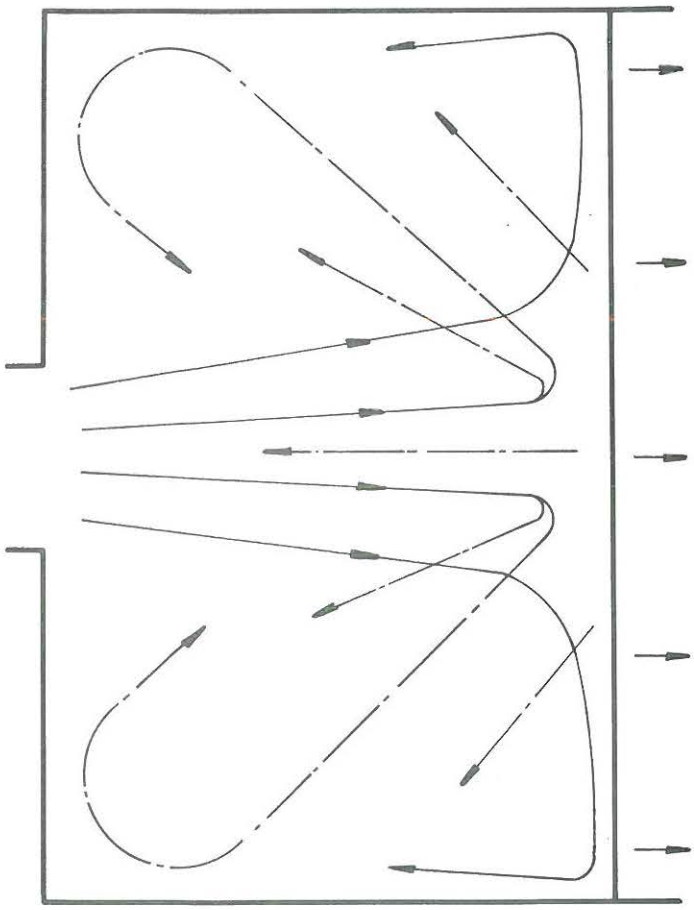

Fig. 2.4.3-6. Flow in model with the length L/H = 3.0 and a narrow supply opening. h/H = 0.025, w/W = 0.2, W/H = 4.7, u/H = 0.16 and Re = 4500.

We see that the dimensions used for the supply opening result in a complicated, three-dimensional, but steady flow. Unlike the corresponding situation in deep rooms, fig. 2.4.2-4, the flow is symmetrical around the median plane through the supply opening.

However, this is only one example of a flow which may arise in a room having one supply opening. Another work worth of mentioning is that of Malmström and Svensson [21] showing that a jet from a single circular supply opening in the median plane of a room may tend to move back and forth in front of the opposite wall.

2.4.4. Flow in models with width W/H = 1.6 and different depths.

This series of experiments is primarily characterized by a limited width in the model. Also the supply opening is smaller than in previous experiments, h/H = o.o2o. The size of the return opening is u/H = o.15.

When discussing the results it is convenient to divide the flow area into three sub areas in the model. The first area is the upper third of the model. Fig. 2.4.4-1 and fig. 2.4.4-2 show that at all lengths of model L/H = 4.9, 4.o, 3.o, 2.o and 1.o there is a flow in this area which, qualitatively, can be characterized as a two-dimensional wall jet. With the length L/H = 4.9 the flow is somewhat unsteady at the farthest point from the supply opening, but the damping from the side walls is significant compared to the flow in a wide model of this length. With the lengths L/H = 4.9, 4.o and 3.o there are two characteristic areas in the lower two thirds of the model. Farthest away from the supply opening there is a recirculating two-dimensional flow originating from the top wall jet, which is turned twice 9o^{o} at the end wall. The velocity is relatively high in this area. Just below the supply opening there is an area of very low velocity, containing a horizontal circulating motion which sometimes occupies the whole width of the model .

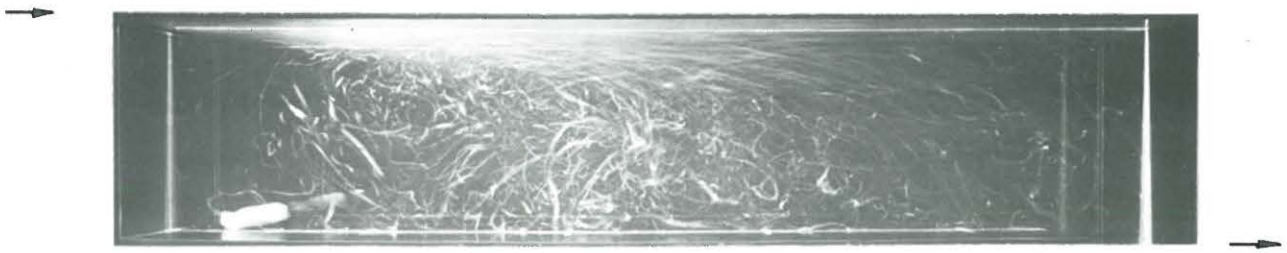

L / H = 4.9

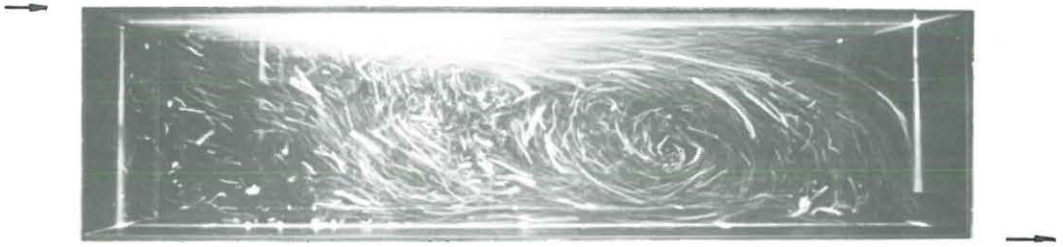

L / H = 4.0

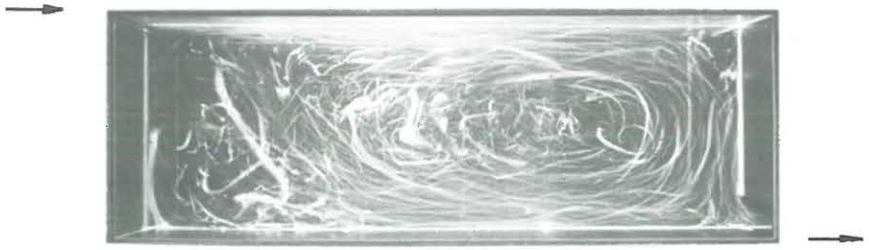

L / H = 3.0

L / H = 1.0

Fig. 2.4.4-1. Flow in models having a width of W/H = 1.6 and different lengths. h/H = o.o2o, w/W = 1.o, u/H = o.15 and Re = 47oo.

With the lengths L/H = 2.o and 1.o the lower two-thirds of the model are completely controlled by the two-dimensional recirculating flow, figs. 2.4.4-1 and 2.4.4-2.

So far, we have only studied the stream line pattern in the median plane of the model. Fig. 2.4.4-2 shows two pictures of stream lines, one from the median plane, x_3/W = o.5, and one from the area close to the side wall, x_3/W = o.o5. For L/H = 2.o in particular, there is a characteristic difference in stream line distribution. We see that the injected jet has a tendency to run down the side walls, something which has also been shown by Linke [19], Urbach [34] and Nagasawa [26]. With the experimental method we use, it is not possible to establish whether this three-dimensional effect has any significant influence on the flow inside the model, i.e. whether the flow inside the model is quantitatively two-dimensional without influence from the side walls.

Fig. 2.4.4-3 shows two situations related to the previously mentioned flow in the area below the supply opening. The flow is a horizontal circulating flow, which sometimes occupies the whole width of the model. It is unsteady and changes its direction every few seconds in the case of V_o = 1o-15 m/s, equivalent to a Reynolds number of 47oo to 71oo. The pictures of the stream lines apply to L/H = 3.0 and illustrate the flow close to the side wall, x_3/W = 0.05. The drawings show the two situations as seen from above. The dividing line between the horizontally circulating flow and the return flow along the side wall is clearly visible on the bottom picture.

With the lengths L/H = 4.0 and 4.9 the velocities are lower than at L/H = 3.0, and the horizontal motion sometimes ceases completely. At all events, flow velocities are so low that they are of no significance to the situation in practice in an air conditioned room.

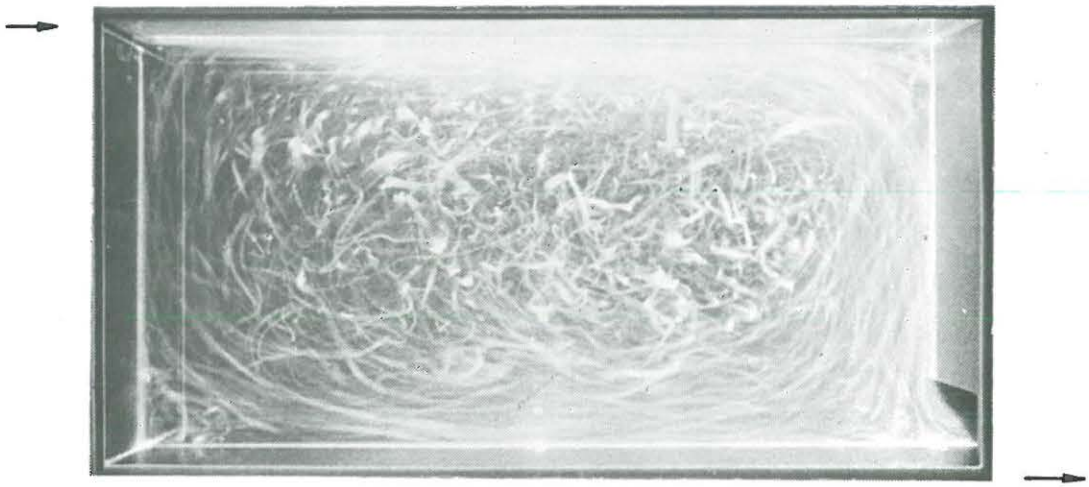

$x_3 / W = 0.5$

$x_3 / W = 0.05$

Fig. 2.4.4-2. Flow in median plane of model, x_3/W = o.5, and at one side wall x_3/W = o.o5. h/H = o.o2o, w/W = 1.o, L/H = 2.o, W/H = 1.6, u/H = o.15 and Re = 47oo.

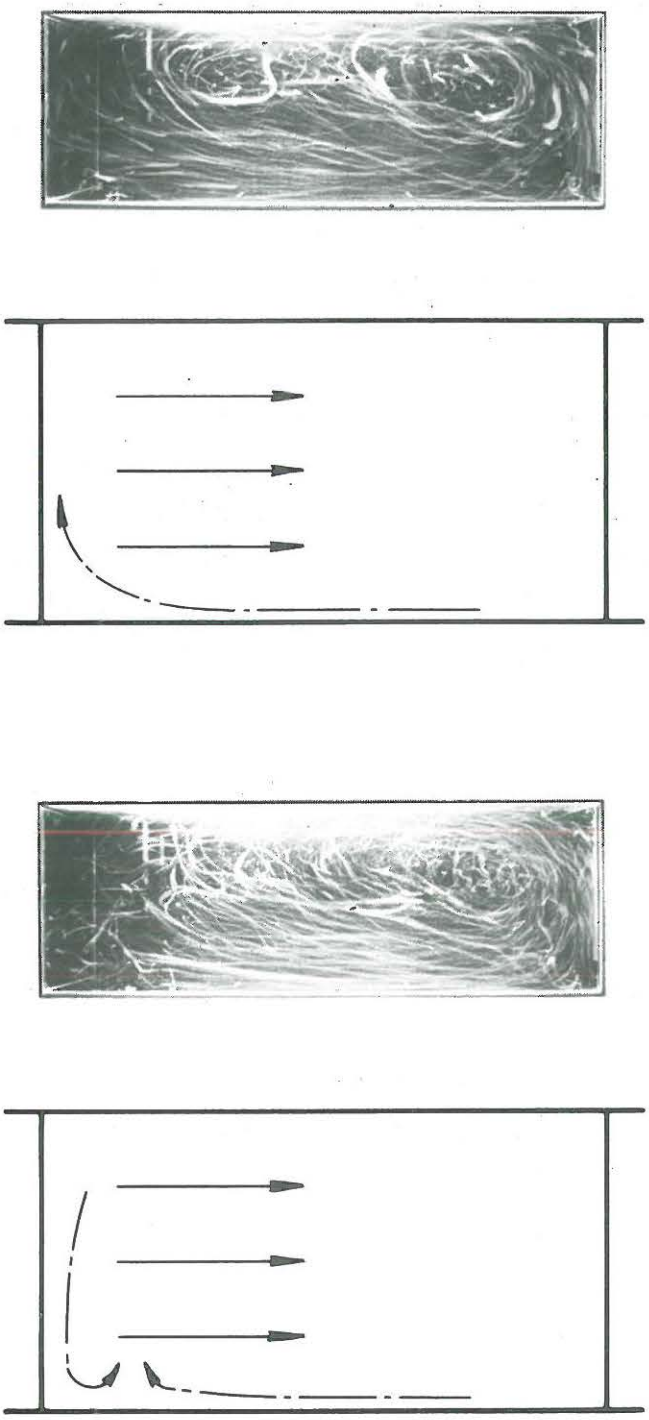

Fig. 2.4.4-3. Two different stream line pictures at the side wall of the model, x_3/W = 0.05. h/H = 0.02, w/W = 1.0, L/H = 3.0, W/H = 1.6, u/H = 0.15 and Re = 4700.

2.4.5. Vertical velocity profile in a model.

Velocity profiles are measured in models having a length of L/H = 3, 3.1 and 4 and widths of W/H = 4.7, 1 and 0.5. The other dimensions are

$$h/H = 0.056$$
$$w/W = 1.0$$
$$u/H = 0.16$$

The vertical velocity profile is measured at $x_1/H = 2.0$. The position is chosen in such a way that it is in the range where the velocity is at a maximum in the lower part of the recirculating flow in the case of a length of L/H = 3.0. This velocity is important in air conditioning because it corresponds to the maximum velocity in the occupied zone of a room.

The velocity profile is also measured close to the centre of the recirculating flow. This gives simple mathematical expressions for the transformation of the signal from the anemometer to velocity and intensity, because the mean velocity in this area is parallel with the x_1-axis.

In a turbulent flow the instantaneous velocity $\hat{v}_i$ may be expressed as the sum of a mean velocity v_i and a time dependent fluctuation v_i' .

$$\hat{v}_i = v_i + v_i' \qquad (2.4.5\text{-}1)$$

When the mean velocity is parallel with the x_1-axis, the total instantaneous velocity should be expressed as

$$\hat{v}_{tot} = \sqrt{(v_1 + v_1')^2 + v_2'^2 + v_3'^2} \qquad (2.4.5\text{-}2)$$

The hot-wire is placed so that the mean velocity v_1 forms a right angle to the probe support, i.e. the x_2 axis is parallel to the probe support and the x_3-axis is parallel to the hot-wire probe.

A hot-wire is sensitive to the direction of flow, and therefore the effective cooling velocity deviates from formula (2.4.5-2), and becomes

$$\hat{v}_{eff} = \sqrt{(v_1 + v_1')^2 + K_1^2 v_2'^2 + K_2^2 v_3'^2} \qquad (2.4.5\text{-}3)$$

where K_1^2 is about 1 and K_2^2 about 0.1 because the hot-wire is only very slightly sensitive to velocity components parallel to the hot-wire. The value of K_1^2 and K_2^2 also depends on the type and geometry of the hot-wire.

If we limit ourselves to situations where fluctuations are small compared to the mean velocity, we may ignore their second power and formula (2.4.5-3) can be written as

$$\hat{v}_{eff} \sim \sqrt{v_1^2 + 2 v_1 v_1'} \sim v_1 + v_1' \qquad (2.4.5\text{-}4)$$

The signal from the anemometer is linearized, and by calibration at a known velocity having a low turbulence intensity the proportionality constant K is determined from the following expression

$$E + E' = K \hat{v}_{eff} \qquad (2.4.5\text{-}5)$$

where E is the mean value of the voltage signal and E' is the fluctuating part. If we suppose that formula (2.4.5-4) can be used in large areas we get the following expressions of the mean velocity v_1 and the turbulence intensity $\sqrt{\overline{v_1'^2}}$.

$$v_1 = E / K \qquad (2.4.5\text{-}6)$$

$$\sqrt{\overline{v_1'^2}} = \sqrt{\overline{E'^2}} / K \qquad (2.4.5\text{-}7)$$

Fig. 2.4.5-1 shows the velocity profile v_1/V_o at a Reynolds number of 4700 in the model having the length L/H = 3 and the width W/H = 4.7. We see that the upper part of the velocity is 0.62 times the supply velocity, which also agrees well with the corresponding velocity of 0.64 calculated for a wall jet after Schwarz and Cosart[32] .

In the middle range of the profile the mean velocity is much lower than the fluctuations. Formula (2.4.5-3) shows that the effective cooling velocity does not become correspondingly low, and Miller and Comings [22] have demonstrated that the signal E/K in this area is an expression of the type

$$\sqrt{\overline{v_1'^2 + v_2'^2}}$$

Since there exists a mixing layer in the middle range with a fairly constant velocity gradient, the dotted curve is a reasonable expression of the mean velocity.

Fig. 2.4.5-1 also shows the profile for intensity $\sqrt{\overline{v_1'^2}}/V_o$. We have chosen to plot this value on the same side as the respective mean velocity, even though it is not to be calculated with signs . In the upper part of the profile the measurements are in good agreement with the results from a wall jet. Thus Nelson [27] , for example finds that the maximum value of $\sqrt{\overline{v_1'^2}}/V_o$ is o.14 in a jet of similar length. It is very characteristic that the intensity reaches a maximum where the gradient of the mean velocity is greatest, and this is due to the production of turbulence by the gradient.

Fig. 2.4.5-2 shows the velocity profile v_1/V_0 and the intensity $\sqrt{\overline{v_1'^2}}/V_o$ at a Reynolds number of 7100. If we compare this with fig. 2.4.5-1, where the Reynolds number is 4700, we see that both the mean velocity and the turbulence are similar at the two supply velocities.

Note the maximum intensity at the lower surface. This maximum is due to the considerable local production of turbulence in the mean velocity shear layer. The corresponding maximum at the upper surface was not found because the hot-wire probe has only been taken a small distance past the mean velocity maximum.

Fig. 2.4.5-3 shows the velocity profile in a model with the length L/H = 3.1 and the width W/H = 4.7, i.e. in practice the same dimensions as those applicable for fig. 2.4.5-1 and 2.4.5-2. The measurements are carried out with a 55K01 anemometer system while the measurements for the two previous figures are made with a 55D01 anemometer system. There is a slight difference between the results for L/H ~ 3.o. The reason may be that the different dimensions of probe support influence the results, because the air flow is at right angles to the probe and the support. Since the sub model used in all the measurements is very small (H = 12.65 cm) and the supply

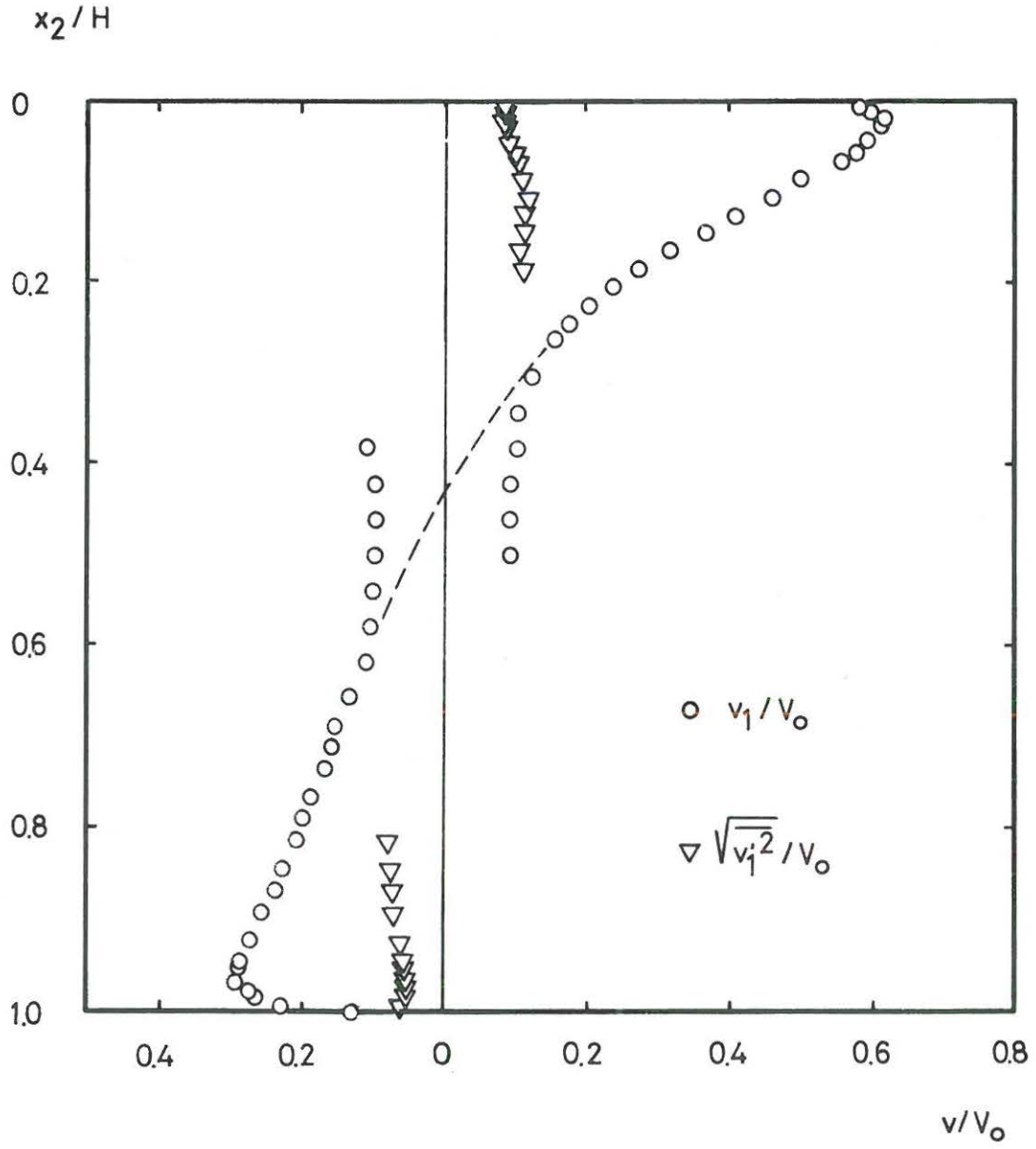

Fig. 2.4.5-1. Vertical velocity profile v_1/V_o and turbulence intensity $\sqrt{\overline{v_1'^2}}/V_o$ in a model of big width. h/H = 0.056, w/W = 1.0, W/H = 4.7, L/H = 3.0 and Re = 4700. The profile is measured at the coordinates x_1/H = 2.0 and x_3/W = 0.5.

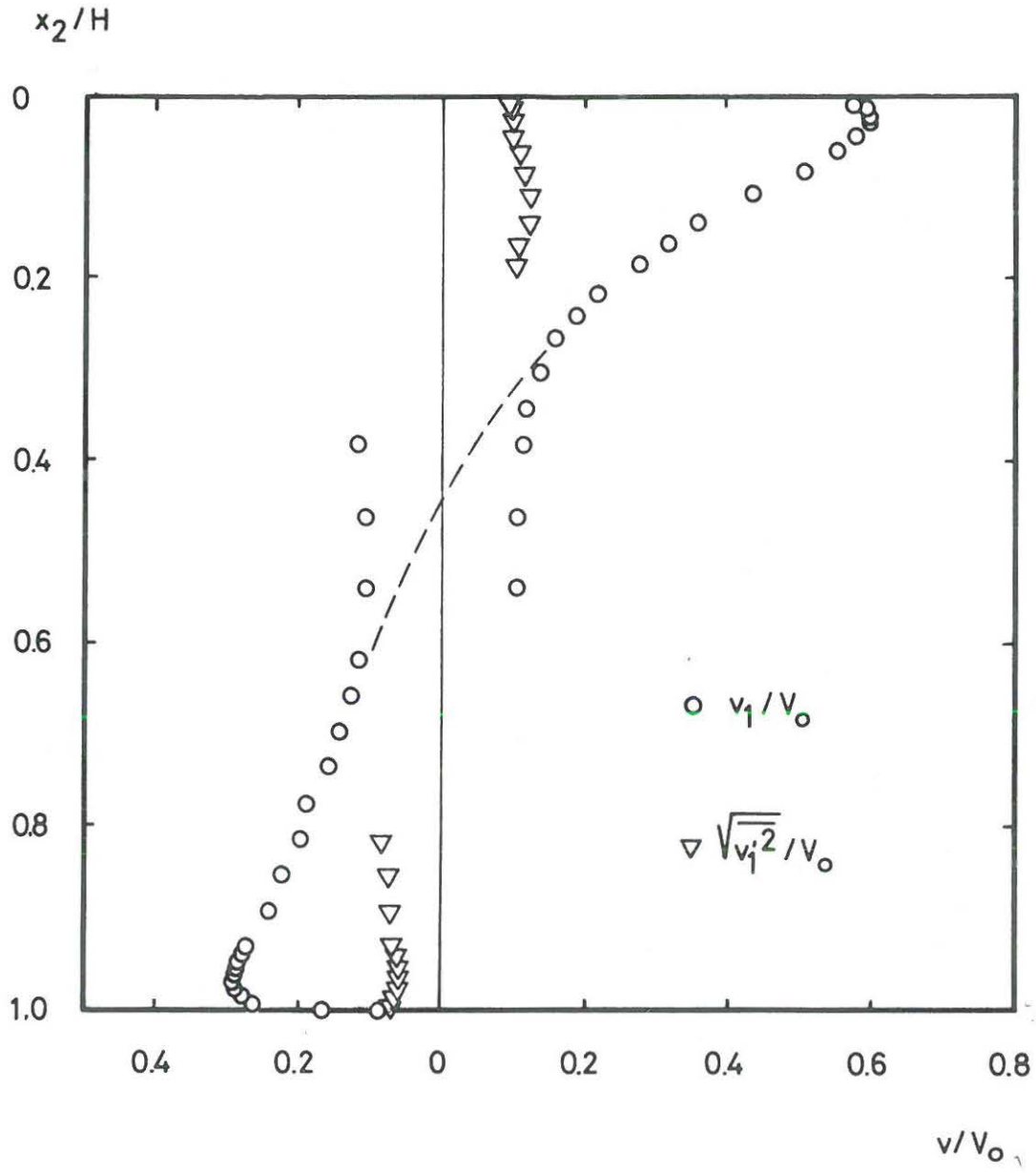

Fig. 2.4.5-2. Vertical velocity profile v_1/V_o and turbulence intensity $\sqrt{\overline{v_1'^2}}/V_o$ in a model of big width. h/H = 0.056, w/W = 1.0, W/H = 4.7, L/H = 3.0 and Re = 7100. The profile is measured at the coordinates x_1/H = 2.0 and x_3/W = 0.5.

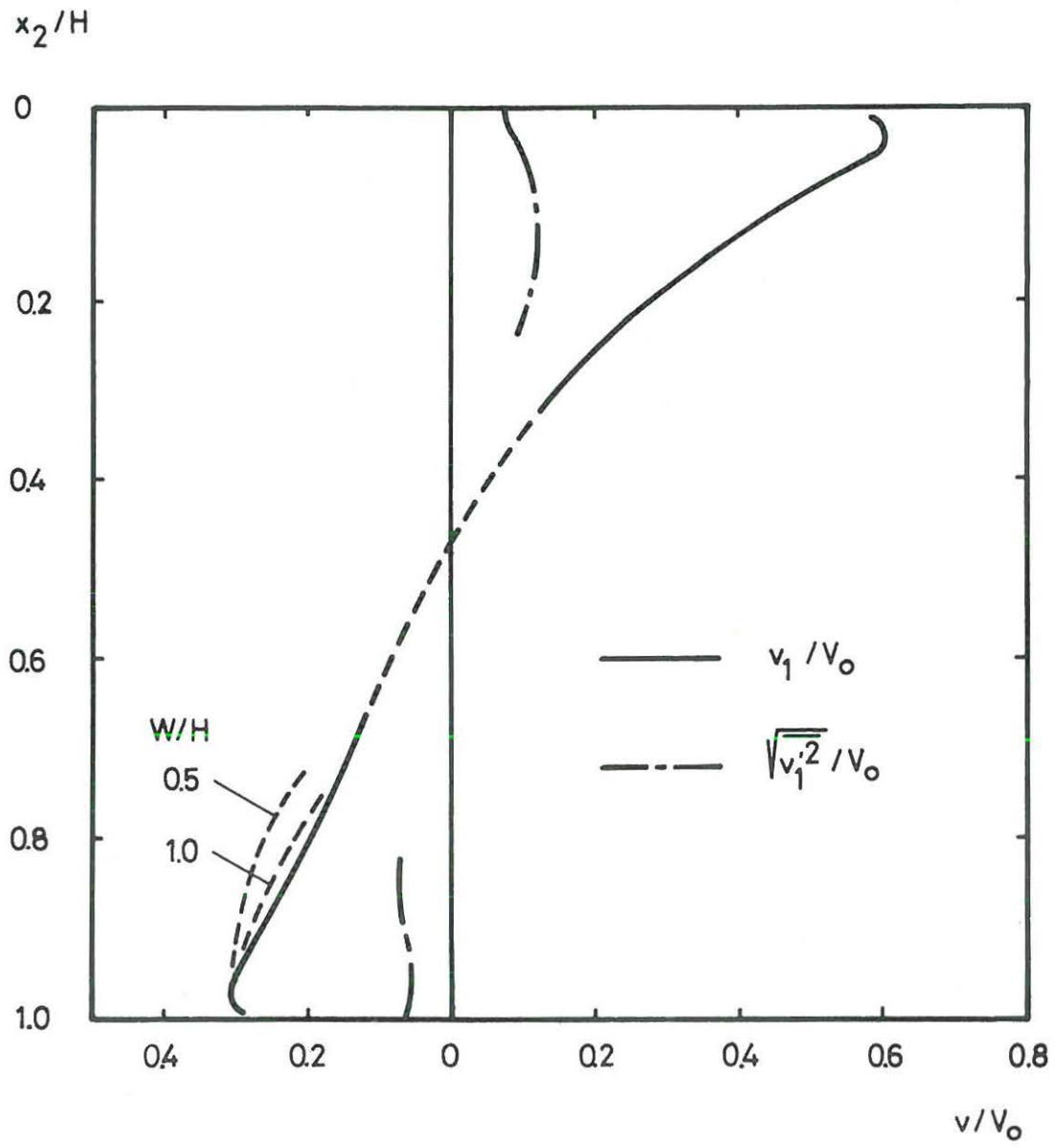

Fig. 2.4.5-3. Vertical velocity profile v_1/V_o and turbulence intensity $\sqrt{\overline{v_1'^2}}/V_o$ in a model of big width. h/H = 0.056, w/W = 1.0, W/H = 4.7, L/H = 3.1 and Re = 7100. The profile is measured at the coordinates x_1/H = 2.0 and x_3/W = 0.5. The results for W/H = 1.0 and 0.5 may be disturbed from the probe support.

opening is difficult to align it is also difficult to recreate a measuring situation with great accuracy.

In the case L/H = 3.1, fig. 2.4.5-3, the velocity profile is also measured at width W/H = 1 and 0.5. There is a tendency for the signal to increase in the lower part of the profile especially in areas just about of the maximum velocity. Owing to the small dimensions and the possibility of disturbances from the probe support, however, it cannot be concluded with certainty, that the change in profile is produced by a three-dimensional effect at the side walls.

Linke [19] is one of the first to show how a three-dimensional effect at the side walls can influence the flow on the median plane. By means of some measurements made in a model with the width W/H = 1.0 and the length L/H = 3.0 he shows that the velocity profile on the median plane does not meet the equation of continuity if the flow is considered two-dimensional. Obviously , the flow in the lower part of the profile is too large. He concludes that the reason is dispersion of the injected jet down and along the side walls, as is also shown on fig. 2.4.4-2, forming a three-dimensional flow.

Urbach's [34] measurements of the velocity profile in a model with the width W/H = 1 show that in practice the flow may be considered two-dimensional in the case of length L/H = 2.0 (the two-dimensional continuity equation was met in the measured velocity profile). At L/H = 4.0 he registers deviations as measured by Linke.

Nagasawa [26] has carried out a complete - though qualitative - measurement of the velocity field in a model having the dimensions h/H = 0.02, L/H = 4.0 and W/H = 1.0. These measurements show how the horizontal velocity profile in the lower part of the model reaches a maximum in the middle and decreases in velocity out to the side walls, i.e. a three-dimensional flow.

Fig. 2.4.5-4 shows the velocity profile in a model with the length L/H = 4.0 and the width W/H = 4.7. The velocity profile is as previously measured at x_1/H = 2.0. Fig. 2.4.3-3 shows that we must expect that the mean velocity in the lower part of the model will have a component in the negative direction of the x_2-axis. We must therefore observe that the velocity on fig. 2.4.5-4 is the total velocity.

2.5. Model tests with temperature distribution.

We shall use a model having the following dimensions

$h/H = 0.056$
$w/W = 1.0$
$W/H = 4.7$
$L/H = 3.0$
$u/H = 0.16$

The flow in the model is steady and two-dimensional, so that the measured temperature distribution is suitable for comparison with the results from the prediction method.

The temperature distribution is created by supplying heat from an ESWA-heating film, placed on the bottom of the model. The temperature is measured at lo points by means of thermocouples. Three thermocouples are placed on the heating film at distance x_1/H = 0.5, 1.0 and 2.0. One thermocouple is placed in the supply opening and two thermocouples are placed vertically above each other in the return opening. The temperature profile in the model is measured on the horizontal plane H/4 corresponding to the coordinates x_2/H = o.75, and the positions in the x_1-direction are x_1/H = 0.1, 0.5, 1.0 and 2.0. All thermocouples are placed on a vertical plane at x_3/W = 0.66.

In addition to the geometrical dimensions, complete specification of the individual experiments includes Reynolds number and Archimedes number according to the formulas (2.2.3-2) and (2.2.3-3).

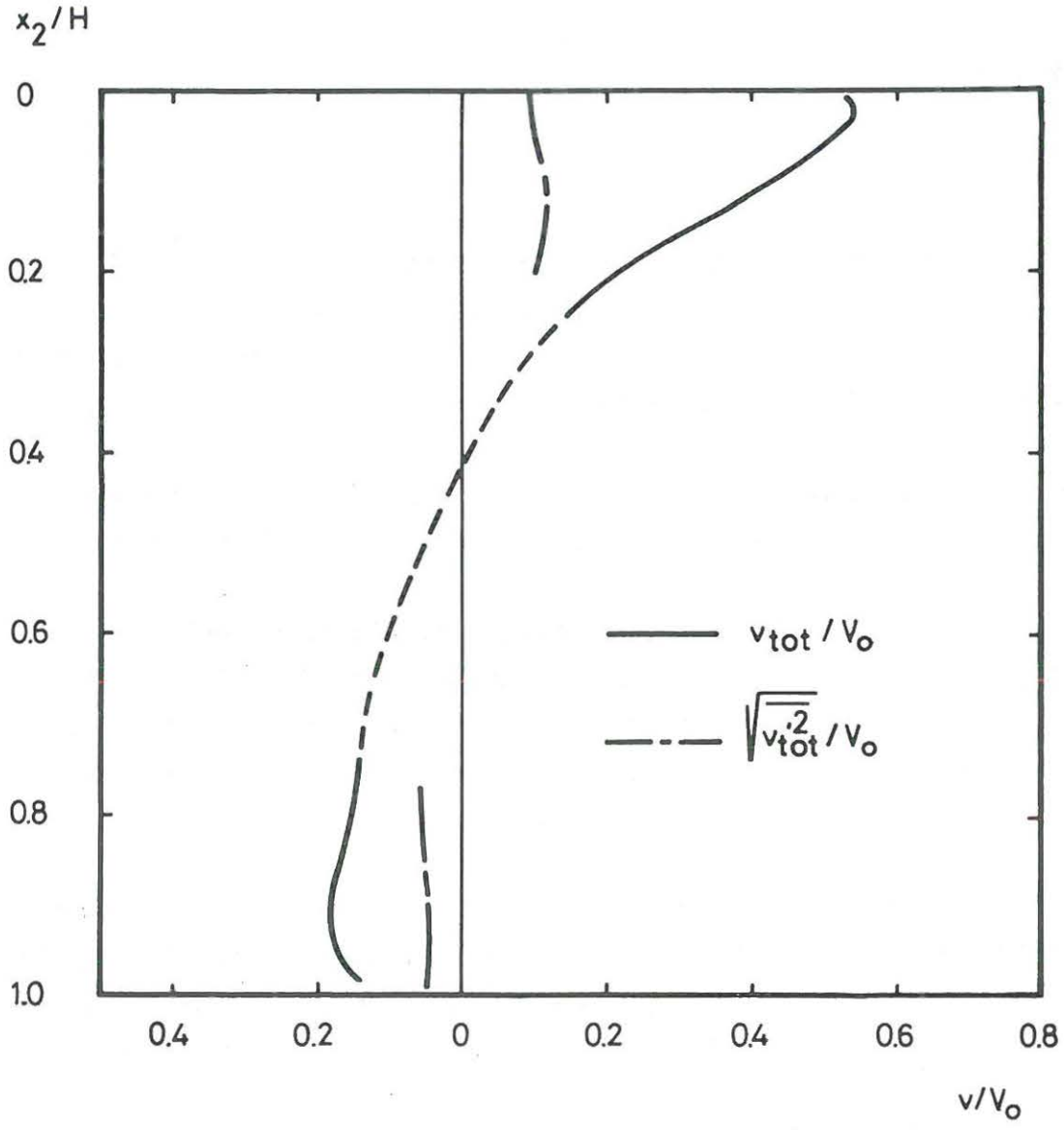

Fig. 2.4.5-4. Vertical velocity profile v_{tot}/V_o and turbulence intensity $\sqrt{\overline{v'^2_{tot}}}/V_o$ in a model of big width. h/H = o.o56, w/W = 1.o, W/H = 4.7, L/H = 4.o and Re = 71oo. The profile is measured at the coordinates x_1/H = 2.o and x_3/W = o.5.

The measured temperature fluctuates just like the velocity and can therefore be expressed as a sum of a mean temperature T and a fluctuation T'.

$$\hat{T} = T + T' \qquad (2.5\text{-}1)$$

Since the thermocouples have a small time constant it is possible to get a qualitative picture of this effect by determining $\hat{T}$ as a function of time on the pen recorder. The mean temperature T is determined graphically.

Figs. 2.5-1, 2.5-2 and 2.5-3 show the horizontal temperature profile in the model at the three Reynolds numbers Re = 2400, 4700 and 7100. The temperatures are given dimensionless according to formula (2.2.1-5). The supply temperature will be $T_o^* = 0$ and the return temperature $(T_o + \Delta T_o)^* = 1$. We see how the temperatures increase in the direction of the recirculating flow and reach their highest level below the supply opening.

The three figures also show the distribution of the surface temperature T_s. Although constant electrical power is supplied, the heat flow is not uniform along the bottom owing to the temperature coefficient of the heating film resistance.

The measurements in fig. 2.5-3 were made at Archimedes numbers so small that the buoyancy is of no importance to the flow, see section 2.2.3. The stream line distribution and the velocity profiles that have been found for isothermal flow in the same model are therefore also applicable for the situation of fig. 2.5-3.

Fig. 2.5-1 shows that the air temperatures are significantly lower than the corresponding temperatures on fig. 2.5-2 and 2.5-3. This change is presumably due to the influence of buoyancy on the flow at the higher Archimedes numbers.

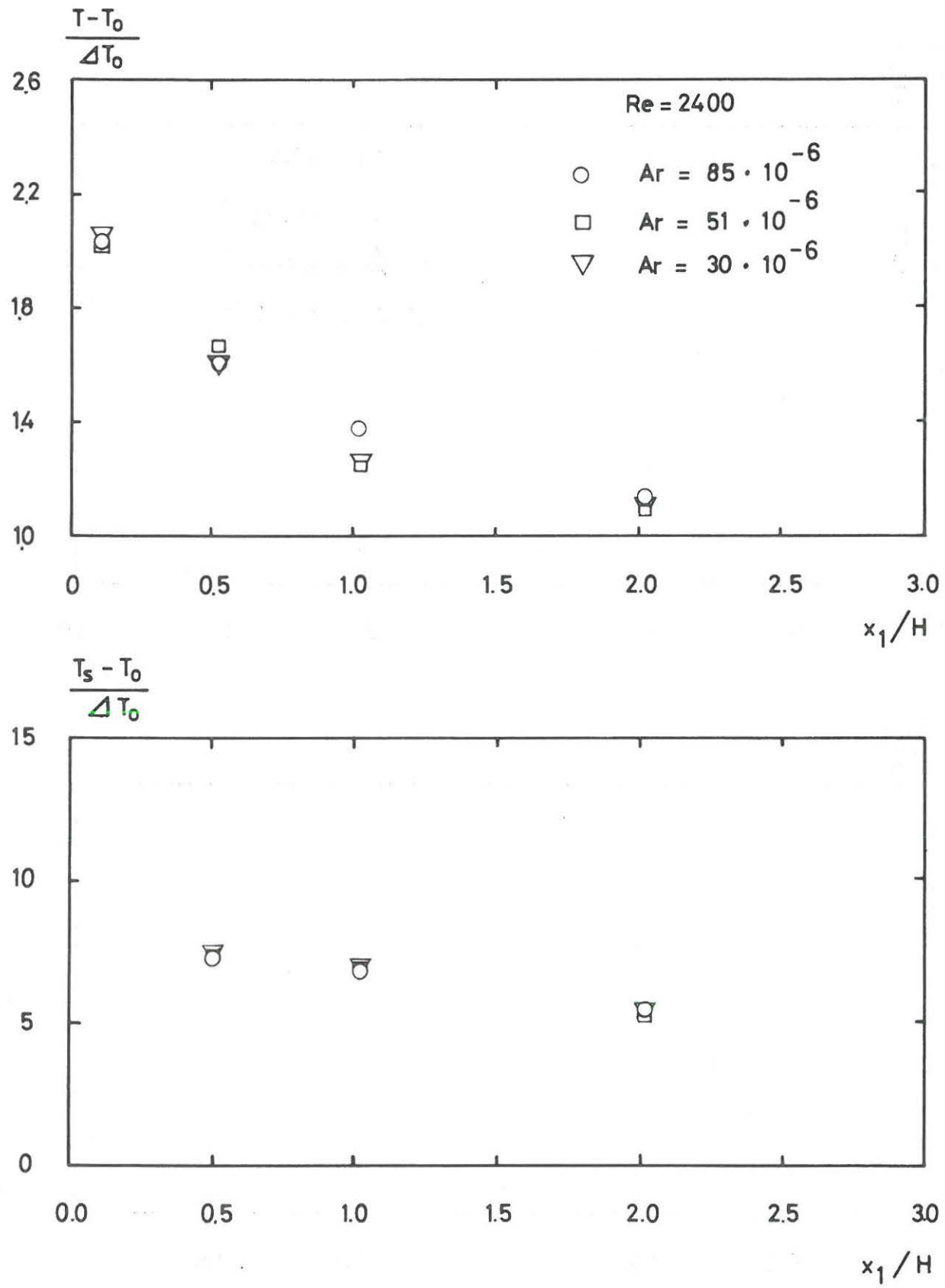

Fig. 2.5-1. Horizontal temperature profile at the height x_2/H = 0.75 and surface temperature profile. h/H = 0.056, w/W = 1.0, W/H = 4.7, L/H = 3.0 and Re = 2400.

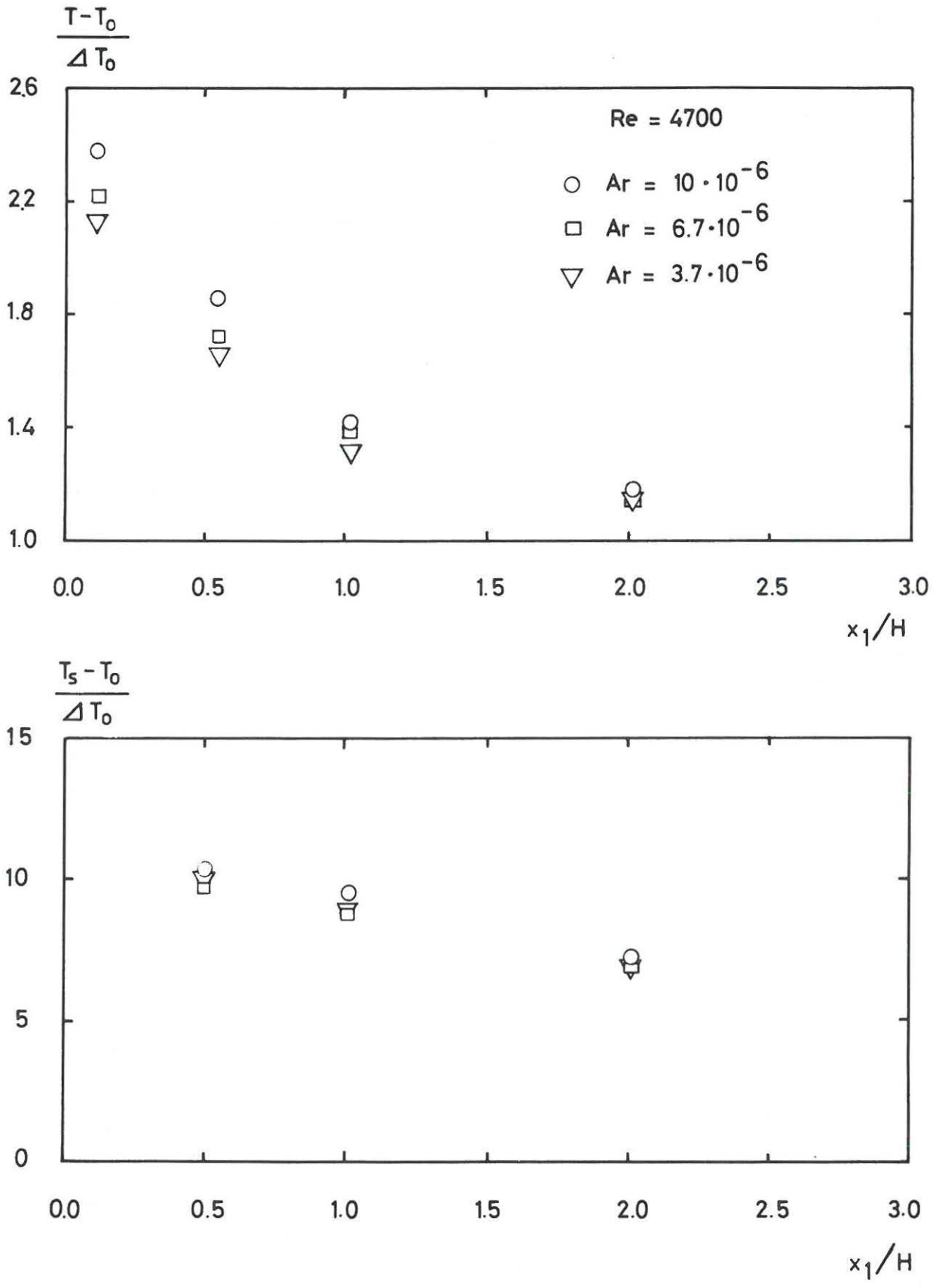

Fig. 2.5-2. Horizontal temperature profile at the height x_2/H = 0.75 and surface temperature profile. h/H = 0.056, w/W = 1.0, W/H = 4.7, L/H = 3.0 and Re = 4700.

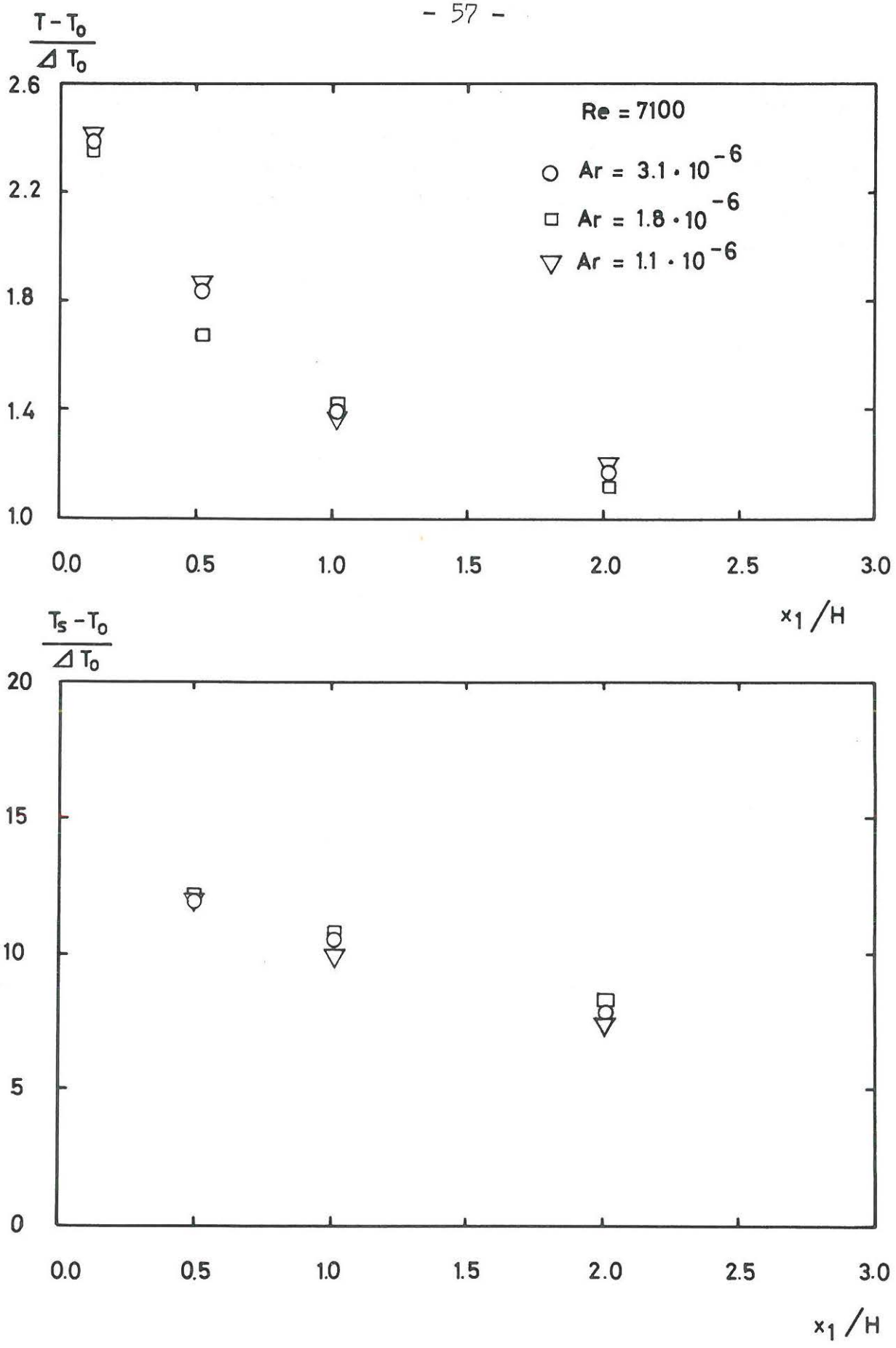

Fig. 2.5-3. Horizontal temperature profile at the height x_2/H = 0.75 and surface temperature profile. h/H = 0.056, w/W = 1.0, W/H = 4.7, L/H = 3.0 and Re = 7100.

If there is a sufficiently big temperature difference it is likely that the supply jet will run down the wall beneath the supply opening and reverse the direction of flow in the model, as is demonstrated by Müllejans [25] in a similar model at a smaller Reynolds number.

3. Numerical prediction of the flow in a room.

In the following section we shall examine a prediction method for determining the air distribution in a room. The method is well suited for the purpose since it predicts air distribution in all areas of the room. This is not the case with the ordinary prediction method, where it is only possible to follow a wall jet or a free jet in the first part of its progression.

The prediction method is based on a numerical solution of the flow equations on a computer. The method requires so much computer space that it is necessary to limit the prediction to steady, two-dimensional flow (The situation in 1971-73).

Section 3.1 to 3.3 gives general information on the numerical method. For more detailed information reference is made to the literature and to appendices I to III. Section 3.3.1 is of special interest, because it shows how the calculations are made for various types of diffusers.

In section 3.4 a comparison is made between measured and predicted results. The primary purpose of this section is to illustrate the applicability of the numerical method. But the section also contains conclusions of general interest to air conditioning , and is therefore recommended to readers even if they have no special interest in the numerical prediction method.

3.1. Two dimensional equations and turbulence model.

If we consider the set of general equations in section 2.1., comprising the equation of continuity (2.1-1) the three equations of motion (2.1-4) and the energy equation (2.1-5), with the five unknowns $\hat{v}_1$,$\hat{v}_2$,$\hat{v}_3$, $\hat{p}$ and $\hat{T}$, we see that they together with the boundary conditions represent a complete description of the flow.

At the velocities and temperature differences prevalent in air conditioned rooms the flow will always be turbulent. The turbulence is described by the fluctuations in the variables involved, and these fluctuations take place at dimensions down to 10^{-3} times the main size of the problem, e.g. the height H. We see that it is difficult to solve the set of general equations by means of a numerical method because such a method requires several difference equations within the length 10^{-3} H, which leads to an untractably large number of difference equations when the whole flow region is to be described.

Instead we shall choose to consider the mean value of the flow as the unknowns. The reason is that the variations in the mean values over a given distance are considerably smaller than the variations in the instantaneous values, and the mean values may therefore be described by a limited number of difference equations.

As a step towards the set of equations which is solved by the numerical method, equations (2.1-1), (2.1-4) og (2.1-5) are rewritten to the following set of equations.

$$\frac{\partial v_i}{\partial x_i} = 0 \qquad (3.1\text{-}1)$$

$$\rho_o\left(\frac{\partial v_i}{\partial t} + v_j\frac{\partial v_i}{\partial x_j}\right) = -\rho_o \beta g_i (T - T_o)$$

$$-\frac{\partial p}{\partial x_i} + \frac{\partial}{\partial x_j}\left(\mu_o\frac{\partial v_i}{\partial x_j} - \rho_o\overline{v_i' v_j'}\right) \qquad (3.1\text{-}2)$$

$$\rho_o\left(\frac{\partial T}{\partial t} + v_j\frac{\partial T}{\partial x_j}\right) = \frac{\partial}{\partial x_j}\left(\frac{\lambda}{c_p}\frac{\partial T}{\partial x_j} - \rho_o\overline{v_j' T'}\right) \qquad (3.1\text{-}3)$$

where

$$v_i + v_i' = \hat{v}_i \tag{3.1-4}$$

$$p + p' = \hat{p} \tag{3.1-5}$$

$$T + T' = \hat{T} \tag{3.1-6}$$

Correlations of type $-\rho_o \overline{v_i' v_j'}$ and $-\rho_o c_p \overline{v_j' T'}$ may be considered as a stress and a heat flux respectively, caused by turbulence. The idea behind the turbulence model is now to replace these correlations by terms containing a turbulent viscosity μ_t according to expressions of the type

$$-\rho_o \overline{v_1' v_2'} = \mu_t \left(\frac{\partial v_1}{\partial x_2} + \frac{\partial v_2}{\partial x_1} \right) \tag{3.1-7}$$

$$-\rho_o \overline{v_1' T'} = \frac{\mu_t}{\sigma_h} \frac{\partial T}{\partial x_1} \tag{3.1-8}$$

where σ_h is the turbulent Prandtl number, see for example, Launder et al.[17] .

The new variable μ_t describes the turbulence on the basis of turbulent kinetic energy k and dissipation of turbulent kinetic energy ϵ .

$$\mu_t = c_\mu \rho_o \frac{k^2}{\epsilon} \tag{3.1-9}$$

c_μ is an empirical constant, and k and ϵ are defined as

$$k = \frac{1}{2}\overline{v_j' v_j'} \qquad (3.1\text{-}10)$$

$$\epsilon = \frac{\mu_o}{\rho_o}\overline{\frac{\partial v_i'}{\partial x_j}\frac{\partial v_i'}{\partial x_j}} \qquad (3.1\text{-}11)$$

Turbulence at a given point is not only dependent on local conditions. It can, via the energy k, be transported around in the flow area, and it is therefore necessary to describe it with the aid of transport equations for k and ϵ . Launder et al.[17] has developed transport equations for these values and reduced them, so that together with the equations for the mean flow they represent a complete description of the flow. The equations are given at the end of this section, and they are disignated (3.1-18) and (3.1-19).

As mentioned we shall confine ourselves to two-dimensional steady flow. We shall also make a reduction of the numbers of equations by leaving the variables v_1, v_2 and p and introducing the vorticity ω and the stream function ψ as new variables.

The vorticity is twice the angular velocity of the air at the examined point and is given by

$$\omega = \frac{\partial v_2}{\partial x_1} - \frac{\partial v_1}{\partial x_2} \qquad (3.1\text{-}12)$$

The stream function describes the vector field (v_1, v_2) by a single scalar quantity ψ.

The stream function is a practical variable when describing the solution to an air conditioning problem, because lines of constant ψ values are stream lines, i.e. lines parallel to the velocity vector. The connection between velocity and stream function is based on the equation of continuity (3.1-1), and it is given by the following expressions.

$$v_1 = \frac{1}{\rho_o} \frac{\partial \psi}{\partial x_2} \qquad (3.1\text{-}13)$$

$$v_2 = -\frac{1}{\rho_o} \frac{\partial \psi}{\partial x_1} \qquad (3.1\text{-}14)$$

We are now able to show the total set of equations in the form which is used in the numerical model. The first equation (3.1-15) is the vorticity transport equation derived from the two equations of motion in the x_1 and x_2 directions. The second equation (3.1-16) is the relation by definition between the vorticity and the stream function, and the third equation (3.1-17) is the energy equation. The last two equations are transport equations for k and ϵ, i.e. equations that represent the model of turbulence.

The set of equations consists of five non-linear partial differential equations. These are all built up with convection terms on the left side and diffusion terms, production terms and dissipation terms on the right side, except equation (3.1-16) in which the diffusion terms are on the left side.

$$\frac{\partial}{\partial x_1}\left(\omega \frac{\partial \psi}{\partial x_2}\right) - \frac{\partial}{\partial x_2}\left(\omega \frac{\partial \psi}{\partial x_1}\right) = \frac{\partial}{\partial x_1}\left(\frac{\partial \mu_t \omega}{\partial x_1}\right)$$

$$+ \frac{\partial}{\partial x_2}\left(\frac{\partial \mu_t \omega}{\partial x_2}\right) + \rho_o \beta g_2 \frac{\partial T}{\partial x_1} \qquad (3.1\text{-}15)$$

$$\frac{\partial}{\partial x_1}\left(\frac{1}{\rho_o}\frac{\partial \psi}{\partial x_1}\right) + \frac{\partial}{\partial x_2}\left(\frac{1}{\rho_o}\frac{\partial \psi}{\partial x_2}\right) = -\omega \qquad (3.1\text{-}16)$$

$$\frac{\partial}{\partial x_1}\left(T \frac{\partial \psi}{\partial x_2}\right) - \frac{\partial}{\partial x_2}\left(T \frac{\partial \psi}{\partial x_1}\right) = \frac{\partial}{\partial x_1}\left(\frac{\mu_t}{\sigma_h}\frac{\partial T}{\partial x_1}\right)$$

$$+ \frac{\partial}{\partial x_2}\left(\frac{\mu_t}{\sigma_h}\frac{\partial T}{\partial x_2}\right) \qquad (3.1\text{-}17)$$

$$\frac{\partial}{\partial x_1}\left(k \frac{\partial \psi}{\partial x_2}\right) - \frac{\partial}{\partial x_2}\left(k \frac{\partial \psi}{\partial x_1}\right) = \frac{\partial}{\partial x_1}\left(\frac{\mu_t}{\sigma_k}\frac{\partial k}{\partial x_1}\right) + \frac{\partial}{\partial x_2}\left(\frac{\mu_t}{\sigma_k}\frac{\partial k}{\partial x_2}\right)$$

$$+ \mu_t \left[2\left(\left(\frac{\partial v_1}{\partial x_1}\right)^2 + \left(\frac{\partial v_2}{\partial x_2}\right)^2\right) + \left(\frac{\partial v_1}{\partial x_2} + \frac{\partial v_2}{\partial x_1}\right)^2\right] - \rho_o \epsilon \qquad (3.1\text{-}18)$$

$$\frac{\partial}{\partial x_1}\left(\epsilon \frac{\partial \psi}{\partial x_2}\right) - \frac{\partial}{\partial x_2}\left(\epsilon \frac{\partial \psi}{\partial x_1}\right) = \frac{\partial}{\partial x_1}\left(\frac{\mu_t}{\sigma_\epsilon}\frac{\partial \epsilon}{\partial x_1}\right) + \frac{\partial}{\partial x_2}\left(\frac{\mu_t}{\sigma_\epsilon}\frac{\partial \epsilon}{\partial x_2}\right)$$

$$+ c_1 \mu_t \left[2\left(\left(\frac{\partial v_1}{\partial x_1}\right)^2 + \left(\frac{\partial v_2}{\partial x_2}\right)^2\right) + \left(\frac{\partial v_1}{\partial x_2} + \frac{\partial v_2}{\partial x_1}\right)^2\right]\frac{\epsilon}{k} - c_2 \rho_o \frac{\epsilon^2}{k} \qquad (3.1\text{-}19)$$

The values c_1, c_2, c_μ, σ_h, σ_k and σ_ϵ are empirical constants whose values are given in table 3.1-1.

The constants are optimized for general fluid mechanics problems, and no changes are made in connection with prediction of the air motion which takes place in air conditioned rooms.

Use of the turbulence model assumes a high Reynolds number flow. It is possible to check whether this assumption is fulfilled in a prediction. The method is described in more detail in appendix I.

3.2. Numerical method.

The principle of the numerical method is to replace the differential equations by a number of difference equations which are solved by means of a modified Gauss iteration. The examined section is divided up into a number of points in a rectangular grid. The distance between the points is chosen in such a way that it is permissible to consider ω, ψ, T, k and ϵ as linear between two points. In areas where gradients of the individual values are great, the points are relatively close together , and in areas where the gradients are small there is a greater distance between the points. We see that the chosen rectangular grid is important to the results of the numerical solution, both with respect to the number of points and the distribution of a given number of points. Appendix II gives a more detailed discussion of how these problems are solved by the numerical predictions.

Evaluation of the difference equations and the lay out of the computer programme which carries out the iteration is described in detail by Gosman et al.[10], and[11]. It will therefore suffice here to mention the principle of the iteration and introduce one or two ideas of importance in connection with the numerical method.

c_1	c_2	c_μ	σ_h	σ_k	σ_ϵ
1,45	2,0	0,09	0,5	1,0	1,3

Table 3.1-1. Empirical constants in the equations (3.1-15) to (3.1-19) and (3.1-9).

The five differential equations are replaced by five difference equations at each point. At point P on fig. 3.2-1, for example, we get

$$\varphi_P = C_E \varphi_E + C_W \varphi_W + C_N \varphi_N + C_S \varphi_S + D \qquad (3.2\text{-}1)$$

where φ denotes ω, ψ, T, k and ϵ. The individual C-coefficients and D are dependent on the unknown variables and the equations are therefore non-linear.

During the iteration the following formula is used

$$\varphi_P^{n+1} = C_E^n \varphi_E^n + C_W^{n+1} \varphi_W^{n+1} + C_N^n \varphi_N^n + C_S^{n+1} \varphi_S^{n+1} + D \qquad (3.2\text{-}2)$$

We will begin by choosing an arbitrary distribution of φ called φ^1. Row by row, we shall now determine a new φ which we shall call φ^2. Equation (3.2-2) shows the calculation of φ_P at iteration n + 1. For points E and N values from iteration n are used and for points W and S values from iteration n + 1 are used, i.e. the latest obtained values are used all the time.

The difference between φ_P^{n+1} and φ_P^n is called the residual R_φ^{n+1}. When convergence takes place, the distance between two successive φ_P values will approach zero, and the iteration will be cut-off when R_φ^{n+1} have all dropped below a certain value

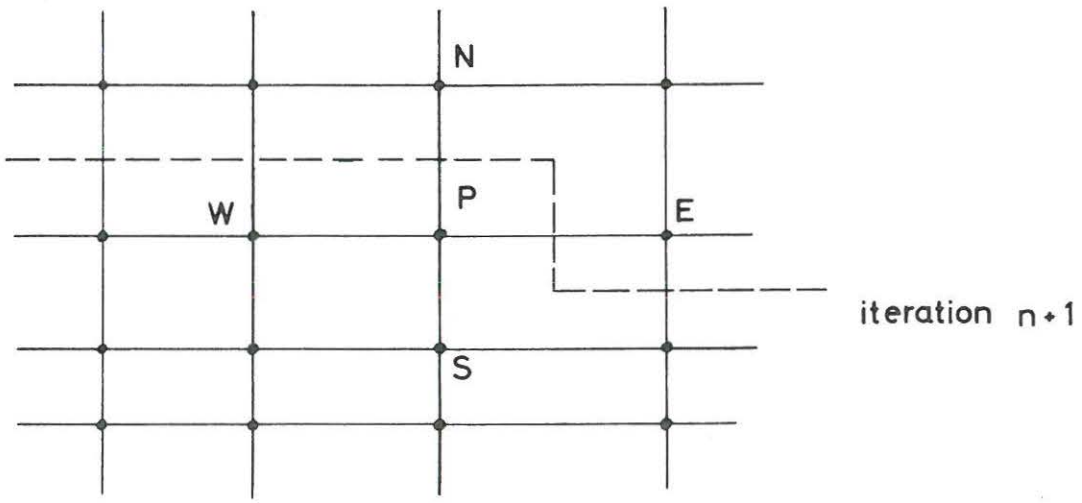

Fig. 3.2-1. Rectangular grid with nodes.

$$\left|\frac{\varphi^{n+1} - \varphi^{n}}{\varphi}\right| < 0.001 \qquad (3.2\text{-}3)$$

It must be pointed out, however, that the condition (3.2-3) is not always sufficient to ensure that the converged solution has been found. By way of a check, the change in some of the individual values φ should be followed to see whether they converge towards a fixed value.

The iteration can be made with successive over-relaxation or under-relaxation using the formula

$$\varphi_P^{n+1} = \varphi_P^{n} + \alpha_\varphi R_\varphi^{n+1} \qquad (3.2\text{-}4)$$

where α_φ is the relaxation parameter. By using over-relaxation where $1 < \alpha_\varphi < 2$, we can accelerate the change in φ_P of which R_φ is an expression, and we can, in some cases, reduce the number of iterations. Similarly with under-relaxation, where $0 < \alpha_\varphi < 1$, we can damp the oscillations in the residual R_φ in an otherwise oscillating iteration, and it is perhaps possible to bring it to convergence. Owing to the non-linearity of the equations we often have to resort to under-relaxation on certain variables in order to ensure convergence, and over-relaxation on other variables to avoid using extensive computer time.

It is generally known that the relaxation parameter ought to be about 1.0 for ω- and ψ-equations and about 0.5 for k-and ϵ-equations. A change in the Reynolds number and a change in grid type may result in divergence in an iteration which would otherwise converge.

Because of the high number of equations a computer of the size loo k bytes must be used. If, for example, a grid with 21 x 21 points is used, we get 21 x 21 x 5 = 22o5 equations and 22o5 unknowns.

3.3. Boundary conditions.

As mentioned earlier, the boundary conditions are a necessary part of the description of a problem, and they are dealt with in the following section on supply opening, return opening and boundary values along surfaces and symmetry planes.

3.3.1 Supply opening.

We shall choose to ignore the details of the flow in the immediate vicinity of the supply opening, and instead describe the supplied jet by values along surfaces "a" and "b", see fig. 3.3.1-1. We obtain two advantages by using these boundary conditions. Firstly, we do not need to use such a fine grid as is necessary to describe the development of the injected jet to a wall jet. Secondly, we can make predictions for supply openings that are three-dimensional, provided that the jets develop into a two-dimensional wall jet or free jet at a certain distance.

Calculation of the boundary values along the surface "a" is started by determining the maximum velocity V_m and the thickness δ_v of the wall jet that has developed at the distance x_a from the supply opening, see reference [32].

$$\frac{V_m}{V_o} = K_v \left(\frac{x_o + x_a}{h} \right)^{-e} \qquad (3.3.1\text{-}1)$$

$$\frac{\delta_v}{h} = D_v \frac{x_o + x_a}{h} \qquad (3.3.1\text{-}2)$$

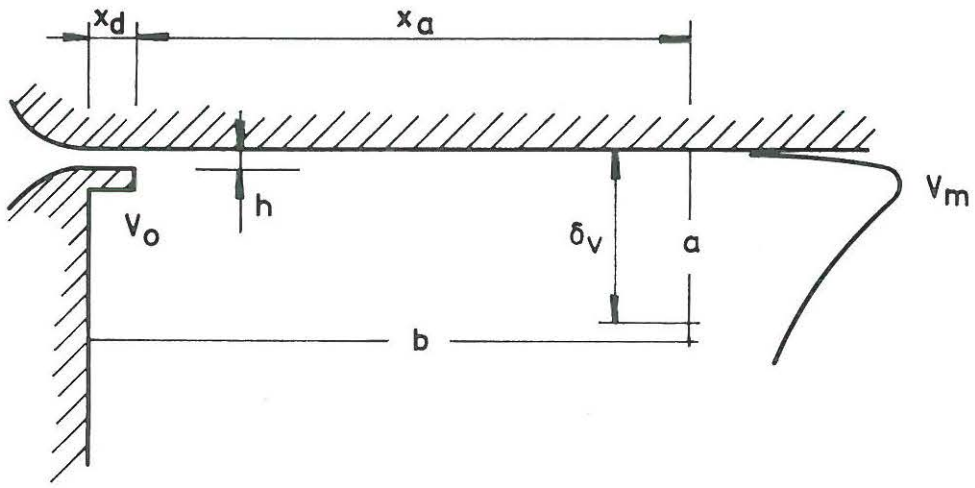

Fig. 3.3.1-1. Boundary and boundary values for a two-dimensional supply opening.

$x_o + x_a$ is the distance to the virtual origin of the jet, and K_v, D_v and the exponent e are constants. The calculations use the constants determined by Schwarz and Cosart [32] .

$$K_v = 5.4$$
$$D_v = 0.068$$
$$x_o/h = 11.2$$
$$e = 0.56$$

If data are available for the actual diffuser, these data should be used.

For maximum or minimum temperature T_m and thickness δ_T we get correspondingly

$$\frac{T_m - T_u}{T_o - T_u} = K_T \left(\frac{x_o + x_a}{h} \right)^{-e} \qquad (3.3.1\text{-}3)$$

$$\frac{\delta_T}{h} = D_T \frac{x_o + x_a}{h} \qquad (3.3.1\text{-}4)$$

T_u is the surrounding temperature, i.e. the mean temperature along surface "b" on fig. 3.3.1-1.

The surrounding temperature is not a fixed value but a function of the maximum or minimum temperature T_m via the flow conditions to be predicted. This connection may give rise to a very slow convergence of the temperature distribution.

The velocity profile v_1/V_m and the distribution of the intensities $\overline{v_1' v_2'}/V_m^2$, $\overline{v_1'^2}/V_m^2$, $\overline{v_2'^2}/V_m^2$ and $\overline{v_3'^2}/V_m^2$ at the surface "a" are universal, and are given for example, by Verhoff [35] and Nelson [27] respectively. By means of these profiles we can determine the distribution of the vorticity ω, stream function ψ, and turbulent kinetic energy k as well as dissipation ϵ. Determination of the dissipation profile involves an evaluation of the distribution of length scale in a wall jet, and this is described in more detail in appendix III.

There is a similarity between temperature profile and velocity profile except in the inner layer, where there is thought to be a constant temperature equal to T_m, which corresponds to an adiabatic surface along the wall jet.

Along the surface "b" the boundary conditions for the stream function are given linearly between the value it has on the surface below the supply opening and the value it has on the profile and the surface "a".

The boundary conditions for the other values along the surface "b" are given as

$$\frac{\partial \varphi}{\partial x} = 0 \qquad (3.3.1\text{-}5)$$

where the x-direction is at right angles to "b" and where φ denotes ω, T, k and ϵ.

The predicted flow conditions are greatly dependent on boundary values and nodal distribution around the supply opening. Therefore, the predicted velocities should always be compared with the velocity in a free jet or wall jet of same length. Such a comparison is shown on fig. 3.4.1-2.

As mentioned previously, it is also possible to predict the flow conditions in the case of special diffuser arrangements. Fig. 3.3.1-2 shows the supply opening of a plane jet at a distance x_s from a parallel surface. Measurements made by Schwartzbach [33] show that the jet is deflected due to the Coanda effect and develops into a wall jet at a distance x_a from the supply opening. The curves on fig. 3.3.1-2 show the values for x_a/h, x_o/h, V_m/V_o and δ_v/h. Based on these data the boundary conditions for a wall jet are determined as before, though it must be pointed out that the turbulence is higher in this case owing to the deflection of the jet.

If a linear supply opening is located at a great distance from parallel surfaces, a two-dimensional free jet may be used as boundary conditions. To examplify the treatment of a three-dimensional supply opening we can mention the arrangement comprising a row of circular openings. Knystautas [15] has shown that the jets develop into a two-dimensional free jet at a distance of about 15 times the distance between the single openings. Assuming that this distance is small compared to H or L, the diffuser arrangement may be replaced by a free jet. Becher [3] has also shown how other types of diffusers may be converted into single wall jets or free jets.

All of the examples shown later are jets which are supplied parallel to a ceiling. The boundary conditions for the supply opening can, of course, also be arranged so that they correspond to supply openings in the floor or in the sill below the window.

In those cases where $h/H \geq 0.1$, the supply opening is used direct as boundary condition , because x_a will otherwise be too great compared to H and L, and because the opening itself can be described by a reasonable number of nodes in this instance.

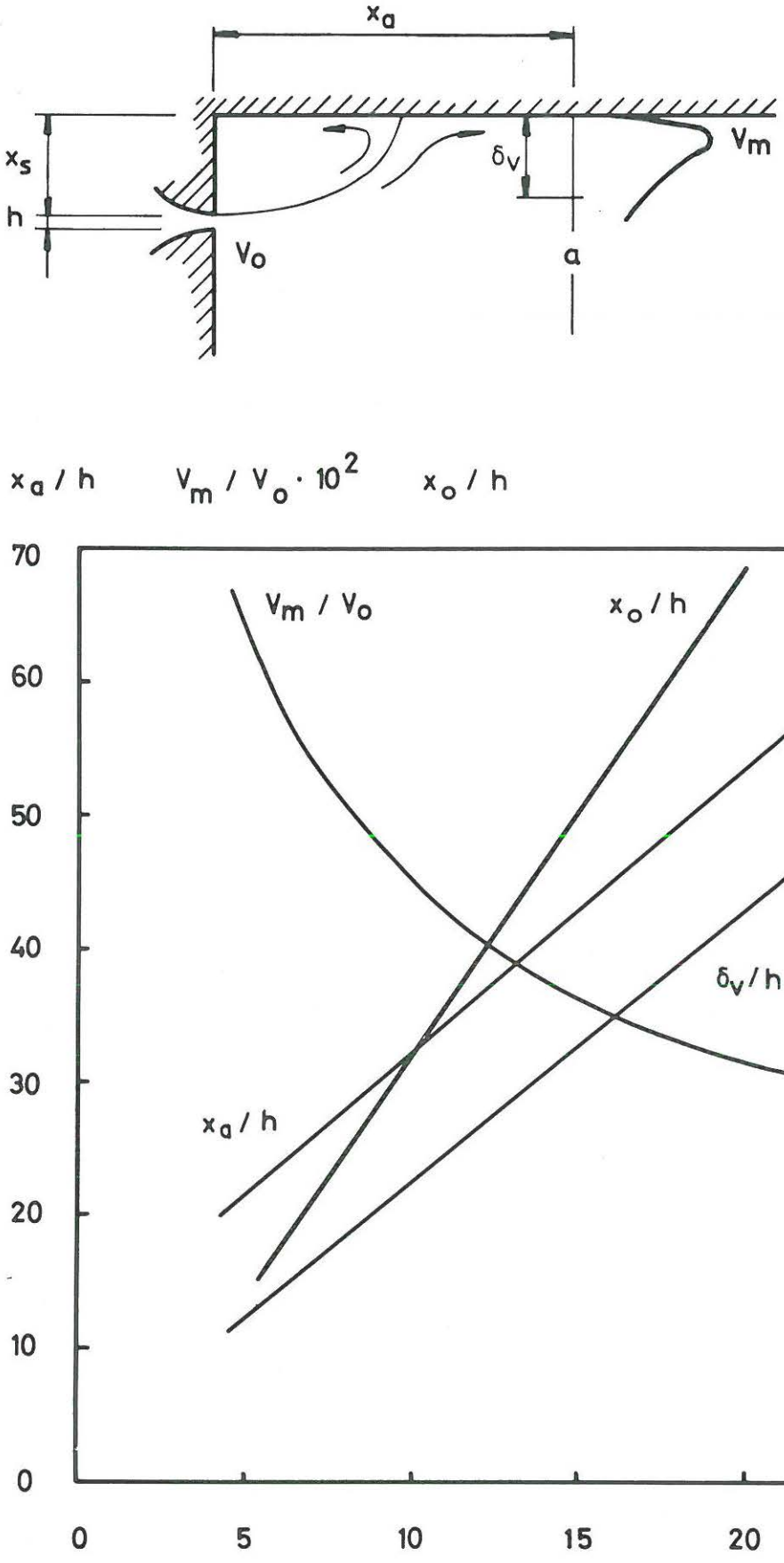

Fig. 3.3.1-2. Two-dimensional jet supplied parallel to a surface. After Schwartzbach [33].

3.3.2. Return opening.

The boundary conditions for the return opening do not have a great influence on the flow. The vorticity ω is assumed to be zero, and the stream function ψ is varied linearly across the opening, corresponding to a parallel flow with rectangular velocity profile. For the other variables we use

$$\frac{\partial \varphi}{\partial x} = 0 \qquad (3.3.2\text{-}1)$$

in the direction of the flow, where φ denotes T, k and ϵ .

3.3.3. Boundary conditions at surfaces.

The gradients in a turbulent boundary layer are big, and a high number of points is required because linearity is assumed between the points right up to the surface. We shall choose instead to let the first point in the flow area, called P, lie just inside the equilibrium layer. Then we use the knowledge we have about the flow in this layer to calculate a slip value at point N on the surface, knowing the value at point P. The slip value is the boundary value which gives the correct slope at point P, assuming a linear variation between N and P, see fig. 3.3.3-1. It is defined by the equation

$$\frac{\varphi_P - \varphi_{sl}}{n_P} = \left(\frac{\partial \varphi}{\partial n}\right)_P \qquad (3.3.3\text{-}1)$$

Wolfshtein [37] has predicted the slip values for v, T and k as functions of the conditions at point P and at point N and has converted them to algebraic forms, which in the following are called the wall functions.

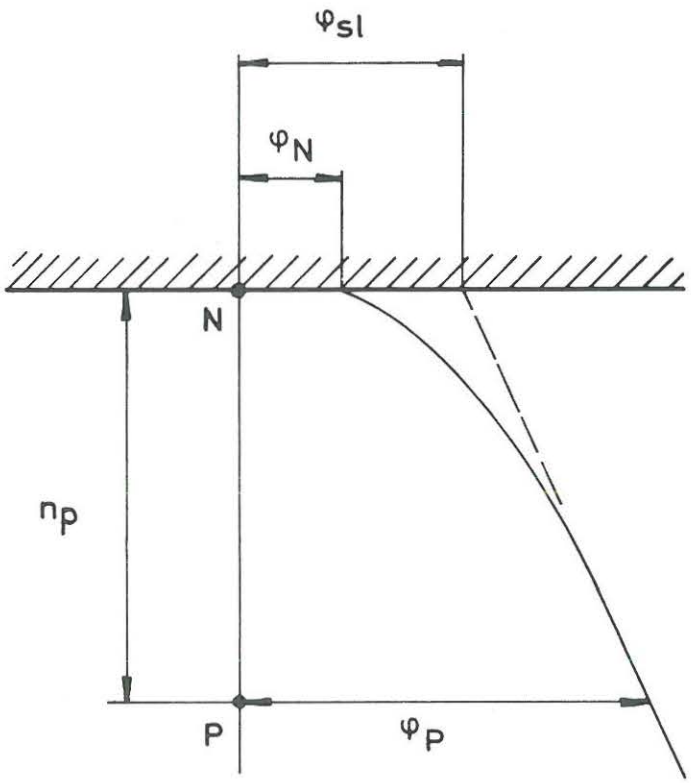

Fig. 3.3.3-1. The slip value at a surface.

The slip values are used as boundary conditions for T and k. Between each iteration there occurs, of course, a calculation of new slip values in accordance with the new conditions at P after a single iteration, and not until the end are the true values φ_N at the surface calculated.

Variation of the vorticity ω between N and P is moderate, and its boundary value may be used direct. It is calculated from the shear stress which is also determined by the wall functions.

In the equilibrium layer between N and P a length scale is used which is proportional to the distance from the surface. The dissipation ϵ is calculated at point P from this length scale and the turbulent kinetic energy. The difference equation for ϵ thus has the boundary value located at the distance n_P from the surface.

The boundary value for the stream function ψ is a fixed given value on the surface between supply and return opening. The gradient of the stream function close to the wall is small, so linearity between N and P is reasonable.

In sufficiently large rooms persons and furniture may be simulated by an equivalent roughness in the wall functions and an "effective height" H. Thermal load from, for example, persons may be simulated by a given heat flux, as shown, for example, on fig. 3.4.2-1.

3.3.4. Plane of symmetry.

In certain situations a section of a two-dimensional flow area will contain a plane of symmetry. This is the case, for example, when two rows of supply openings are placed in a plane symmetrical geometry with plane symmetrical boundary conditions. The discharged supply air will, after possible deflections, meet on the symmetry plane and proceed parallel with this.

In this situation it is sufficient to consider the flow in one area. On the symmetry plane boundary conditions are based on the vanishing of all φ gradients at right angles to this plane.

$$\frac{\partial \varphi}{\partial x} = 0 \qquad (3.3.4\text{-}1)$$

3.4. Results.

3.4.1. Predictions at small Archimedes numbers.

The following predictions apply in situations where velocities are high and temperature differences are low. The forced convection is dominant compared to the free convection, and this means that we can ignore the source term of buoyancy in the transport equation for vorticity. A prediction is completely characterized by the Reynolds number and the geometry of the room, while the influence from the Archimedes number is vanishing.

First comparisons are made with some measurements from a full scale test room at the Technical University of Norway, Trondheim [12]. The test room is 8.3 m long, 3.4 m wide, and 2.8 m high. The supply is located below the ceiling at a distance of 22 cm from the one end wall. The opening runs along the width of the room and has a height h of 15 mm. Two return openings are located in the bottom corners of the opposite end wall. The velocity is measured by spherical anemometers, and the air flow direction is determined by injecting smoke into the room.

The upper section on fig. 3.4.1-1 shows the predicted and measured velocity distribution in the room. The velocity is indicated as "isovels", i.e. lines of constant velocity, and both the predicted and the measured velocity field v_{tot}/V_o are given dimensionless by dividing with the supply velocity.

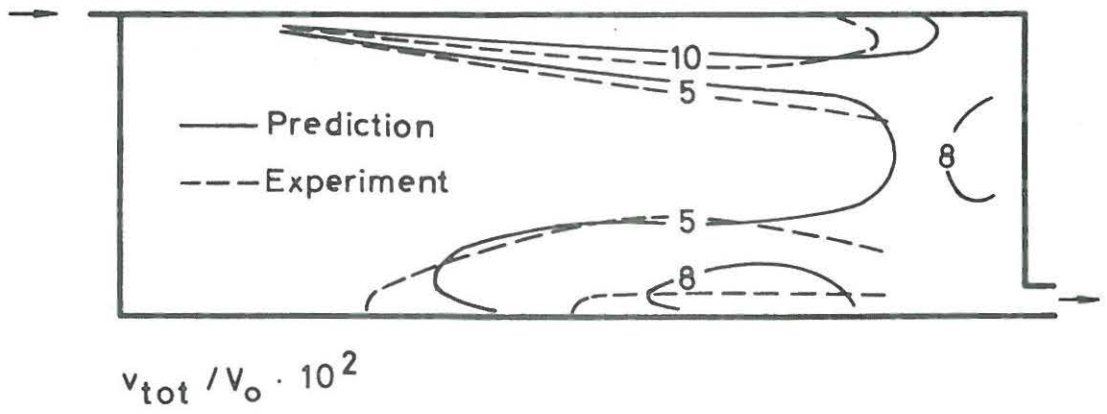

$v_{tot} / V_o \cdot 10^2$

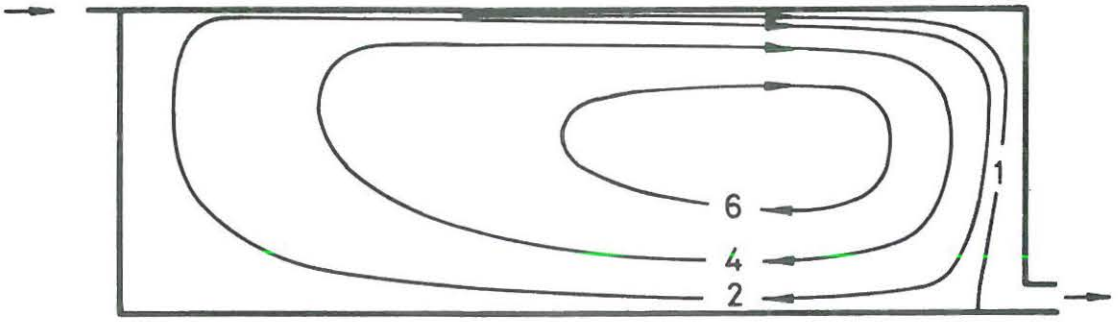

$\psi / h \rho_o V_o$

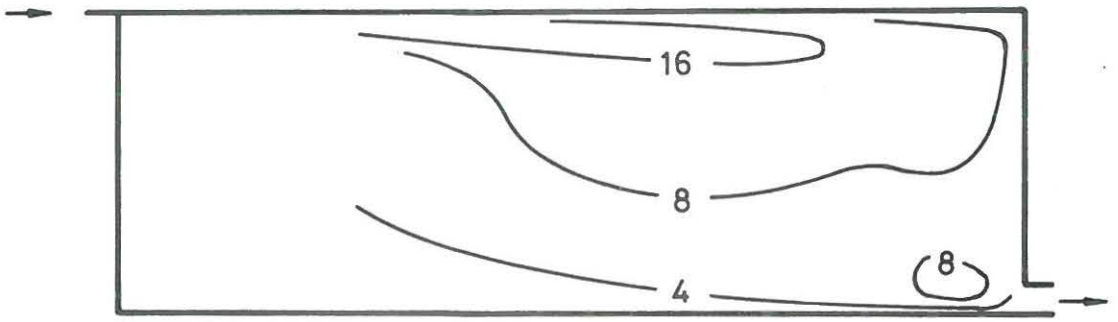

$k / V_o^2 \cdot 10^4$

Fig. 3.4.1-1. Velocity distribution, stream line distribution and distribution of turbulent kinetic energy. Comparison with measured velocity distribution [12] . h/H = o.oo5, x_d/H = o.o8, L/H = 3.o, u/H = o.1, 15 x 21B and Re = 18oo.

$$v_{tot} = \sqrt{v_1^2 + v_2^2} \qquad (3.4.1\text{-}1)$$

The velocity is 8 per cent of the supply velocity at floor level in the right side of the occupied zone and then decreases to less than 2 per cent in the upper and left section of the occupied zone. The predictions and the test have been made at a Reynolds number of 1800, corresponding to a supply velocity of 1.8 m/s. The velocity in the occupied zone, therefore, lies between 14 and 4 cm/s.

It appears that in practice the dimensionless velocity is rather independent of larger variations in supply velocity, because the structure of the turbulence in the recirculating flow will be similar and thereby independent of Reynolds number. If the supply velocity increases to 3.6 m/s, it results in a velocity in the occupied zone which lies between 28 and 8 cm/s. It will be seen that a doubling of the supply velocity means both a doubling of the maximum velocity and a doubling of the velocity gradients. It is thus more difficult to obtain a uniform state of thermal comfort in the whole occupied zone at high velocities than at low velocities in the case of isothermal flow.

The middle section on fig. 3.4.1-1 shows the distribution of the stream lines in the room. The amount of air which is transported between two stream lines is constant, and therefore, the velocity is high where the stream lines are close and low where the distance is great. The stream function is made dimensionless by division with the supplied mass flow.

$$\psi^* = \psi / h \rho_o V_o \qquad (3.4.1\text{-}2)$$

Between stream lines 4 and 6, for example, twice the supply amount is transported, and in all, an amount of air approximately seven times the injected amount is set into motion.

It must be pointed out that the stream lines are only expressing mean values. At a fixed point, the stream line is parallel to the mean velocity, but because of the various directions of the instantaneous velocities a transfer of mass and energy takes place across the stream lines. If the air is injected at a high temperature, heat diffusion will take place across the upper stream lines down into the room.

The bottom section of fig. 3.4.1-1 shows the distribution of dimensionless turbulent kinetic energy k/V_o^2. Turbulent kinetic energy is produced by the turbulent stresses. These stresses are, in the applied model of turbulence, expressed as velocity gradients of different types as will be seen from the production term for turbulent kinetic energy in the transport equation (3.1-18).

$$\mu_t \left[2\left(\left(\frac{\partial v_1}{\partial x_1} \right)^2 + \left(\frac{\partial v_2}{\partial x_2} \right)^2 \right) + \left(\frac{\partial v}{\partial x_2}_1 + \frac{\partial v}{\partial x_1}_2 \right)^2 \right] \qquad (3.4.1\text{-}3)$$

If we compare the turbulent energy with the distribution of isovels we may see that the energy is high where the velocity gradient between the discharged jet and the surrounding air is great. The energy is also high in the thin shear layer between jet and ceiling.

Close to the return opening there is an area where the energy has a local maximum. This energy is due to the deceleration of the jet and is produced by turbulent normal stresses.

It should be noted that distribution of energy does not follow the distribution of energy production everywhere. Turbulent energy is produced in certain areas and transported in the mean flow direction by convection and, perpendicular to the mean flow direction, by turbulent diffusion. The figure shows that the

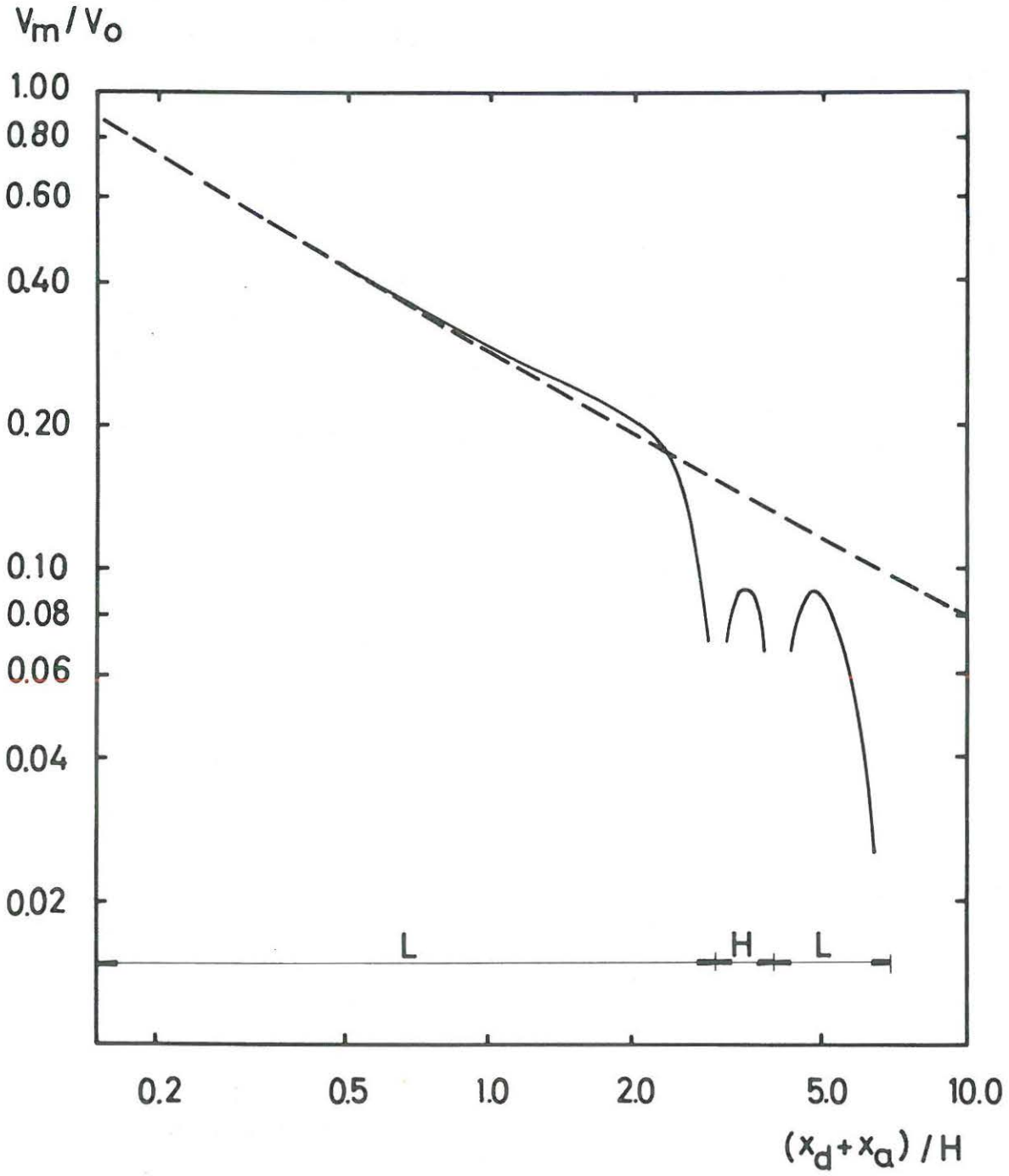

Fig. 3.4.1-2. Decay of velocity in a jet in a closed room. h/H = 0.005, x_d/H = 0.08, L/H = 3.0, u/H = 1.0, 15 x 21B and Re = 1800.

velocity gradient between the discharged jet and the surrounding air gives the most important production of turbulence and that it diffuses from this area giving an even, high level of turbulence everywhere in the room.

Fig. 3.4.1-2 shows the decay of the maximum velocity in the jet which runs along the ceiling, the end wall, and the floor. The dotted curve shows the decay of velocity in a wall jet of corresponding length. We see that the jet drops in velocity in the corners. It increases in velocity along the end wall and along the floor, but does not reach a velocity as high as a wall jet of similar length. The two open areas on the curve denote the length, which is added to the jet because it is ignored that the jet does not follow the corners.

Fig. 3.4.1-3 shows a comparison between a measured and a predicted velocity profile in the following case

$$h/H = 0.056$$
$$L/H = 3.0$$
$$Re = 7100$$

The measurement of the velocity profile is mentioned in section 2.4.5. Both profiles are dimensionless by division with the respective inlet velocities. It will be seen that the calculation gives a satisfactory velocity profile over the whole area.

It is also possible to compare the calculated turbulent kinetic energy with the measured fluctuation $\sqrt{\overline{v_1'^2}}$ .If we assume that the flow may be characterized as a wall jet the following formula applies

$$\sqrt{\overline{v_1'^2}} \sim \sqrt{k} \qquad (3.4.1\text{-}4)$$

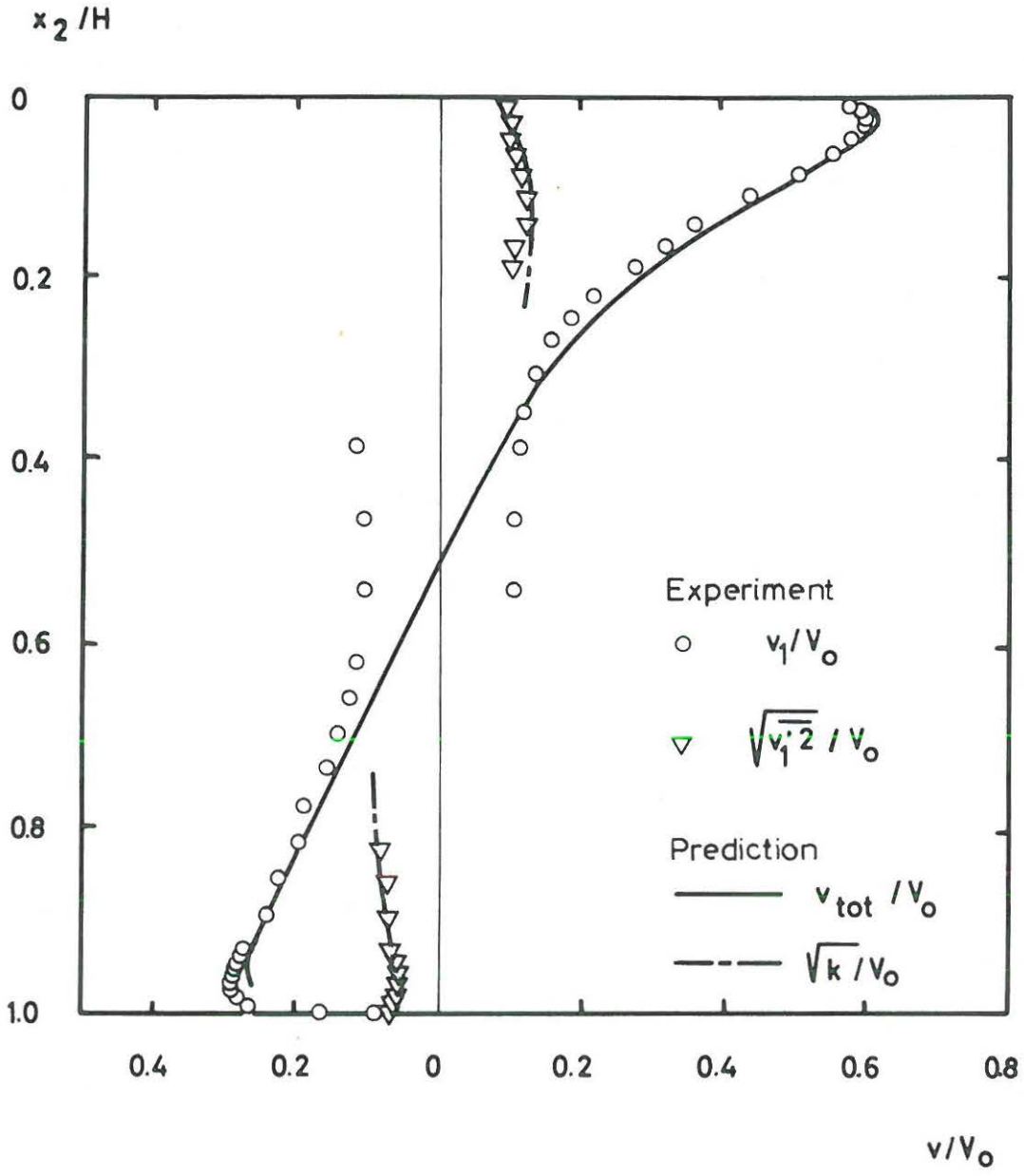

Fig. 3.4.1-3. Comparison between predicted and measured velocity- and turbulence intensity profile. h/H = 0.056, L/H = 3.0, 15 x 21B and Re = 7100.

The experimental results indicated in fig. 3.4.1-4 are from Urbach [34] . They are made in a model 2 m long, 1 m wide and 1 m high. The supply opening is situated below the ceiling at one end wall and runs along the whole width of the model. The size of the opening h can be set at various values. The return opening is situated at the bottom of the opposite wall.

As can be seen from formula (3.4.1-2) the maximum value of the stream function is an expression of the amount of air set into motion compared with the supplied amount. Fig. 3.4.1-4 shows how this quantity increases with the decreasing height of supply opening. The supplied amount is always the same, i.e. the supply velocity increases with a decrease in supply opening. It is an advantage that the maximum value of the stream function ψ_m^* is big. The following figs. 3.4.1-5 and 3.4.2-1 show how the temperature differences in a room become more even with a decrease in the height of the supply opening, which also means an increase in ψ_m^* .

At a given amount of supply air - the quantity of which may be set according to a thermal or hygienic criterion - the entrainment and the amount of air set into motion in the room must be limited. The reason is that the supply velocity increases with decreasing supply opening and causes an increasing velocity in the occupied zone. Thus this velocity and the noise generated by the diffuser limits the minimum size of the supply opening.

In section 2.5. the temperature distribution is measured in the following situation:

$$h/H = 0.056$$
$$L/H = 3.0$$
$$Re = 7100$$

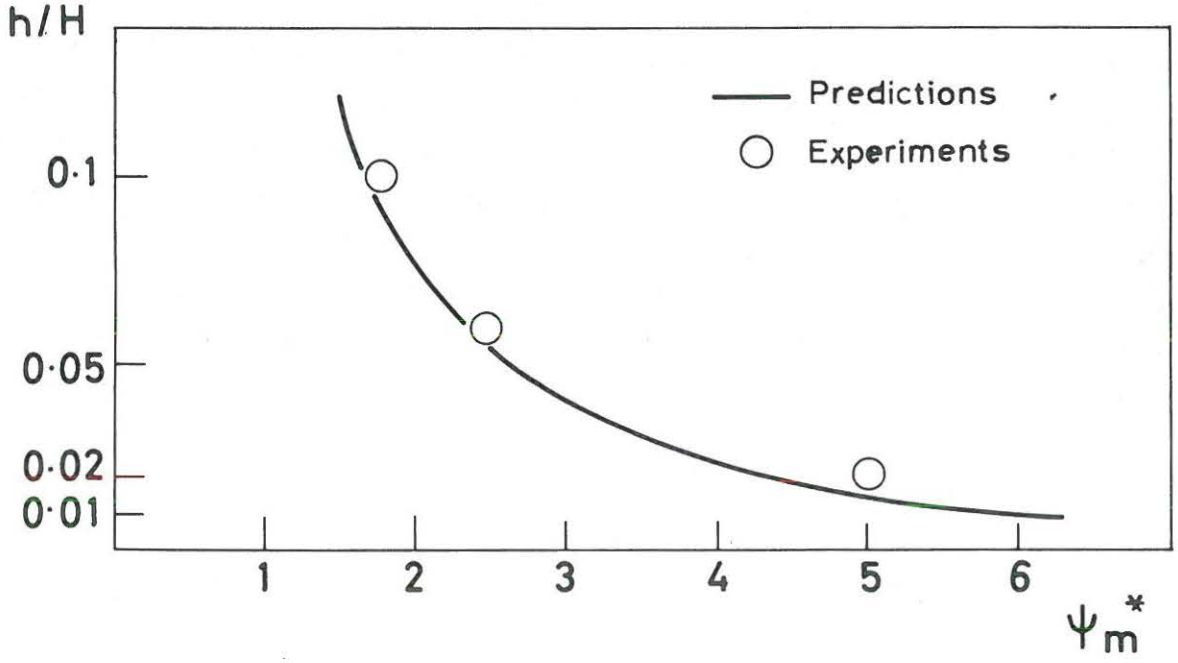

Fig. 3.4.1-4. Effect of supply opening geometry on recirculation. L/H = 2.0, W/H = 1.0, 15 x 19 and Re = 7400.

Fig. 3.4.1-5 shows a comparison between these measurements and corresponding predictions. In section 2.2.2 we have shown that the influence from thermal radiation falls proportional to the decreasing value of the scale 1/M. Therefore, thermal radiation can be excluded from the calculations. The Archimedes number in the measurements is so low that buoyancy is also neglected in the calculations.

The temperatures in fig. 3.4.1-5 are given in dimensionless form. The reason is that a dimensionless solution contains many solutions if the Archimedes number is low. All temperatures T are given in reference to the supply temperature T_o by subtracting this temperature, because a solution is independent of the temperature level. A positive temperature T^* is therefore greater than the supply temperature T_o, and a negative temperature is less than T_o. At low Archimedes numbers a solution is independent of the difference ΔT_o between the supply temperature and the return temperature. Therefore, the temperature distribution is made dimensionless by dividing with ΔT_o.

$$T^* = \frac{T - T_o}{\Delta T_o} \qquad (3.4.1\text{-}5)$$

or

$$T = T^* \Delta T_o + T_o \qquad (3.4.1\text{-}6)$$

At a supply temperature T_o of 22°C and a temperature difference ΔT_o of 1°C, the dimensionless temperature $T^* = 1.6$ corresponds to 23.6°C, see formula (3.4.1-6). If the load is doubled at

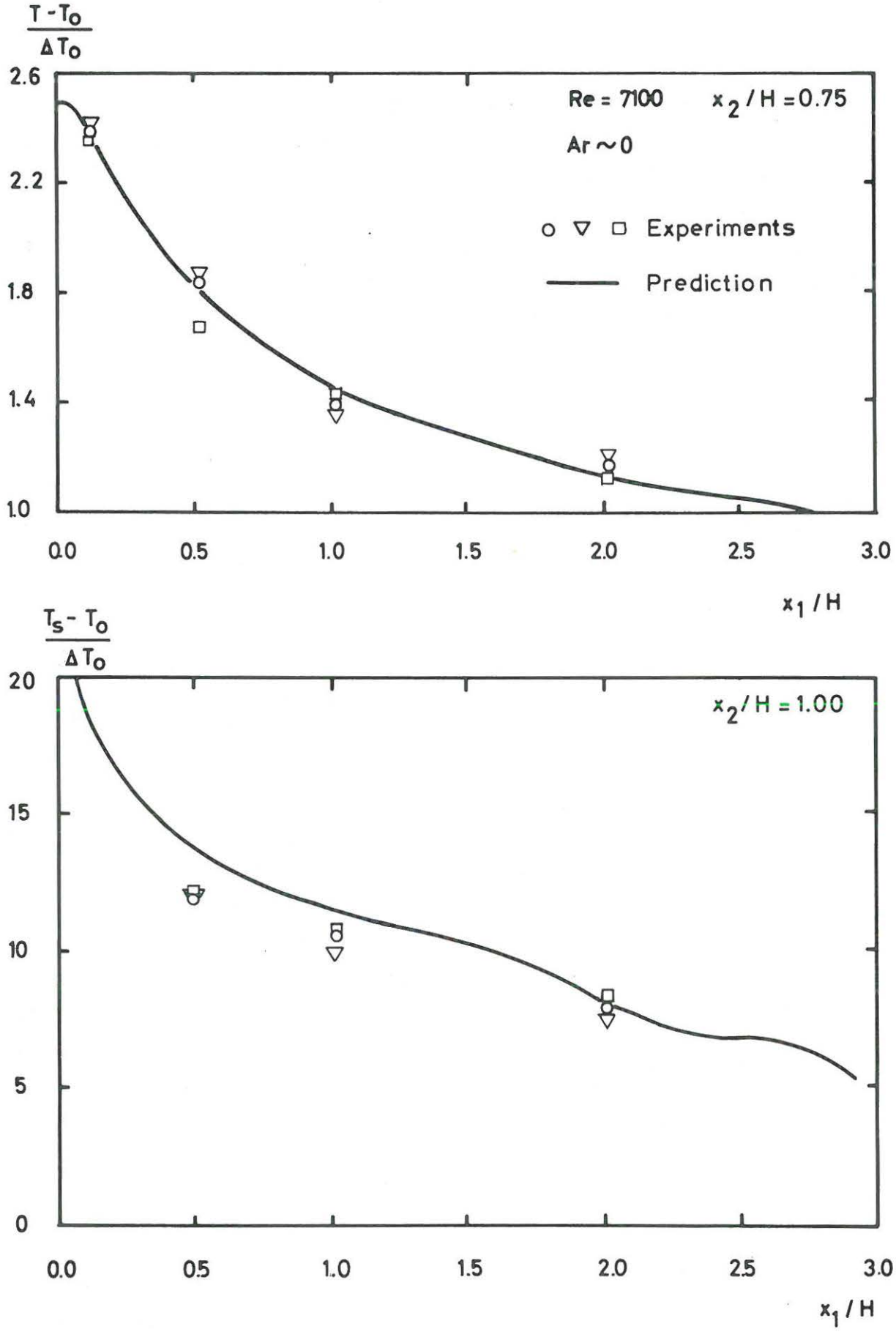

Fig. 3.4.1-5. Comparison between measured and predicted air temperature- and surface temperature profile. h/H = 0.056, L/H = 3.0, 15 x 21B and Re = 7100.

the same air flow rate, so that ΔT_o becomes 2°C, the dimensionless temperature distribution is unchanged. The dimensionless temperature $T^* = 1.6$ corresponds in this instance to 25.2°C. If the Archimedes number is so high that the buoyancy has a significant influence on the flow it is not possible to attach more values to ΔT_o. Predictions must be made for the actual values of ΔT_o and, therefore, of all the Archimedes numbers, see section 3.4.2.

The turbulent Prandtl number is, in principle, a function of the turbulence. However, it varies only slightly compared to the other turbulent parameters, and is of the magnitude 1. For boundary layer flow a value of 0.9 is often used, while for free turbulent flow a value of 0.5 is used. For the predictions made here a value of 0.5 is used.

When the temperature distribution along the surface "a" at the supply opening is calculated it is assumed that K_T is 0.9 K_V, see equations (3.3.1-1), (3.3.1-3) and fig. 3.3.1-1.

So far, the predictions mentioned have embraced situations where the flow is in practice steady and two-dimensional. If we predict the flow in a deep room, we shall of course, get a solution that also in this case represents steady two-dimensional flow. In the case of h/H = 0.056 a preliminary prediction in a coarse grid gives a penetration of $l_{re}/H \sim 6.5$, and this is not much in conflict with the measurements showing that $l_{re}/H \sim 4$-5, see section 2.4.2. It is also in agreement with various values given by Bradshaw and Wong [5] for reattachment behind an obstacle in a turbulent shear layer.

Since, in this case, the flow really is unsteady or steady three-dimensional, it will be seen that one should always have knowledge of the nature of the flow before making a prediction. Section 2.4 gives some data on the nature of the flow in different situations. In special cases it is recommended that a preliminary model experiment should be made.

Hitherto we have described the supply opening by the ratio h/H. Although this ratio is a principal parameter, it is not, however, sufficient to describe the two-dimensional flow from the jet. Constructive details such as turbulence-generating corners before the inlet, sectional division of the nozzle, grid arrangement and alignment with the ceiling may be of importance to the established wall jet. These factors can be difficult to express geometrically, but their effect is expressed by the coefficients in formulas (3.3.1-1), (3.3.1-2), (3.3.1-3) and (3.3.1-4).

Based on Förthmanns measurements of isothermal velocity profiles [9] the following set of coefficients can be derived

$$K_v = 4.1$$

$$D_v = 0.082$$

$$x_o/h = 6.6$$

$$e = 0.5$$

The coefficients are formed by first describing δ_v as a function of x_a, formula (3.3.1-2). This gives us x_o and D_v. If we assume that e = 0.5, K_v can then be found from formula (3.3.1-1).

If we compare this with Schwarz' and Cosart's coefficients [32] it will be seen that there are some deviations.

Myers et al. [24] expresses the velocity decrease and the increase in boundary layer thickness in a wall jet as follows

$$\frac{V_m}{V_o} = z = \frac{1}{\sqrt{1 + 0.381\left(\frac{x_a/h}{7} - 1\right)}} \qquad (3.4.1\text{-}7)$$

$$\frac{\delta_v}{h} = \frac{2.05}{z^2\,Re^{1/5}}\left(0.65\,Re^{1/5} - 1 + 0857rz\right) \qquad (3.4.1\text{-}8)$$

where

$$r = \left(0.523\, z^{10} + 0.477\, z^{-1}\right)^{4/5}$$

Fig. 3.4.1-6 shows a comparison of V_m/V_o in the three cases mentioned, reference [32] , [9] and [24]. In all three situations, the size of the opening is h/H = o.oo15 and it is seen that this ratio does not clearly describe the center line velocity that will take place in the wall jet. Results from the linear diffusers used in air conditioning will undoubtly indicate even greater dispersion in V_m/V_o as a function x_a.

Fig. 3.4.1-6 also shows prediction of the velocity decrease in the jet running along the perimeter of the room. In the full-drawn curve Schwarz' and Cosart's wall jet [32] is used as boundary conditions while in the case of the dotted curve it is Förthmann's wall jet [9] that is used as boundary conditions. It will be seen that the results of the calculations are greatly dependent on the wall jet chosen as boundary conditions. We can thus conclude that the ratio h/H is not quite sufficient to characterize the supply opening, and this must be borne in mind when comparing with measuring results taken from tests in rooms.

Matters may become further complicated by the fact that V_m/V_o may be somewhat dependent on the length L/H. Urbach [34] has established this dependency with the relatively large supply opening, h/H = o.o2, in models having a width of W/H = 1.o. If this effect is present at more realistic h/H and W/H ratios, it can be suppressed to a large extent by selecting a small x_a.

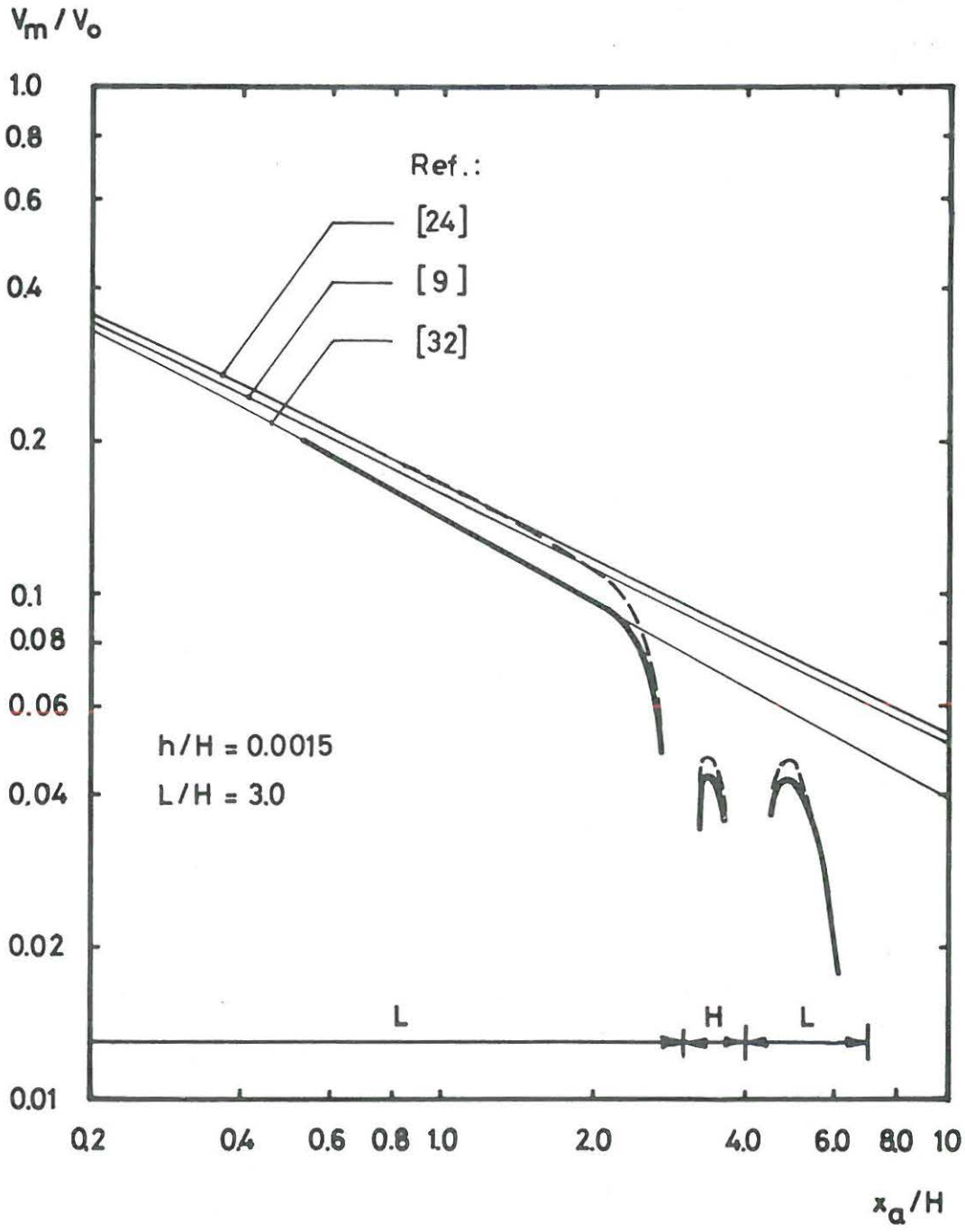

Fig. 3.4.1-6. Decay of center line velocity in a wall jet according to three different references. Center line velocity in a closed room using two of the different wall jets as boundary conditions is also shown. h/H = o.oo15, L/H = 3.o, u/H = o.1, 15 x 21 B and Re = 214o.

3.4.2. Predictions at high Archimedes numbers.

We shall now look at some predictions where the Archimedes number is so high that the buoyancy has a considerable influence on the flow.

Fig. 3.4.2-1 shows the temperature and stream line distribution in a room under the following conditions:

$$h/H = 0.005$$

$$x_d/H = 0.08$$

$$L/H = 3.0$$

$$u/H = 0.1$$

$$Re = 3600$$

The dimensionless supply temperature is $T_o^* = 0$, and the return temperature is $(T_o + \Delta T_o)^* = 1$. Ceiling and wall are adiabatic while a constant heat flux is supplied through the floor. These boundary values are stated as gradients on the respective surfaces, see fig. 3.4.2-1 at the top.

The contribution from buoyancy to the vorticity appears from the last term of the equation (3.1-15). It will be seen that it is proportional to the horizontal temperature gradient, which also seems physically reasonable. The upper section on fig. 3.4.2-1 shows the dimensionless temperature distribution given at low Archimedes numbers. The temperature distribution shows, in particular, steep horizontal gradients on the left side of the room below the supply opening. The lower section on the figure shows the stream line distribution in the case of Ar = 0 and Ar = $4 \cdot 10^{-4}$. We see that there is a big change in stream line distribution in the area with steep horizontal temperature gradients. The maximum value of the stream function rises from about 7 to about 8.5 with this increase in the Archimedes number.

Fig. 3.4.2-2 shows the stream line distribution in a room, where the wall opposite the supply opening may have a constant temperature as boundary value. This temperature may be higher

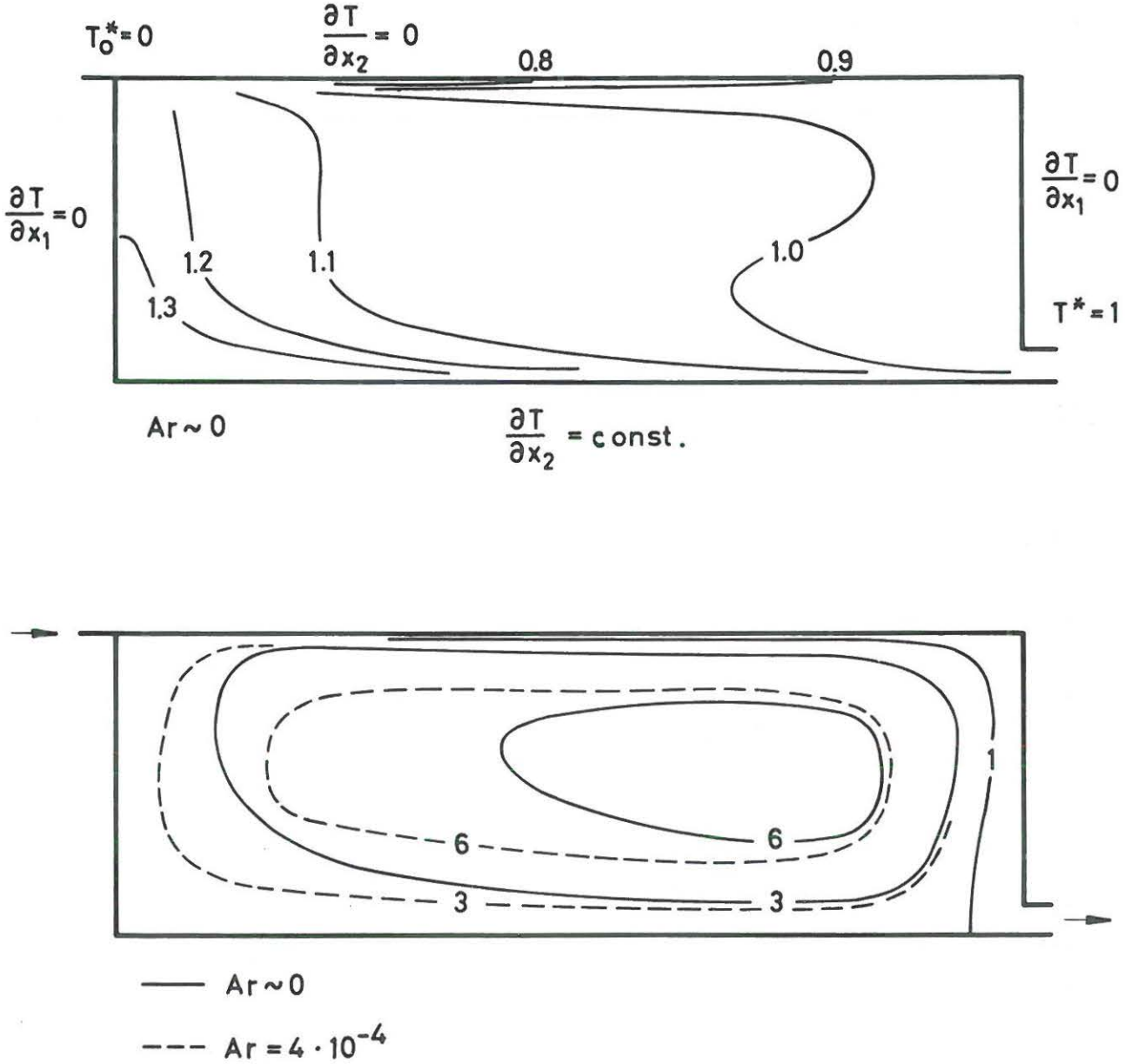

Fig. 3.4.2-1. Temperature distribution. Stream line distribution at low and high Archimedes number. h/H = 0.005, x_d/H = 0.08, L/H = 3.0, u/H = 0.1, 13 x 17A and Re = 3600.

or lower than the supply temperature. This corresponds, for example, to a window exposed to either low outdoor temperatures or direct solar radiation. The other surfaces are considered adiabatic. The predictions apply to the following geometry and Reynolds number.

$$h/H = 0.005$$
$$x_d/H = 0.08$$
$$L/H = 3.0$$
$$u/H = 0.1$$
$$Re = 3600.$$

The upper figure shows the stream line distribution in the case of isothermal flow. The next figure shows the flow pattern when the end wall is colder than the supply air. It will be seen that cool downdraught has removed the recirculating flow at the bottom corner. The lower figure shows the situation where the end wall is warmer than the supplied air. The warm current rising in front of the surface creates an area of recirculating flow and the injected jet leaves the ceiling before it reaches the end wall. The flow conditions are in accordance with the measurements made by Miller and Nash [23] in a somewhat similar situation. They use the ADPI index to express the thermal comfort in different situations. They show that it is advantageous to raise the velocity to a level such that there will only be a small area of recirculating flow in front of the warm end wall.

By comparing the isothermal stream line distribution in fig. 3.4.2-2 with the stream line distribution in fig. 3.4.1-1 we can estimate the influence from changes in the position of the return opening. The maximum value of the stream function ψ^*_m is, in practice, independent of the position of the return opening. If the return opening is moved from one end wall to the other the amount of recirculating air in the lower part of the room will change by $\psi^* = 1$, corresponding to the injected amounts. The change in air velocity in the occupied zone will thus be of the magnitude $1/\psi^*_m$.

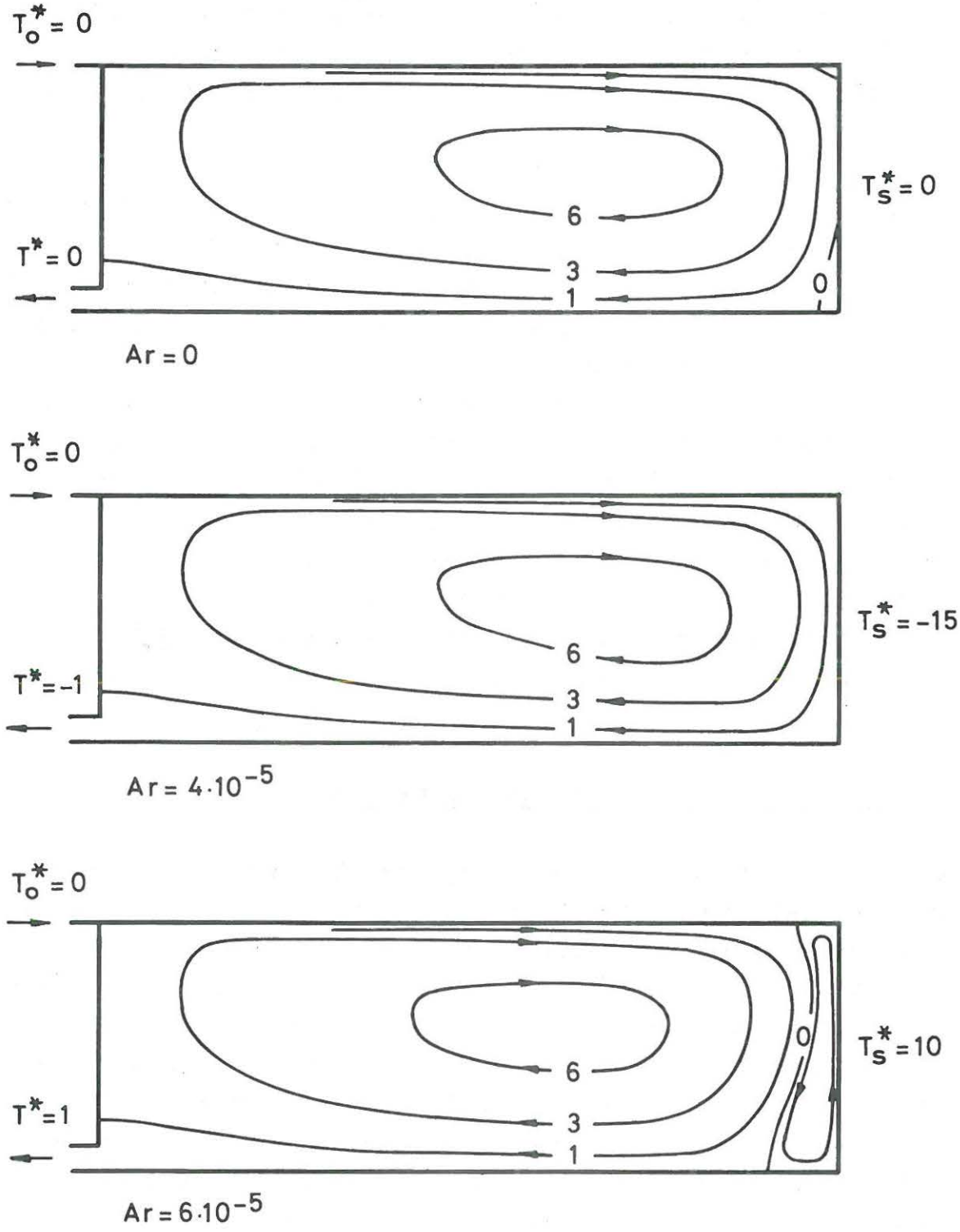

Fig. 3.4.2-2. Stream line distribution in the case of three different temperatures on the right end wall. h/H = 0.005, x_d/H = 0.08, L/H = 3.0, u/H = 0.1, 14 x 17A and Re = 3600.

If ψ_m^* is suitably high, as is the case with small supply openings, see fig. 3.4.1-4, the influence from the position of the return opening will be small. This is the case in practice, where the supply opening is often of the size h/H < o.ol.

Fig. 3.4.2-3 shows the horizontal velocity profile at the end wall in the three situations examined on fig. 3.4.2-2. With isothermal flow the profile can be characterized as a wall jet. In the case of a cold surface the maximum velocity is increased. The buoyancy generates a strong vorticity in the shear layer at the surface where the horizontal temperature gradients are greatest. This vorticity gives the shown change in the shape of the profile, and a typical velocity profile for downdraught is obtained. In the case of a warm surface the vorticity changes sign and gives the corresponding change in profile. The three profiles represent the same volume flow because the maximum value of the stream function ψ_m^* is the same in all three situations.

3.5. Extension of the prediction method.

One of the objects of predicting the flow conditions in an air conditioned room is to obtain information on the level of thermal comfort in different areas of the room. This can be done by examining the various factors: air temperature, mean radient temperature and air velocity. It is obvious, however, to extend the prediction method so that it integrates these physical quantities into a single variable, which in itself expresses the level of thermal comfort in the area. To this end we can use the distribution of "Predicted Percentage of Dissatisfied" persons - PPD - an index developed by Fanger [8]. The previously mentioned ADPI-index can also be used to make an integrated estimation of the thermal comfort conditions of a room, see Nevins and Miller [28] .

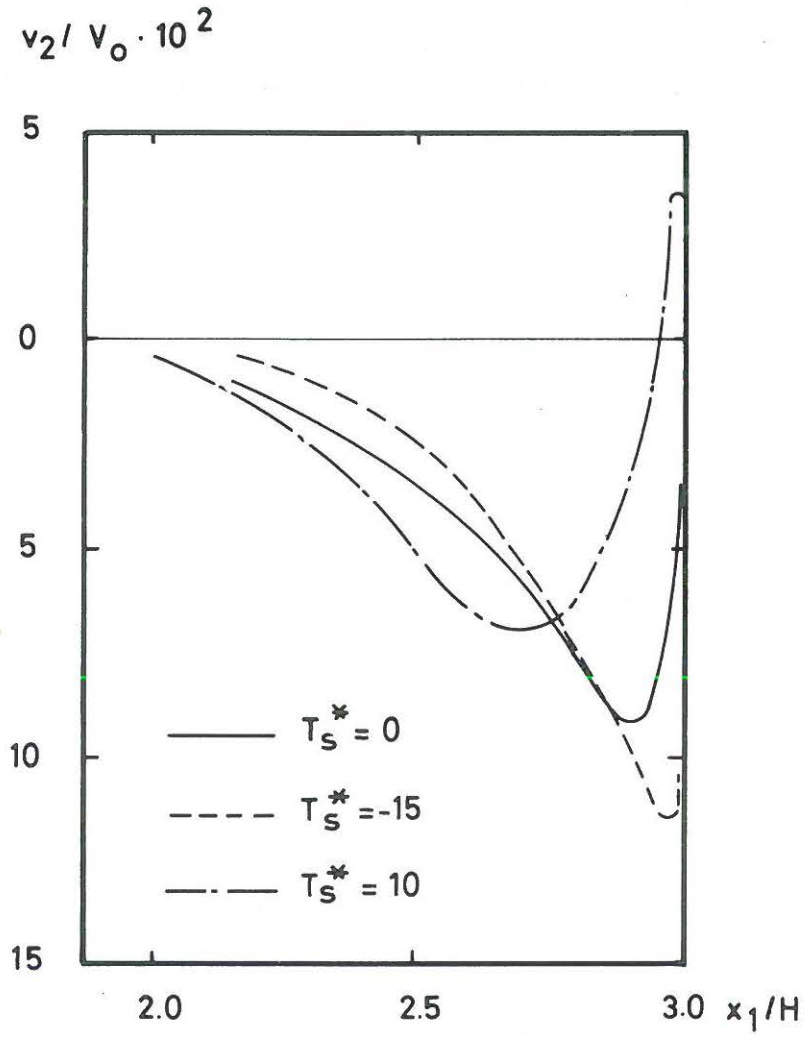

Fig. 3.4.2-3. Velocity profiles at the right end wall (x_2/H = 0.37) for three different temperatures of the wall. Same conditions as in fig. 3.4.2-2.

The prediction method can also be extended to apply to other physical factors. Transport equations of the same type as (3.1-17) can be derived for humidity in air. Solution of a set of equations containing this equation will be of interest in connection with the design of, for example, cold stores. Similarly, a transport equation for the concentration of particles in air could be used to examine the flow conditions in "clean rooms", operating theatres etc.

4. Numerical prediction of convective heat transfer in cavities.

Heat transfer in a cavity is a subject which is of interest in connection with insulation of buildings. In this section will be shown some results of numerical prediction of this type of heat transfer.

In cavity wall insulation, double glazing and similar applications, laminar flow exists under normal temperature conditions, and we shall confine us to this type of flow.

The flow conditions are dependent on the orientation of the hot and cold surfaces compared to the direction of gravity. In the following predictions the surfaces are placed parallel to the direction of gravity.

Dropkin and Somerscales [7] together with Probert et al.[29] have discussed the effect when the surfaces form and angle to the gravitational acceleration. Horizontal surfaces with the hot surface at the bottom have been studied by, among others, Wantland [36] . When the hot surface is uppermost, a convective current may be created by a temperature distribution which varies over the surface. This has been studied by Berkovsky and Fertman [4] . Also relevant is a study made by Bankvall [2] regarding flow in cases where the cavity is filled with an insulating material.

4.1. Basic equations and boundary conditions.

The set of equations, which describes steady two-dimensional laminar flow, is

$$\frac{\partial}{\partial x_1}\left(\omega \frac{\partial \psi}{\partial x_2}\right) - \frac{\partial}{\partial x_2}\left(\omega \frac{\partial \psi}{\partial x_1}\right) = \mu_o\left(\frac{\partial^2 \omega}{\partial x_1^2} + \frac{\partial^2 \omega}{\partial x_2^2}\right)$$

$$+ \rho_o \beta g_2 \frac{\partial T}{\partial x_1} \qquad (4.1\text{-}1)$$

$$\frac{\partial}{\partial x_1}\left(\frac{1}{\rho_o}\frac{\partial \psi}{\partial x_1}\right) + \frac{\partial}{\partial x_2}\left(\frac{1}{\rho_o}\frac{\partial \psi}{\partial x_2}\right) = -\omega \qquad (4.1\text{-}2)$$

$$\frac{\partial}{\partial x_1}\left(T\frac{\partial \psi}{\partial x_2}\right) - \frac{\partial}{\partial x_2}\left(T\frac{\partial \psi}{\partial x_1}\right) = \frac{\lambda}{c_p}\left(\frac{\partial^2 T}{\partial x_1^2} + \frac{\partial^2 T}{\partial x_2^2}\right) \qquad (4.1\text{-}3)$$

These equations are identical to the equations (3.1-15), (3.1-16), and (3.1-17), apart from the following points: They contain the viscous stress terms in (4.1-1) and the molecular diffusion terms in (4.1-3), while the corresponding turbulent contributions are disregarded.

The boundary conditions for this set of equations are given on fig. 4.1-1. The cavity is characterized by a height H and a width W.

The gravitational acceleration acts in the direction of the x_2-axis. The stream function has a constant value $\psi = 0$ along the whole closed surface. The boundary conditions for the vorticity are given from the value of the stream function at near wall node and wall node, see Gosman et al.[11]. The vertical surfaces have constant temperatures and the horizontal surfaces are adiabatic

Since the solution domain is surrounded by a closed surface, it is appropriate to select other reference values than those used in the foregoing chapters. The following dimensionless numbers together with boundary conditions will specify the flow in the case of convective heat transfer.

$$Pr = \frac{\mu_o c_p}{\lambda} \qquad (4.1\text{-}4)$$

$$Gr_w = \frac{\rho_o^2 g_2 \beta \Delta T_o W^3}{\mu_o^2} \qquad (4.1\text{-}5)$$

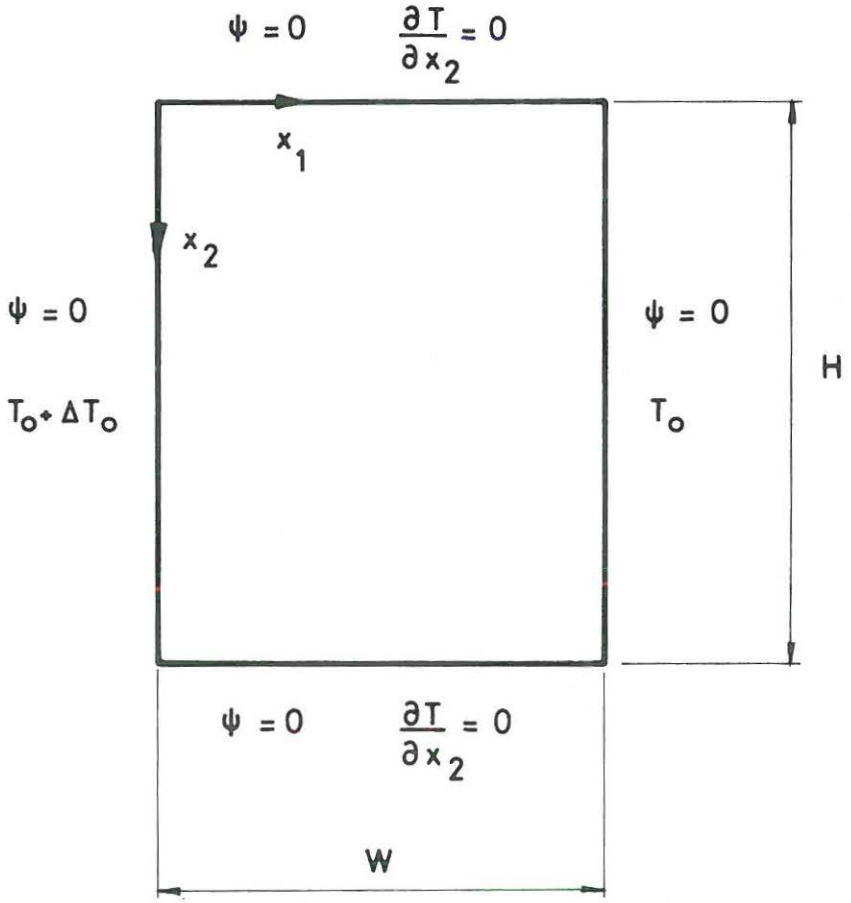

Fig. 4.1-1. Cavity with specification of dimensions and boundary conditions.

ΔT_o is defined on fig. 4.1-1.

When calculating heat transfer the Rayleigh number Ra_w is often used as a variable

$$Ra_w = Gr_w \cdot Pr \qquad (4.1\text{-}6)$$

The heat transfer in the cavity is given by the Nusselt number. This number is the ratio between the actual heat transfer and that which would take place, if there were only conduction.

$$Nu_w = \frac{\varkappa\, W}{\lambda} \qquad (4.1\text{-}7)$$

$\varkappa$ is the coefficient of convective heat transfer. In the predictions $\varkappa$ is given by the following expression

$$\varkappa\, \Delta T_o H = -\int_0^H \left(\frac{\partial T}{\partial x_1}\right)_{x_1=0} \lambda\, dx_2 \qquad (4.1\text{-}8)$$

4.2. Results.

Fig. 4.2-1 shows stream lines and temperature distribution in a cavity having the ratio H/W = 1.0.The stream lines are given for

0.2, 0.4, 0.6 and 0.8 times ψ_m and the isotherms for o.2, o.4, 0.6 and 0.8 times ΔT_o.

At a Grashof number below $1o^2$ there is pure conduction and the isotherms are straight lines which are equally spaced. The first prediction illustrated, applies to a Grashof number of $2.4 \cdot 1o^3$. It will be seen, that the isotherms are slightly deformed by the flow and a small part of the heat transfer takes place by means of convection. If the Grashof number is increased to $3 \cdot 1o^4$ a further change in the distribution of the isotherms is noticed and the maximum value of the stream function will increase.

While the flow at $Gr_w = 2.4 \cdot 1o^3$ may be characterized as asymptotic, reference [2o] , the flow at a Grashof number of $3 \cdot 1o^4$ and $1o^5$ is a laminar boundary layer flow. This is confirmed by the fact, that the isotherms are close at the vertical surfaces, indicating that there are large gradients at the surfaces and small ones in the middle of the cavity. The stream function shows two maxima, as have also been found by MacGregor and Emery [2o] .

Fig. 4.2-2 shows the predicted heat transfer in cavities with different dimensions. For comparison purposes predictions by MacGregor and Emery [2o] are shown for H/W = 1.0 and 10.0. An increase in H/W reduces the heat transfer through the cavity, as is seen from the results for H/W = 1.0 and 10.0 and also from the results in [2o] .

It is also evident that the heat transfer is reduced if the ratio H/W is reduced in the range $H/W < 1.0$. This is because the convective flow is greatly restricted by the horizontal surfaces. In practice however, it should be borne in mind that horizontal surfaces give rise to conductive heat transfer. Predictions are made for Rayleigh numbers up to $\sim 1o^5$. At a Rayleigh number of $1o^6$ the flow will become unsteady and in the range $Ra_w > 1o^7$ the flow is turbulent.

ψ - distribution

T - distribution

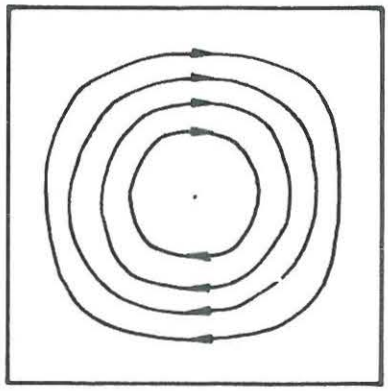

$Gr_w = 2.4 \cdot 10^3$

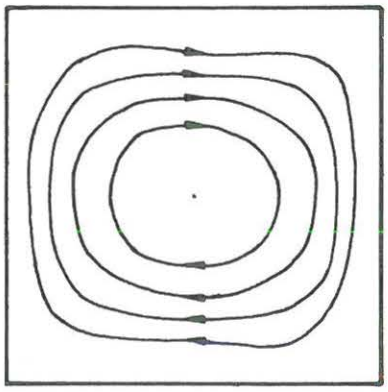

$Gr_w = 3 \cdot 10^4$

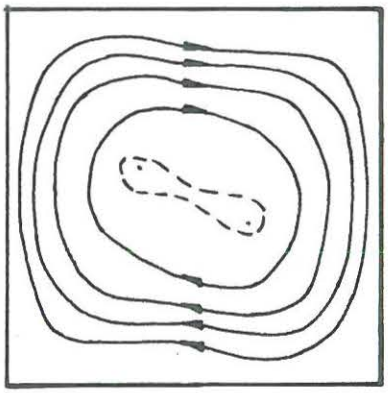

$Gr_w = 10^5$

Fig. 4.2-1. The influence of Grashof number on the stream line- and temperature distribution. H/W = 1.o, Pr = o.7.

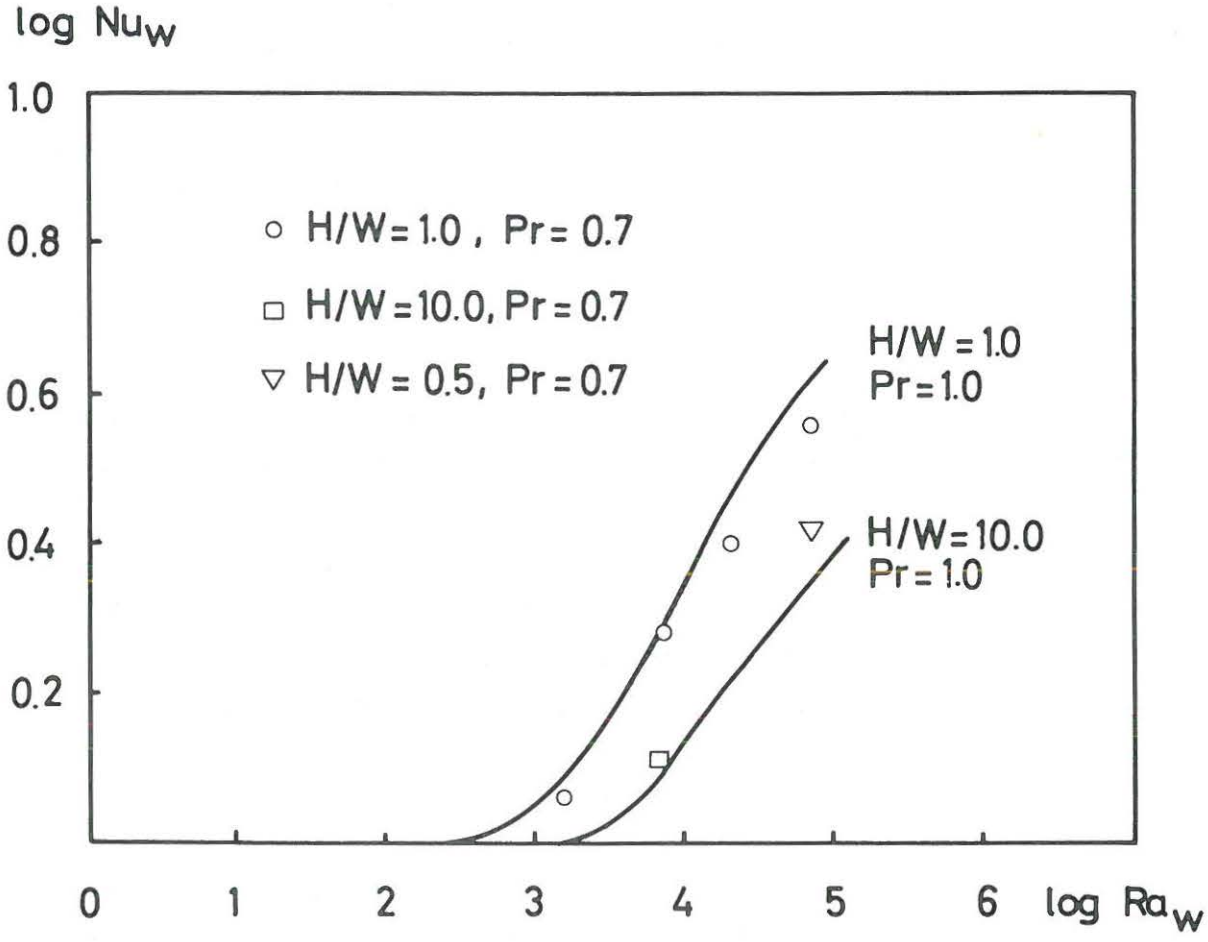

Fig. 4.2-2. Predicted heat transfer in a cavity at different Rayleigh numbers and heights H/W, Pr = o.7. The curves are from reference [2o] , Pr = 1.o.

5. Summary.

Air distribution in air conditioned rooms is investigated by model experiments and by numerical solutions of the flow equations.

The theory of similarity for the flow in air conditioned rooms and models is derived from the flow equations and include evaluations of thermal radiation.

A model (6o x 6o x 18o cm) is made and by dividing it into sections, isothermal air distribution is investigated in about 25 different model sizes.

These experiments show that in a deep, wide model, very unsteady flow conditions may arise. When the air supply opening is only a fraction of the model width, steady unsymmetrical flow may result.

In models of limited depth, (where the length of the model is less than 3-4 times its height), steady two-dimensional flow will take place. It is assumed that the supply opening is located close beneath the "ceiling" and covers the full width of the model.

Stream line measurements are made by illuminating metaldehyde particles and photographing or filming the flow. In a model which indicates steady two-dimensional flow, velocity profiles are also measured at different Reynolds numbers.

It is found that the velocity and stream line distributions are similar at the various Reynolds numbers covered by the investigation.

Temperature distribution is determined by a series of tests in which heat is supplied from the bottom of the model.

Numerical solution of the flow equations is used to predict the air distribution in a section where the flow may be considered steady and two-dimensional. Comparisons are made between predicted values and values measured by full-scale and model-scale experiments. Comparison with test results shows that the prediction method used is suitable for investigation of air distribution in air conditioned rooms.

The method fully takes account of situations where the free convection is significant compared to the forced convection. For instance an example is given of air distribution in a room into which air is injected from one end wall while along the other end wall air is forced thermally up or down, governed by temperature differences.

The prediction method provides everywhere in the room the information necessary for evaluation of thermal comfort, i.e. air velocity, air temperature, surface temperature, velocity- and temperature gradients and turbulent kinetic energy.

Finally, it is shown how convective heat transfer in a cavity is predicted by means of a numerical method.

6. References.

[1] Aris, R., Vectors, tensors, and the basic equations of fluid mechanics, Prentice-Hall, London, 1962.

[2] Bankvall, C.G., Natural convective heat transport in insulated structures, Lunds Inst. of Tech., Rep.38, Div. of Building Tech., Sweden, 1972.

[3] Becher, P., Varme og ventilation 3 (Heating and ventilation 3), Teknisk Forlag, Copenhagen, 1972.

[4] Berkovsky, B.M., and V.E. Fertman, Advanced problems of free convection in cavities, Heat Transfer 197o, vol. IV, Elsevier Publishing Comp., Amsterdam, 1971.

[5] Bradshaw, P., and F.Y.F. Wong, The reattachment and relaxation of a turbulent shear layer, J. Fluid Mech., vol. 52, part 1, 1972.

[6] Daws, L.F., A.D. Penwarden, and G.T. Waters, A visualization technique for the study of air movement in rooms, J. Inst. Heating and Ventilation Engineers, 33, 1965.

[7] Dropkin, D., and E. Somerscales , Heat transfer by natural convection in liquids confined by two parallel plates which are inclined at various angles with respect to the horizontal, J. Heat Transfer, February 1965.

[8] Fanger, P.O., Thermal comfort - analysis and applications in environmental engineering, McGraw-Hill Books Co. New York, 1973.

[9] Förthmann, E., Uber turbulente Strahlausbreitung, Ing. Archiv 5, 1934.

[10] Gosman, A.D., B.E. Launder and W.M. Pun, Calculation of recirculating flows, Imperial College, Mech.Eng.Dept. Rep., June 1971.

[11] Gosman, A.D., W.M. Pun, A.K. Runchal, D.B. Spalding and M. Wolfshtein, Heat and mass transfer in recirculating flows, Academic Press, London, 1969.

[12] Hestad, T., Private communication, Institute for VVS, NTH, Trondheim, 1971.

[13] Jones, W.P., and B.E. Launder, The calculation of low - Reynolds-number phenomena with a two-equation model of turbulence, Imperial College, Mech.Eng.Dept. Rep. TM/TN/A/17, 1972.

[14] Katz, P., Wurfweite, Eindringtiefe und Lauflänge von Zuluftstrahlen im klimatisierten Raum, HLH, No. 3, 1974.

[15] Knystautas, R., The turbulent jet from a series of holes in line, The Aeronautical Quarterly, vol. XV, February 1964.

[16] Launder, B.E., Private communication, Imperial College, Mech. Eng. Dept., 1973.

[17] Launder, B.E., D.B. Spalding and J.H. Whitelaw, Turbulence models and their experimental verification, Imperial College, Mech. Eng. Dept., April 1973.

[18] Libby, P.A., and H.R. Reiss, The design of two-dimensional contraction sections, Quarterly of Applied Mathematics, vol. 9, 1951.

[19] Linke, W., Strömungsvorgänge in künstlich belüfteten Räumen, Forschungsberichte des Wirtschafts- und Verkehrsministeriums NRW No. 259, 1956.

[2o] MacGregor, R.K., and A.F. Emery, Free convection through vertical plane layers - moderate and high Prandtl number fluids, J. Heat Transfer, August 1969.

[21] Malmström, T. and A. Svensson, Hastighetsmätningar i ventilationsluftstrålar (Velocity measurements in jets of ventilating air), (Swedish) VVS, August, 1971.

[22] Miller, D.R., and E.W. Comings, Force-momentum fields in a dual-jet flow, J. Fluid.Mech., p. 237, 196o.

[23] Miller, P.L., and R.T. Nash, A further analysis of room air distribution performance, ASHRAE transactions, vol. 77, part II, 1971.

[24] Myers, G.E., Schauer, J.J., and R.H. Eustis, Plane turbulent wall jet flow development and friction factor, J. Basic Eng., March, 1963.

[25] Müllejans, H., Über die Ähnlichkeit der nicht-isothermen Strömung und den Wärmeübergang in Räumen mit Strahllüftung, Diss., T.H. Aachen, 1963.

[26] Nagasawa, Y., Strömungs- und Temperaturverhältnisse in einem Modellraum mit Bodenheizung, Lehrstuhl für Wärmeübertragung und Klimatechnik RWTH, Aachen, 1974.

[27] Nelson, J.L., An experimental investigation of the turbulent and mean flow properties of a plane two-dimensional turbulent wall jet. Dissertation, University of Tennessee, Dep. of Chem.Eng., 1969.

[28] Nevins, R.G., and P.L. Miller, Analysis, evaluation and comparison of room air distribution performance - a summary, ASHRAE transactions, vol. 78, part II, 1972.

[29] Probert, S.D., M. Dixon and N.M. Pediaditakis, The optimal separation of hot and relatively cool parallel walls, J. Institute of Fuel, February 1971.

[30] Rubel, A., and F. Landis, Laminar natural convection in a rectangular enclosure with moderately large temperature differences, Heat Transfer 1970, vol. IV, Elsevier Publishing Comp., Amsterdam, 1971.

[31] Schmidt, W., Turbulente Ausbreitung eines Stromes erhitzter Luft, Z. Angew.Math.Mech., bd. 21, No. 5 and 6, 1941.

[32] Schwarz, W.H., and W.P. Cosart, The two-dimensional turbulent wall-jet, J. Fluid.Mech., vol. lo, p. 481, June 1961.

[33] Schwartzbach, C., Private communication, Dept. of Fluid Mech., DTH, Copenhagen, 1973.

[34] Urbach, D., Modelluntersuchungen zur Strahllüftung, Diss., TH Aachen, 1971.

[35] Verhoff, The two-dimensional turbulent wall jet with and without an external free stream, Princeton University, Dep. Aeronautical Eng., rep.no. 626, May 1963.

[36] Wantland, J.L., A numerical evaluation of the thermal and hydrodynamic characteristics of laminar cellular convection between rigid horizontal surfaces, Heat Transfer 197o, vol. IV, Elsevier Publishing Comp., Amsterdam, 1971.

[37] Wolfshtein, M., Convection processes in turbulent impinging jets, Imperial College, Mech.Eng.Dept. Rep. SF/R/I/2, 1967.

Appendix I. Low Reynolds number flow.

Jones and Launder [13] have developed a set of equations with a turbulence model suitable for both low and high Reynolds number flow. In principle, this set of equations differs from the one used here in the following points: It contains the viscous stress terms and the molecular diffusion terms in the transport equations, and the coefficients c_μ and c_2 are functions of a turbulent Reynolds number.

The turbulent Reynolds number is a local parameter that can be expressed as

$$R_t = \frac{1}{c_\mu} \frac{\mu_t}{\mu_o} \qquad \text{(I-1)}$$

The coefficients c_μ and c_2 are given as the following functions of the turbulent Reynolds number, Launder [16] .

$$c_\mu = 0.09 \exp(-3.0/(1+R_t/50)^2) \qquad \text{(I-2)}$$

$$c_2 = 2.0(1 - 0.3 \exp(-R_t^2)) \qquad \text{(I-3)}$$

A model of turbulence for high Reynolds number flow may be considered as a special version of the above mentioned model. When the turbulent Reynolds number exceeds 400, the contributions from the viscous stress terms and molecular diffusion terms are negligible compared to the turbulent contributions. From formulas (I-2) and (I-3) it will be seen, that c_μ and c_2 have attained their constant values for $R_t \geq 400$, and the two models of turbulence are identical.

This means that a prediction in which the turbulent Reynolds number is greater than 400 in every point of the flow domain is correctly described by the turbulence model used in section 3.

For c_μ = o.o9 and R_t > 4oo the following condition is obtained by means of formula (I-1).

$$\mu_t > 40 \cdot \mu_o \qquad \text{(I-4)}$$

The turbulent Reynolds number at a point, R_t, increases with an increase in the Reynolds number Re, but it is also a function of the geometry of the room. In a prediction specified by

h/H = o.oo5
L/H = 3.o
u/H = o.1

R_t is greater than 4oo at Re = 18oo. If h/H is increased to o.o56, it is necessary to raise the Reynolds number to about 4ooo-5ooo in order to obtain an R_t greater than 4oo. In both cases there exists, even at high Reynolds numbers, a very small area at the end wall opposite the injected jet where R_t is less than 4oo. This is assumed to be negligible

Near the surfaces the viscous stress and the molecular diffusion will always be of significance, but these effects are taken into account through the wall functions.

Appendix II. Choice of grid distribution.

In section 4 a grid having a constant distance between nodes is used. The accuracy of the results is evaluated, making predictions for the grid with various numbers of points and observing how the predicted value approaches a fixed value at an increasing number of points. Although the difference between the predicted and the analytical solution decreases with an increase in the number of points the accumulated round-off error on the computer will increase. Therefore, an optimum number of grid points exists, beyond which the predicted solution diverges with a further increase in the number of points. Experiments with grids of the type 11 x 11, 15 x 15, 17 x 17, 21 x 21, and 31 x 31 all gave a ψ_m which only deviated 1-2 % for $Gr = 10^4$ and H/W = 1.0. This implies that a grid of the type 11 x 11 is sufficient for practical predictions.

In section 3 a grid with non-uniform distance between the nodes is used. The gradients are, in some areas, so large that we must rule out the use of a grid with uniform node distance if we wish to confine ourselves to a number of nodes of about 300, and this is necessary (in 1971-73) taking the number of difference equations into consideration.

A primary rule in the distribution of nodes is to place them close together where velocity gradients are large, i.e. where ω is great. Velocity gradients occur in source terms in the k- and ϵ-equations and therefore have great influence on the turbulence. Generally speaking, this means that the greatest number of nodes is in the x_2 direction, and that they are very close together at the uppermost surface and fairly close together at the lowest surface.

Two types of grids are used. Grids of type A having a rather great number of nodes close to the surfaces, and type B having a more even distribution, though still with small node distance close to the surfaces compared to the node distance in the middle of the area.

In the case of h/H = o.oo5 and Re = 18oo the variation in ψ_m is less than 7 % for grids of the type 13 x 17A, 15 x 21A and 15 x 21B. It must be borne in mind that the node distribution along surface "a" on fig. 3.3.1-1 is different for each grid type, and this has a great influence on the results. If surfaces "a" and "b" are given a suitable location, fig. 3.3.1-1, it is possible especially with a grid of the type 15 x 21B, to obtain a continuous progression of the velocity profile, see figs. 3.4.1-2 and 3.4.1-6.

Since the computer time is increased considerably when the number of points exceeds approx. 4oo, it has proved necessary to develop the grid distribution by comparing the predictions obtained with measuring results.

Appendix III. Turbulent viscosity and dissipation in a wall jet.

By means of the measured values for the mean velocity v_1, turbulent kinitic energy k and the intensity $\overline{v_1' v_2'}$ in a wall jet, Verhoff [35] and Nelson [27], it is possible to calculate turbulent viscosity and dissipation. The turbulent viscosity may be determined from the Boussinesq hypothesis.

$$- \rho_o \overline{v_1' v_2'} = \mu_t \frac{\partial v_1}{\partial x_2} \qquad \text{(III-1)}$$

This hypothesis assumes that there is a vanishing shear stress at the velocity maximum. This is not the case in asymmetrical jets such as wall jets, and if μ_t is determined according to (III-1) it will thus approach plus and minus infinity around the velocity maximum in the wall jet. Uppermost in fig. III-1 this progression is shown with the dotted curve as a function of η where η is a dimensionless thickness of the wall jet.

$$\eta = x_2 / \delta_v \qquad \text{(III-2)}$$

If the turbulence length scale is determined by the calculated μ_t distribution and by the formula

$$l = \mu_t / c_\mu k^{0.5} \rho_o \qquad \text{(III-3)}$$

we get the distribution shown by the dotted curve at the bottom of fig. III-1.

It is not reasonable to use these values as boundary values, since they assume conditions which are disregarded in the model of turbulence. Instead we shall develop some new values based on the length scale and the following points:

1. The length scale is proportional to the distance from the wall in the near wall area.

2. In the range $\eta > 0.5$ the results are not disturbed by the definition problems, and the length scale has a constant value.

The chosen length scale is shown on the lower figure. This length scale is used to determine μ_t according to (III-3), and the result is the curve on the upper figure. In addition the length scale is used to determine the distribution of the dissipation according to the formula

$$\epsilon = k^{3/2} / l \qquad \text{(III-4)}$$

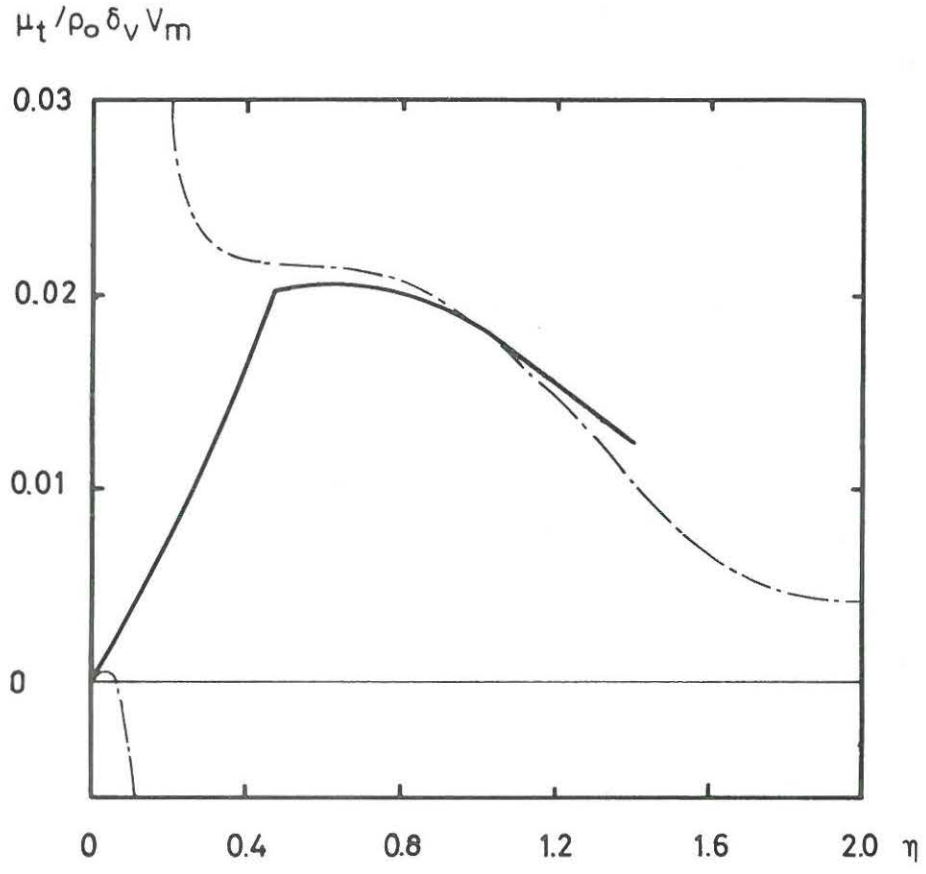

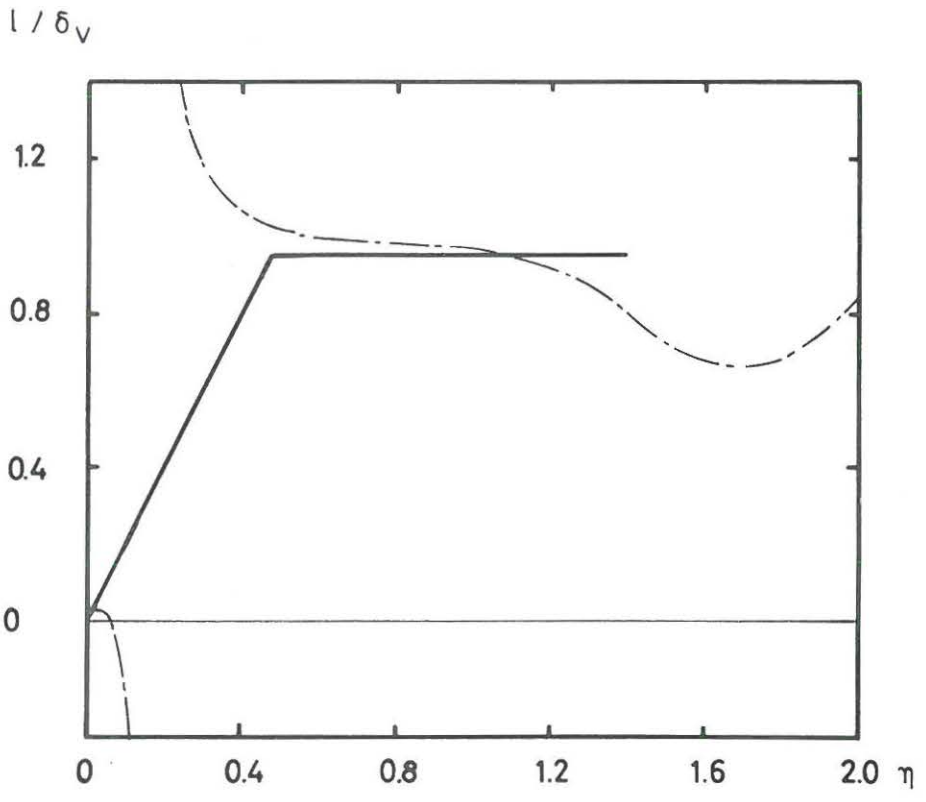

Fig. III-1. Distribution of turbulent viscosity and turbulent length scale in a wall jet.